Advanced Digital Signal Processing in Coherent Fiber Optic Communication Systems

Mahdi Malekiha

Department of Electrical & Computer Engineering
McGill University
Montréal, Canada

August 2016

A thesis submitted to McGill University in partial fulfillment of the requirements for the degree of Doctor of Philosophy.

Abstract

To satisfy the explosive growth in global Internet traffic, the development of transmission links that not only have high-capacity but are also flexible, reconfigurable, and adaptive is imperative. The advents of high speed digital-to-analog and analog-to-digital converters, and recent progress in complementary metal–oxide–semiconductor (CMOS) technology has facilitated the development of optical transceivers relying on coherent detection and digital signal processing (DSP) for the compensation of fiber impairments. Next generation coherent optical networks are anticipated to further approach the Shannon limit and deliver 400 Gb/s or 1 Tb/s data rates per channel, while providing flexibility and agility to maximize the utilization of the network resources. This thesis explores novel system architectures and advanced DSP algorithms to fulfill these design targets.

Currently, chromatic dispersion (CD) compensation and forward error correction (FEC) decoders are the major power consuming (more than 50%) blocks of a conventional transceiver application-specific integrated circuit (ASIC). This thesis presents the concepts and architectures of multi-sub-band (MSB) signaling for mitigation of CD, and eliminating the need for a CD compensating equalizer in reduced-guard-interval (RGI) orthogonal frequency-division multiplexing (OFDM) and single carrier systems. The performance of the proposed techniques are experimentally evaluated using a leading-edge optical long-haul transmission test-bed. It is shown that the MSB technique, in addition to the evidently lower computational complexity, allows for a highly efficient adaptive rate smart transceiver implementation with lower system overhead and simplified parallelism, while attaining the same or better transmission reach and performance as the conventional transceiver. This is due to its higher tolerance to fiber nonlinearity.

With coherent technology and advanced FEC, it is known that the capacity of current fiber optic transmission systems is fundamentally limited by fiber nonlinearities. We have optimized the perturbation based nonlinearity compensation (PB-NLC) equalization scheme and proposed a novel adaptive nonlinear equalizer. The performances of the aforementioned DSP equalization schemes are numerically and experimentally studied. It is found that the optimized technique demonstrates lower computational complexity over conventional PB-NLC. In addition, the proposed adaptive nonlinear equalizer does not require prior calculations of perturbation coefficients and detailed knowledge of the transmission link parameters. It achieves comparable performance to the PB-NLC. Unlike previously studied adaptive nonlinear equalization techniques, our algorithm takes advantage of common symmetries, avoids replication of operations, and only uses a few adaptive nonlinear coefficients. Finally, its computational complexity is smaller than previously proposed adaptive nonlinear equalization schemes, which meets the requirements of next generation optical networks.

Résumé

Pour satisfaire la croissance explosive du trafic Internet mondial, le développement des liaisons de transmission qui ont non seulement une grande capacité, mais qui sont aussi flexibles, reconfigurables, et adaptables est impératif. L'avancement en vitesse des convertisseurs numériques-analogiques et analogiques-numériques, et les progrès récents dans la technologie des semi-conducteurs complémentaires à l'oxyde de métal (CMOS) ont facilité le développement d'émetteurs-récepteurs optiques utilisant la détection cohérente et le traitement numérique du signal (DSP) pour la compensation des détériorations de la fibre. Il est prévu que les réseaux optiques cohérents de la prochaine génération approcheront la limite de Shannon en livrant des débits de données de 400 Gb/s ou 1 Tb/s par canal, tout en offrant la flexibilité et l'agilité pour optimiser l'utilisation des ressources du réseau. Cette thèse explore de nouvelles architectures de systèmes et algorithmes DSP pour répondre à ces objectifs de conception.

Présentement, la compensation pour la dispersion chromatique (CD) et la correction d'erreur directe (FEC) sont les principales consommatrices d'énergie (plus de 50%) des blocs d'un circuit intégré spécifique (ASIC) d'un émetteur-récepteur. Cette thèse présente les concepts et architectures de signalisation multi-sous-bande (MSB) pour diminuer l'effet de la CD et éliminer la nécessité d'un égaliseur CD dans les systèmes à garde-intervalle réduite (RGI) à multiplexage par répartition en fréquence orthogonale (OFDM). La performance des techniques proposées est expérimentalement évaluée à l'aide d'un banc d'essai de transmission optique à longue distance. Il est démontré que la technique MSB, en plus de réduire la complexité de calcul, permet le traitement en parallèle et rend possible de réaliser un émetteur-récepteur intelligent très efficace avec une faible surcharge. Tout cela en atteignant la même ou une meilleure portée de transmission et de performance que l'émetteur-récepteur classique. Ceci est dû à sa plus grande tolérance à la non-linéarité de la fibre.

Avec la technologie cohérente et FEC moderne, il est connu que la capacité des systèmes de transmission à fibre optique est essentiellement limitée par la non-linéarité de la fibre. Nous avons optimisé la technique de compensation de non-linéarité à base de perturbation (PB-NLC) et proposé un nouvel égaliseur de non-linéarité adaptable. La performance de ces algorithmes DSP est numériquement et expérimentalement étudiés. On démontre que la technique optimisée a une complexité de calcul plus faible que la PB-NLC classique. En outre, cet égaliseur non linéaire adaptable ne nécessite pas de calculs antérieurs des coefficients de perturbation et de connaissance détaillée des paramètres de liaison de transmission. Il réalise des performances comparables à la PB-NLC classique. Contrairement aux techniques non linéaires d'égalisation adaptable étudiées précédemment, notre algorithme tire parti des symétries communes, évite la répétition des opérations, et utilise seulement quelques coefficients adaptables. Enfin, sa complexité de calcul est plus petite que des systèmes non linéaires proposés précédemment, il est donc conforme aux exigences des réseaux optiques de la prochaine génération.

Acknowledgments

I would like to express my most sincere gratitude to my supervisor, Prof. David Plant, for his support, resources, advice, experience, and guidance in the completion of this work. I am grateful to him for believing in my research ideas and for providing the right environment to make them flourish. Moreover, I highly appreciate Prof. Plant's dedication to his work, which has resulted in a laboratory with high-end equipment that is necessary to perform not only my research but also that of other students in the Photonic Systems Group.

I would like to acknowledge Prof. Shiva Kumar for giving me my first opportunity as a researcher, and for his countless suggestions and long discussions in research and life. Furthermore, I would like to express my appreciation of Dr. Igor Tselniker for having worked together on various topics in optical communications. I am profoundly impressed by his ideas, as well as his passion, and rigor.

During the course of my graduate studies, I met incredible individuals without whom this thesis could not have been completed. Many thanks to my talented colleagues: David Patel, Mohamed Morsy-Osman, Qunbi Zhuge, Xian Xu, Mathieu Chagnon and everyone else that have helped me in various forms to realize this project.

My deepest love and appreciation goes to my parents for their unconditional love, support, and patience during my entire life. They devoted their heart and soul to advance my education and encourage me to love learning and work hard. I dedicate this thesis to my wife Mehrnoosh. I would not be where I am if it was not for her love and perseverance. I feel considerably lucky for having her by my side throughout my graduate studies.

Mahdi Malekiha

May 2016

Associated Publications

The content of this thesis is based on published journal papers and conference proceedings. A list of the publications that I have authored is provided below. The contribution of the co-authors is stated below each item for the journal and conference papers directly related to this thesis.

Journal Articles Directly Related to This Thesis

[1] **M. Malekiha**, I. Tselniker, and D.V. Plant,"Efficient nonlinear equalizer for intra-channel nonlinearity compensation for next generation agile and dynamically reconfigurable optical networks," *Optics Express*, vol. 24, no. 4, pp. 4097-4108, 2016.

I conceived the idea, performed the simulation and experiment, and wrote the paper. The co-authors contributed in editing the paper and discussing the idea.

[2] **M. Malekiha**, and D.V. Plant,"Adaptive Optimization of Quantized Perturbation Coefficients for Fiber Nonlinearity Compensation," *IEEE Photonic Journal*, vol. 6, no. 3, pp. 1-7, 2016.

I conceived the idea, performed the simulation and experiment, and wrote the paper. The co-authors contributed in editing the paper and discussing the idea.

[3] **M. Malekiha**, I. Tselniker, and D.V. Plant, "Chromatic dispersion mitigation in long-haul fiber-optic communication networks by sub-band partitioning," *Optics Express*, vol. 23, no. 20, pp. 32654-32663, 2015.

I conceived the idea, performed the simulation and experiment, and wrote the paper. The co-authors contributed in editing the paper and discussing the idea.

[4] **M. Malekiha**, I. Tselniker, M. Nazarathy, A. Tolmachev, and D.V. Plant, "Experimental demonstration of low-complexity fiber chromatic dispersion mitigation for

reduced guard-interval OFDM coherent optical communication systems based on digital spectrum sub-band multiplexing," *Optics Express*, vol. 23, no. 25, pp. 25608-25619, 2015.
I conceived the idea, performed the simulation and experiment, and wrote the paper. The co-authors contributed in editing the paper and discussing the idea.

Conference Proceedings Directly Related to This Thesis

[5] **M. Malekiha**, and D.V. Plant,"Complexity reduction of dispersion mitigation based on sub-band partitioning," *Photonics North*, Paper F71S, 2016.
I conceived the idea, performed the simulation, and wrote the paper. The co-authors contributed in editing the paper and discussing the idea.
[6] **M. Malekiha**, and D.V. Plant,"Adaptive quantization of perturbation coefficients for nonlinearity compensation," *Photonics North*, Paper J9K8, 2016.
I conceived the idea, performed the simulation and experiment, and wrote the paper. The co-authors contributed in editing the paper and discussing the idea.

Journal Articles Not Directly Related to This Thesis

[7] X. Xu, Q. Zhuge, B. Châtelain, M. Chagnon, M. Morsy-Osman, **M. Malekiha**, M. Qiu, Y. Gao, W. Wang, and D.V. Plant, "Experimental investigation on the nonlinear tolerance of root M-shaped pulse in spectrally efficient coherent transmissions," *Optics Express*, vol. 23, no. 2, pp. 31966-31982, 2015.

[8] L. Xiaojun, S. Kumar, J. Shao, **M. Malekiha**, and D.V. Plant. "Digital compensation of cross-phase modulation distortions using perturbation technique for dispersion-managed fiber-optic systems," *Optics Express*, vol. 22, no. 17, pp. 20634-20645, 2014.

[9] A. Rhys, M. Spasojevic, M. Chagnon, **M. Malekiha**, J. Li, D.V. Plant, and L.R. Chen. "Wavelength conversion of 28 Gbaud 16-QAM signals based on four-wave mixing in a silicon nanowire," *Optics Express*, vol. 22, no. 4, pp. 4083-4090, 2014.

[10] S.A. Nezamalhosseini, L.R. Chen, Q. Zhuge, **M. Malekiha**, F. Marvasti, and D.V. Plant. "Theoretical and experimental investigation of direct detection optical OFDM transmission using beat interference cancellation receiver," *Optics Express*, vol. 21, no. 13, pp. 15237-15246, 2013.

[11] **M. Malekiha**, D. Yang, and S. Kumar, "Comparison of optical back propagation schemes for fiber-optic communications," *Optical Fiber Technology*, vol. 19, no. 1, pp. 4-9, 2013.

Conference Proceedings Not Directly Related to This Thesis

[12] R. Adams, M. Spasojevic, M. Chagnon, **M. Malekiha**, J. Li, D.V. Plant, and L.R. Chen, "Four Wave Mixing Based Wavelength Conversion and Multicasting of 16QAM Signals in a Silicon Nanowire," *IEEE Photonics Conference*, Post-deadline Paper PGS, 2013.

[13] S.A. Nezamalhosseini, L.R. Chen, Q. Zhuge, **M. Malekiha**, F. Marvasti and D.V. Plant, "A novel receiver for spectrally efficient direct detection optical OFDM," *IEEE Photonics Conference*, pp. 539-540, 2013.

Contents

List of Figures

List of Tables

List of Abbreviations

ADC	Analog-to-digital converter
ASE	Amplified spontaneous emission
ASIC	Application-specific integrated circuit
AWGN	Additive white Gaussian noise
BER	Bit error rate
BPF	Bandpass filter
BPSK	Binary phase-shift keying
CD	Chromatic dispersion
CO	Coherent optical
CP	Cyclic prefix
CPR	Carrier phase recovery
CW	Continuous wave
DAC	Digital-to-analog converter
DBP	Digital back-propagation
DD-LRD	decision-directed least radius distance
DD-LMS	decision-directed least mean square
DEPN	Dispersion-enhanced phase noise
DGD	Differential group delay

DP	Dual-polarization
DPSK	Differential phase-shift keying
DSP	Digital signal processing
DWDM	Dense wavelength-division multiplexing
ECL	External cavity laser
EDFA	Erbium-doped fiber amplifier
EEPN	Equalization-enhanced phase noise
ENOB	Effective number of bits
FEC	Forward error correction
FFT	Fast Fourier transform
FIR	Finite-duration impulse response
FO	Frequency offset
FPGA	Field-programmable gate array
FWM	Four-wave mixing
GN	Gaussian noise
GVD	Group velocity dispersion
ICI	Inter-carrier interference
IFFT	Inverse fast Fourier transform
IFWM	Intrachannel four-wave mixing
IM/DD	Intensity modulation / direction detection
ISI	Intersymbol interference
ISPM	Intrasymbol self-phase modulation
LMS	Least-mean square
LO	Local oscillator

MSB	Multi-sub-band
ML	Maximum-likelihood
MZM	Mach-Zehnder modulator
NLSE	Nonlinear Schrödinger equations
OSA	Optical spectrum analyzer
OFDM	Orthogonal frequency-divsion multiplexing
OSNR	Optical signal-to-noise ratio
PAPR	Peak-to-average power ratio
PC	Polarization controller
PD	Photodetector
PDM	Polarization-division multiplexing
PLL	Phase-locked loop
PDPR	Pilot-to-data power ratio
PMD	Polarization mode dispersion
PRBS	Pseudo random binary sequence
PS	Pilot subcarrier
QAM	Quadrature amplitude modulation
QPSK	Quadrature phase-shift keying
RDE	Radius directed equalization
RGI	Reduced-guard-interval
RF	Radio frequency
ROADM	Reconfigurable optical add-drop multiplexer
RRC	Root-raised-cosine
SC	Single-carrier

SMF	Single-mode fiber
SNR	Signal-to-noise ratio
SPM	Self-phase modulation
SSFM	Split-step Fourier method
SSMF	Standard single-mode fiber
SW	Switch
TDF	Time-domain filter
TF	Tunable filter
TS	Training symbol
VOA	Variable optical attenuator
WDM	Wavelength-division multiplexing
XPM	Cross-phase modulation

"Only a life lived for others is a life worthwhile."

Albert Einstein

Chapter 1

Introduction

THe past decade has been marked by a significant increase in Internet access media and an abundance of cloud-based storage, high-definition multimedia streaming, and services providing software and platforms. This has resulted in an unprecedented demand in the speed and volume of data transfers. As forecasted by Cisco (Fig. 1.1), this demand will definitely continue to grow and global data traffic will increase nearly 3-fold from 2014 to 2019. By the year 2019, 10.4 zettabytes of data will be transferred per year [1].

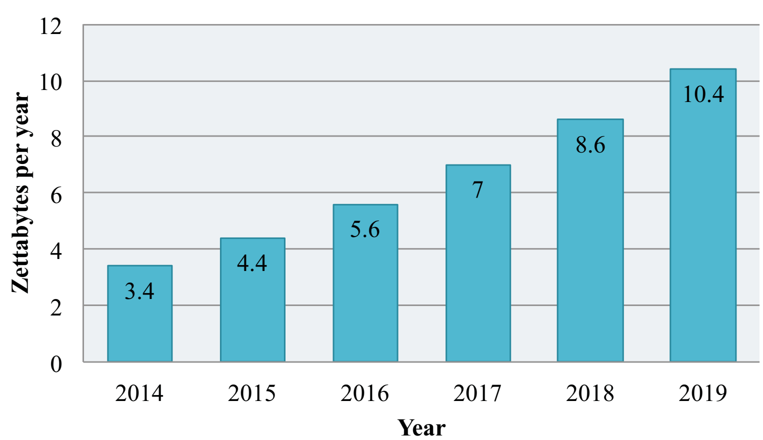

Fig. 1.1 Network traffic predictions for years 2014 to 2019 in zettabytes per year. Figure produced from data in [1].

This remarkable growth has put tremendous pressure on existing infrastructures to increase the transmission throughput by increasing the bandwidth and its efficient usage, extending the transmission reach, and higher standards for the signal quality [2]. These improvements are required at every tier of the technology, ranging from core to metro, and even access networks. In addition, the migration of transmission systems to higher capacity is expected to reduce the costs of installation, design, maintenance, and operation, altogether quantified by the "dollar per transmitted bit" measure. These two phenomena have greatly driven the deployment of underlying high capacity communication networks.

1.1 Overview

Prior to the introduction of fiber optical communications, microwave communication systems evolved considerably. In the late 1960s, microwave systems were able to operate at a bit rate of up to 200 Mb/s and close to their fundamental limit [3]. In the 1950s, it was realized that optical waves could increase the system capacity by several orders of magnitude due to its much higher carrier frequency. However, it was not until the 1970s that optical fibre communication systems became possible due to the development of low-loss silica fibres and efficient double-heterojunction structure semiconductor lasers [4–6]. After the first successful field trial in Chicago in 1977, fiber optical communication systems were commercially deployed in 1980 [7] with the invention of the erbium-doped-fibre-amplifier (EDFA). The advent of the wavelength-division multiplexing (WDM) technique started a revolution that resulted in a doubling of the system's capacity every 6 months or so and led to lightwave systems operating at bit rates of 10 Tb/s by 2001 [3]. In the mid 2000s, the realization of coherent detection and advanced digital signal processing (DSP) techniques enabled by the emergence of high speed electronics allowed information to be encoded in all four available degrees of freedom, namely amplitude and phase of the electric field along with the two orthogonal polarizations [8–10]. This not only enabled pre- and/or post-compensation of the fibre transmission impairments using DSP algorithms but also allowed for the transmission of spectrally efficient advanced modulation formats with maximum power efficiency. Current fiber optic transmission systems design aims for large system capacity, high spectral efficiency, and long transmission reach. Table 1.1 summaries a few record breaking transmission experiments.

Table 1.1 A summary of a few record breaking hero experiments in the fifth generation fiber optical transmission systems. (PDM: polarization-division multiplexing; QPSK: quadrature phase-shift keying; QAM: quadrature amplitude modulation; OFDM: orthogonal frequency-division multiplexing)

Year	Ref.	Modulation Format	Baudrate [Gbaud]	Spectral Efficiency [b/s/Hz]	Capacity [Tb/s]	Reach [km]
2007	[11]	PDM QPSK	10	0.8	1.6	3200
2008	[12]	PDM QPSK	27.75	2	16.4	2550
2009	[13]	PDM 8QAM	19	4	32	580
2010	[14]	PDM 36QAM	10.7	8	64	320
2011	[15]	PDM 128QAM OFDM	N/A	11	101.7	165
2012	[16]	PDM 256QAM OFDM	N/A	11.15	0.23	800
2013	[17]	PDM QPSK	107	3.3	4.28	4800
2014	[18]	PDM 16QAM	32.4	5.4	49.3	9100
2015	[19]	PDM 64QAM	32.4	7.1	63.5	5380

1.2 Motivation

Fiber optical communications have been widely employed in submarine, terrestrial, metro and even access networks because of their wider bandwidth, longer transmission distance, and lower attenuation. Since the mid 2000s, coherent technologies along with DSP and strong forward error correction (FEC) coding techniques have substantially increased the capacity of fiber optic networks [20]. 100 Gb/s coherent optical transports have been commercialized and are being deployed globally since 2009 [21] and 1 Tb/s is expected to be standardized between 2015 and 2020 [22]. Nonetheless, industry and academia are still being challenged to satisfy future network traffic growth, and new technologies to further reduce the cost per bit are being intensively researched and explored. In addition to higher data rates and longer transmission distances, agility is crucial for the next generation fiber optic communication systems. Agility enables the impending software-defined optical networks to dynamically add, drop, and route the optical channels at any individual nodes in order to address the ever-changing and unpredictable Internet data traffic, and to save on unnecessary transponder costs associated with the optical-to-electrical (O/E) and electrical-to-optical (E/O) conversions [23–27]. In addition, smart software-defined transceivers can autonomously optimize the network resources [28, 29].

The objective of this thesis is to investigate and develop advanced technologies for next generation flexible coherent transceivers. In this work, a DSP algorithm to increase the transmission capacity and reach by compensation of fiber nonlinearity is proposed. Additionally, digitally generated multi-sub-band (MSB) data architecture is investigated as an alternative to conventional single-carrier (SC) systems. MSB systems reduce the cost of future optical networks by eliminating the need for a chromatic dispersion (CD) compensating equalizer, simpler parallelization, and efficient flexible optical transceiver implementation without having to re-design and install new transponders or transmission links.

1.3 Thesis Objective and Contribution

This section presents the motivations and original contributions of the work discussed in this thesis.

Multi-Sub-Band Data Architecture

Optical transmission systems can generally be categorized into single-carrier and multi-carrier systems. Current commercial coherent products adopt single-carrier systems due to its simpler transceiver design. In addition, digital-to-analog converters (DACs) are not necessary in single-carrier systems because the current 50 GHz grid is wide enough to contain the 100 Gb/s non-return-to-zero (NRZ) quadrature phase-shift keying (QPSK) signal. In multi-carrier systems, however, the transmitted data is divided into many lower rate parallel streams to be transmitted over multiple carrier frequencies. This leads to efficient parallelization of DSP tasks by deploying multiple independent sub-band processors running at a lower clock rate. However, most multi-carrier systems require both transmitter and receiver side DSP.

As the available bandwidth of a fiber becomes exhausted, spectral efficiency and pulse shaping at the transmitter becomes crucial for a fiber optic communication system. Moreover, optical network agility can efficiently and intelligently utilize network resources for higher spectral efficiency and lower costs. These two requirements have greatly driven the deployment of the transmitter-side DSP for single-carrier communication systems.

In this work, we propose a novel digitally generated sub-band multiplexed data architecture for chromatic dispersion mitigation. Currently, the high power usage and area requirements of a CD compensating equalizer in long-haul and metro line-card application-specific integrated circuits (ASICs) is one of the major obstacles for implementing advanced DSP techniques such as nonlinearity compensation. Using this approach, the transmitted signal bandwidth is divided into multiple narrow-bandwidth sub-bands, each operating at a lower baud rate. Within each sub-band, the CD frequency response can be approximated as a linear-phase band-pass filter, which can be considered as an analog time delay that does not require additional compensation. Therefore, the resulting receiver digital signal processing is simplified due to the removal of the CD compensating equalizer. Furthermore, flexible optical transceivers (with reconfigurable rates and modulation formats) may be efficiently realized using this filter-bank based digital sub-banding approach. For example, it allows flexible spectral occupancy by turning on and off certain sub-bands. Also, when operating with a fixed spectral occupancy, this allows changing the constellation size of all or a sub-set of the sub-bands in order to engineer the desired data throughput.

Adaptive Nonlinear Equalization

Fiber Kerr nonlinearities constitute a fundamental limit in high capacity long-haul optical transmission systems because they restrict the maximum optical launch power into the fiber, and thereby also limit the achievable optical signal-to-noise ratio (OSNR), transmission reach, and system capacity. Mitigation and compensation of fiber nonlinearities have been an active topic of research and will increase the capacity of a single fiber. Currently, most nonlinearity compensation algorithms require link information, such as transmission distance, dispersion, and other fiber parameters. However, these link information may not always be available in agile optical networks which may consist of links with various types of fibers and dispersion maps.

In this work, the conventional perturbation based nonlinearity compensation (PB-NLC) technique was optimized and a novel adaptive low-complexity nonlinear equalizer was proposed. In the optimized PB-NLC, the complexity was reduced by using a decision-directed least mean square (DD-LMS) algorithm for the optimization of the quantized perturbation coefficients at the receiver. Next, an all adaptive nonlinear equalizer was proposed. This novel technique does not require any prior calculation or detailed knowledge of the transmission system. For efficient implementation, the fiber nonlinearities were compensated independently after the equalization of the linear impairments. Therefore, this algorithm can be easily implemented in currently deployed transmission systems after the conventional linear DSP stack. The complexity of the proposed algorithm is lower than previously studied adaptive nonlinear equalizers by more than an order of magnitude. In addition, this novel algorithm takes advantage of common symmetries of the perturbation coefficients and avoids replication of

1.4 Thesis Structure

Chapter 1: Introduction

This chapter provided a brief introduction to high capacity coherent fiber optical transmission systems and the motivations behind the work presented in the thesis.

Chapter 2: Fundamentals of coherent optical transmissions

In this chapter, the basics of the linear and nonlinear impairments in an optical fiber channel and that are relevant to the work in this thesis is reviewed. Topics include fiber attenuation, amplified spontaneous emission (ASE) noise, chromatic dispersion, polarization mode dispersion (PMD) and fiber nonlinearity. Then, a generic architecture of coherent optical transmission systems and corresponding DSP algorithms for mitigating or compensation of these impairments is presented. Detailed explanations of the DSP algorithms implemented in our coherent transmission systems are also provided.

Chapter 3: Low Complexity Transceiver Based on Multi-Sub-Band Reduced-Guard-Interval OFDM

In this chapter, the concepts behind filter-bank based multi-sub-band communication and its application for chromatic dispersion mitigation is reviewed. The efficient implementation of such a system and experimentally obtained performance of the recently proposed multi-sub-band reduced guard interval OFDM (MSB-RGI-OFDM) technique is then presented. Finally, a comparison of the the MSB-RGI-OFDM performance against conventional single carrier modulation formats is performed. At the same total data rate, both systems have comparable performance and transmission reach, however, the proposed method allows for a significant reduction in computational complexity due to the removal of the CD pre/post compensating equalizer.

Chapter 4: Chromatic Dispersion Mitigation Based on Multi-Sub-Band Single-Carrier

In this chapter, the application of multi-sub-band (MSB) communication technique for CD mitigation in a single-carrier modulation format with high spectral efficiency is studied. The next-generation ultra-dense wavelength-division multiplexing (UD-WDM) and super channel communications typically require filters with very small roll-off factor to limit the linear cross-talk between neighboring channels. This results in high computational complexity. MSB technique offers efficient frequency domain parallelization and lower computational complexity due to the elimination of CD compensation from the receiver DSP. Finally, we experimentally demonstrate that filter-bank based multi-sub-band signaling offers longer transmission reach, better tolerance to nonlinearity, and simpler realization of flexible optical transceivers. This demonstrates the potential of multi-sub-banding for next-generation flexible data-rate adaptive and spectrally efficient high-speed communication systems.

Chapter 5: Perturbation-Based Adaptive Nonlinear Equalizer

In this chapter, the concept behind the perturbation-based fiber nonlinearity compensation (PB-NLC) technique is first explained. Afterwards, an optimized PB-NLC and a novel adaptive low-complexity nonlinear equalizer is proposed and experimentally demonstrated. The proposed equalizers operate at one sample per symbol and require only one computation step. In addition, it allows for the compensation of linear and nonlinear impairments independently, which permits a more efficient implementation and facilitates integration with conventional DSP approaches. Therefore, this algorithm can be easily implemented in currently deployed transmission systems following conventional linear DSP.

In contrast to previously proposed adaptive nonlinear equalization techniques, this novel algorithm identifies common symmetries between perturbation coefficients to avoid duplicate and unnecessary operations. In the optimized PB-NLC, to further reduce the complexity and simplify its implementation, a decision-directed least-mean-square (DD-LMS) algorithm for the optimization of quantized perturbation coefficients at the receiver is developed. Only a few adaptive filter coefficients is used by grouping multiple nonlinear terms and dedicating only one adaptive nonlinear filter coefficient to each group. Finally, the complexity of the proposed algorithm is shown to be lower than previously studied nonlinear equalizers by more than one order of magnitude. In comparison to conventional PB-NLC, this new nonlinear equalizer does not require prior calculation of perturbation coefficients, symmetric dispersion maps, or a large memory to store all possible perturbation coefficients for reconfigurable network scenarios. Experimentally, a transmission distance of 2818 km for a 32 Gbaud DP 16QAM signal was achieved.

Chapter 6: Conclusion

This chapter summarizes the key achievements of the work presented in this thesis. In addition, future research directions for this work are discussed.

Chapter 2

Fundamentals of Coherent Optical Transmissions

2.1 Introduction

Coherent transceivers were first introduced for fiber optic communications in the 1980s because of their ability to transmit longer distances without repeaters and because of their higher receiver sensitivity [30–33]. However, coherent detection was not commercialized until the advent of high speed electronics, particularly the digital-to-analog and analog-to-digital converters (DAC/ADC), which occurred in the mid 2000s [34–38]. Coherent detection offers improved receiver sensitivity which in turn allows for longer transmission distance. In addition, coherent detection enables transmission of spectrally-efficient polarization-division multiplexed (PDM) advanced modulation formats such as high-order QAM, orthogonal frequency-division multiplexing (OFDM) and other multidimensional modulation formats. Moreover, in coherent communication, the optical field is fully linearly mapped to the electrical field, which permits digital pulse shaping as well as the compensation or mitigation of linear and nonlinear optical fiber channel impairments. Finally, coherent detection is inherently frequency selective due to the use of a local oscillator, which enables colorless reception of any wavelength division multiplexing (WDM) channel using a single receiver. As a result, coherent detection and advanced digital signal processing (DSP) techniques have substantially increased the capacity of optical communication networks [20].

This chapter is devoted to the fundamental aspects of coherent optical transmission systems. The linear and nonlinear impairments of the optical fiber channel relevant to this thesis are first described. Generic coherent optical transmitter and receiver architectures are then presented. Finally, a detailed review of the DSP algorithms implemented in our systems to compensate fiber channel impairments is given.

2.2 Impairments in Fiber Channels

The propagation of a single polarization optical field in an optical fiber can be described by the nonlinear Schrödinger equations (NLSE) [39]:

$$\frac{\partial}{\partial z}u(t,z)+j\frac{\beta_2(z)}{2}\frac{\partial^2}{\partial t^2}u(t,z)=j\gamma(z)|u(t,z)|^2u(t,z)+\frac{1}{2}(g(z)-\alpha_L(z))u(t,z)+f_n(t,z). \quad (2.1)$$

where, $u(t,z)$ is the optical field as a function of the transmission distance and time (z and t, respectively). $\beta_2(z)$ is the group velocity dispersion, $\gamma(z)$ is the nonlinear coefficient, $g(z)$ is the gain coefficient of the optical amplifier, $\alpha_L(z)$ is the attenuation coefficient of the optical fiber, and f_n is the fluctuations induced by spontaneous emission and is responsible for the amplifier's noise. It should be noted that the third order dispersion is neglected in this NLSE since it is not a dominant factor in the presence of second order dispersion.

In this section, the impairments presented in Eq. (2.1) will be explained. In order to isolate to the impairments of relevance, the NLSE is first simplified.

2.2.1 Attenuation

Originating from the material absorption of silica and the Rayleigh scattering [39], the fiber attenuation leads to a reduction of the average signal power with increasing transmission distance. Considering only the attenuation in Eq. (2.1), the NLSE can be simplified to:

$$\frac{\partial u}{\partial z} = -\frac{1}{2}\alpha_L \cdot u. \tag{2.2}$$

The solution of this equation is:

$$u(z) = u(0)\exp(-\frac{1}{2}\alpha_L z). \tag{2.3}$$

Attenuation is typically expressed in units of decibel per length (e.g., dB/km). It can be converted to dB by using the following relationship:

$$\alpha_{dB} = -\frac{10}{z}\log_{10}\left[exp(-\alpha_L z)\right] = 4.343\,\alpha_L. \tag{2.4}$$

It should be noted that the attenuation is a function of wavelength. In long-haul optical transmission systems, the operating wavelength is usually chosen at the minimum attenuation region (0.16 dB/km at a wavelength of 1550 nm in silica fibers) [40]. Hence, the wavelengths used in the thesis are all around 1550 nm.

It should also be noted that the attenuation has an impact on the strength of the nonlinear effects in a fiber. As the signal power decreases exponentially when traveling down the fiber, the nonlinear effects also get weaker and weaker. Therefore, the nonlinear effects are the strongest at the outputs of the transmitter and each amplifier stage.

2.2.2 ASE Noise

Long-haul transmissions usually extend over thousands of kilometers and the fiber attenuation is compensated periodically at intervals of 60 km to 120 km using Erbium-doped fiber amplifiers. In the amplification process, spontaneous emission generates photons with random phase, direction and state of polarizationz, which perturbs both the amplitude and the phase of the signal. Since the spontaneous emission generated noise is additive [41] and has a flat frequency power spectrum, it can be modeled as an additive white Gaussian noise (AWGN). The term $f_n(z,t)$ in Eq. (2.1) comes from spontaneous emission and its power spectral density can be written as [3]:

$$\rho_{ASE} = NF \cdot h \cdot \nu \cdot (G-1)/2 \tag{2.5}$$

where, NF is the Erbium-doped fiber amplifier (EDFA) noise figure, h is Planck's constant, ν is the optical carrier frequency, and G is the gain of the amplifier. The total noise power can be obtained by summing up the noise over the entire amplifier bandwidth. Typically, an optical filter is placed after the amplifier to reduce the out-of-band noise power. Hence, the total power of the amplified spontaneous emission noise can be expressed as:

$$P_{ASE} = 2 \cdot \rho_{ASE} \cdot BW_{Amp} = NF \cdot h \cdot \nu \cdot (G-1) \cdot BW_{Amp} \tag{2.6}$$

where, BW_{Amp} is the effective bandwidth of an amplifier, and the factor of 2 represents the two orthogonal polarized modes supported by a single-mode fiber.

2.2.3 Chromatic Dispersion

Dispersion is the broadening of a light pulse in time as it propagates down the fiber. As a result, short pulses become longer, which leads to significant intersymbol interference (lSI) and therefore, severely degrades the performance. Single-mode fibers (SMFs) effectively eliminate inter-modal dispersion by limiting the number of modes to just one by the use of a small core diameter. However, pulse broadening still occurs in SMFs due to intra-modal dispersion. This originates from the frequency-dependent refractive index of a fiber and the frequency-dependent optical field distribution in the fiber. These two phenomena are respectively termed material and waveguide dispersion [3]. Therefore, by properly designing optical fibers, different chromatic dispersion values can be obtained. There are two equivalent parameters to quantify the chromatic dispersion: 1) group velocity dispersion (GVD) β_2 [s^2/m], and 2) dispersion parameter D [ps/(nm*km)]. The dispersion parameter is defined as the derivative of group velocity β_1 with respect to the the wavelength λ. With a dispersion coefficient of D, two signals with wavelength separation of $\Delta\lambda$ walk-off by a time of $D\Delta\lambda L$ after a distance of L. The relationship between D, β_1 and β_2 can be found as follows [3]:

$$D = \frac{d\beta_1}{d\lambda} = -\frac{2\pi c}{\lambda^2}\beta_2 \approx -\frac{\lambda}{c}\frac{d^2 n}{d\lambda^2} \tag{2.7}$$

where, c and λ are the speed of light in vacuum and the optical carrier wavelength, respectively. It can be seen that D has the opposite sign of β_2. If chromatic dispersion (CD) is the only impairment of interest here, the NLSE can be simplified to include only the term with the group velocity dispersion parameter β_2:

$$\frac{\partial}{\partial z}u(t,z) + j\frac{\beta_2(z)}{2}\frac{\partial^2}{\partial t^2}u(t,z) = 0. \tag{2.8}$$

This equation can be solved by using the Fourier transform method and the solution is given by:

$$u(t,z) = \frac{1}{2}\int_{-\infty}^{\infty} U(\omega,0)\exp\left(j\omega t - j\frac{\beta_2 z\omega^2}{2}\right)d\omega. \tag{2.9}$$

where, ω is the angular frequency and $U(\omega,0)$ is the Fourier transform of the input optical field. Equation (2.9) can be interpreted in the frequency domain as:

$$U(\omega,z) = U(\omega,z)H_{CD}(\omega,z) \tag{2.10}$$

where,

$$H_{CD}(\omega,z) = \exp(j\frac{\beta_2 z\omega^2}{2})d\omega. \tag{2.11}$$

It can be seen that the transfer function of CD is an all-pass filter with a quadratic phase response and that the phase of each spectral component within a pulse is affected differently. In the time domain, this leads to pulse broadening and when a sequence of pulses are transmitted, the broadening results in overlapping pulses leading to inter-symbol interference (ISI).

Another way to interpret Eq. (2.11) is that different spectral components in the same pulse travel at different speeds depending on the sign of β_2 [39]. If $\beta_2 < 0$ (or $D > 0$), it is said that the optical signal exhibits normal dispersion. In the normal dispersion regime, high-frequency components of optical signal travel slower than low-frequency components. On the contrary, when $\beta_2 > 0$ (or $D > 0$), there is anomalous dispersion. In the anomalous dispersion regime, high-frequency components of optical signal travel faster than low-frequency components. It should be noted that in a standard single-mode fiber, the wavelengths around 1550 nm fall into the anomalous dispersion regime. Since the work in this thesis is around the telecom wavelength of 1550 nm, the anomalous regime is of the most interest.

The interaction between dispersion and nonlinearity is an important issue in lightwave system design. On one hand, within the same optical channel, different spectral components of neighboring pulses may interact with each other due to the pulse broadening and lead to intra-channel nonlinearity effects [42]. On the other hand, in WDM systems, the inter-channel nonlinearity interaction may occur when the pulse in the fast moving channels walks through the pulse in the slow moving channels.

Currently, CD equalizer's high power and area requirements in next generation long-haul and metro (400 Gb/s and 1 Tb/s) line-card application-specific integrated circuitries (ASICs) [43, 44] is one of the major obstacles for implementing advanced DSP techniques such as nonlinearity compensation. This is the motivation behind the work of this thesis, which proposes a novel low complexity DSP technique for CD mitigation.

2.2.4 Polarization Mode Dispersion

Single-mode optical fiber supports two orthogonal polarization modes. Ideally, the core of an optical fiber is perfectly circular, and therefore has the same index of refraction for both polarization states. However, mechanical and thermal stresses introduced during manufacturing breaks the symmetries in the fiber core geometry. This asymmetry introduces small differences in the index of refraction of the two polarization states, a property called birefringence [3]. As a result, the state of polarization (SOP) of the transmitted signal randomly changes inside an optical fiber. Polarization mode dispersion (PMD) refers to the optical pulse broadening that occurs due to the polarization dependent refractive index. The birefringence results in a periodic power exchange between the two modes. The period is known as the beat length and is given by:

$$L_B = \frac{\lambda}{|n_x - n_y|} \tag{2.12}$$

where, n_x and n_y denote the indices of the orthogonally polarized modes.

Unless a linearly polarized light is polarized along one of the principle axes, in which case it will remain linearly polarized during the transmission, the state of polarization of the light will periodically change from linear to elliptical and then back to linear over the length L_B.

Birefringence causes one polarization mode to travel faster than the other, resulting in a difference in the propagation time called the differential group delay (DGD). For a signal propagating in a fiber with constant birefringence, the DGD at a distance of L can be calculated by [39]:

$$\Delta\tau = \left|\frac{L}{v_{g,x}} - \frac{L}{v_{g,y}}\right| = |\beta_{1,x} - \beta_{1,y}| = L\Delta\beta_1 \tag{2.13}$$

where, x and y denote the two principle SOPs, v_g is the group velocity, and $\beta_1 = 1/v_g$.

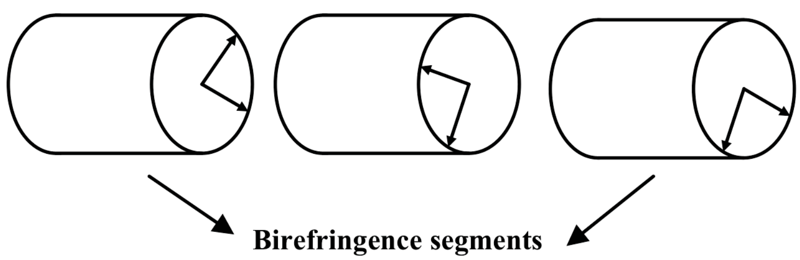

Fig. 2.1 Illustration of PMD modelling in a fiber.

In reality, the birefringence varies randomly with time and along the fiber. Therefore, the SOPs change randomly during the propagation. One way to model the PMD in conventional fibers is to divide the fiber into a large number of sections [45]. The DGD and the SOPs remain constant within each segment but change randomly from one segment to another segment, as shown in Fig. 2.1.

The transfer function of PMD in each birefringence segments can be characterized using the Jones matrix formalism as [46]:

$$H_i(\omega) = R_i^{-1} D_i(\omega) R_i \tag{2.14}$$

where, the following diagonal matrix

$$D_i(\omega) = \begin{bmatrix} e^{j\omega\tau_i/2} & 0 \\ 0 & e^{-j\omega\tau_i/2} \end{bmatrix} \tag{2.15}$$

characterizes the DGD τ between the principle SOPs, and the following rotation matrix

$$R_i = \begin{bmatrix} \cos(\theta_i) & \sin(\theta_i) \\ \sin(\theta_i) & \cos(\theta_i) \end{bmatrix} \tag{2.16}$$

characterizes the rotation from current SOPs to the principle SOPs with a rotation angle θ. The transfer function of PMD in the entire fiber length can be obtained by multiplying the individual transfer function of PMD in each birefringence segment:

$$H(\omega) = \prod_{i=1}^{N} H_i(\omega) \tag{2.17}$$

Since PMD is a random process, its effect on pulse broadening is characterized by the root-mean-square value of the DGD. It was shown that the DGD follows a Maxwellian distribution with the mean DGD growing as the square root of the fiber length and calculated by [47]. The mean DGD is typically in the range of 0.01-10 ps/(km)$^{1/2}$. For direct-detection systems, the random SOPs are not an issue as the photodiodes can only detect power and are insensitive to the SOPs. However, the PMD induced pulse broadening may introduce ISI and could become a limiting factor. For coherent systems, the polarization state must be recovered at the receiver, especially for long-haul high bit rate systems on legacy links.

2.2.5 Fiber Nonlinearity

Fiber nonlinearities are considered to be the main factor limiting the fiber channel capacity [48]. The response of any dielectric to light becomes nonlinear for intense electromagnetic fields, and optical fibers are no exception. For the long-haul fiber optic transmission system and WDM systems, to combat accumulated noise added by the amplifier chain along the transmission link, the launch power must be increased to keep the signal-to-noise ratio (SNR) high enough for the error-free detection at receiver. As the launch power increases, the nonlinearity of the fiber becomes significant and leads to a severe degradation in performance. There are two sources for the fiber nonlinear effects. One source is the fact that the fiber refractive index is a function of light intensity. The origin of this nonlinear response is related to anharmonic motion of bound electrons under the influence of an applied field. This phenomenon is called the Kerr effect. The second source is the non-elastic scattering of photons in fibers, which results in stimulated Raman and stimulated Brillouin scattering phenomena. As the power thresholds for stimulated inelastic scattering are normally much higher than the practical launch power used in optical transmission systems, they are usually not a major limiting factor [3]. Hence, the work presented in this thesis mainly considers the Kerr nonlinearity. The dependence of refractive index on the light intensity can be written as [39]:

$$n(\omega, u(z,t)) = n_0(\omega) + n_2|u(z,t)|^2 \tag{2.18}$$

where, n_0 is the linear part of the refractive index, n_2 is the nonlinear index coefficient. Fiber Kerr nonlinearity distorts the signal by imposing a pattern dependent nonlinear phase shift to the signal.

As mentioned in the previous section, CD and attenuation also have an impact on the fiber nonlinearity. Therefore, the simplified NLSE should include the terms associated with CD and attenuation, as well as the nonlinear effect. This is expressed as:

$$\frac{\partial}{\partial z}u(t,z) + j\frac{\beta_2(z)}{2}\frac{\partial^2}{\partial t^2}u(t,z) + \frac{\alpha}{2}u(t,z) = j\gamma|u(t,z)|^2 u(t,z). \tag{2.19}$$

where, the nonlinear coefficient γ is related to the nonlinear-index coefficient n_2 as:

$$\gamma(\omega) = \frac{n_2\omega}{cA_{eff}} \tag{2.20}$$

where, A_{eff} is the effective mode area. It should be noted that $u(t,z)$ in Eq. (2.19) contains all the optical field present in the fiber. For example, in the case that $u(t,z)$ is an aggregate of three individual WDM channels u_1, u_2 and u_3, it can be written as $u = u_1 + u_2 + u_3$. Therefore, Eq. (2.19) can be separated into three coupled equations, one for each channel. For instance, the equation describing the evolution of u_2 is given by [49]

$$\frac{\partial u_2}{\partial z} + j\frac{\beta_2}{2}\frac{\partial^2 u_2}{\partial t^2} + \frac{\alpha_L}{2}u_2 = \underbrace{j\gamma|u_2|^2 u_2}_{\text{SPM}} + \underbrace{2j\gamma(|u_1|^2 + |u_3|^2)u_2}_{\text{XPM}} + \underbrace{2j\gamma u_1 u_3 u_2^*}_{\text{FWM}} \tag{2.21}$$

where, the three terms on the right hand side represent self-phase modulation (SPM), cross-phase modulation (XPM) and four-wave mixing (FWM) nonlinearity effects. SPM refers to the self-induced power-dependent phase shift experienced by an optical field during its propagation in the optical fiber and it is responsible for the spectral broadening of the optical pulses. XPM is the nonlinear phase shift due to optical pulses from other channels or from other states of polarization. The XPM effects are quite important for WDM lightwave systems since the phase of each optical channel is affected by both the average power and the bit pattern of all other channels. FWM stems from the refractive index modulated by the power profile of at least three optical channels and FWM leads to new waves at new frequencies from the beating of three different channels.

Equation (2.19) does not generally have analytical solutions unless the fiber dispersion can be neglected. Under such an assumption, the NLSE can be written as:

$$\frac{\partial}{\partial z}u(t,z) + \frac{\alpha}{2}u(t,z) = j\gamma|u(t,z)|^2 u(t,z). \tag{2.22}$$

Its solution for the SPM effect at a transmission distance of L is:

$$u(t,L) = u(t,0)\exp(-\alpha L/2)\exp(j\phi_{SPM}(t,L)) \tag{2.23}$$

where, the SPM induced phase shift is expressed as:

$$\phi_{SPM}(t,L) = \gamma|u(t,0)|^2 L_{eff} \tag{2.24}$$

where, L_{eff} is the effective length defined as:

$$L_{eff} = \frac{1-\exp(-\alpha L)}{\alpha} \tag{2.25}$$

As can be seen, the SPM effect applies a pattern dependent phase shift on the signal in the time domain.

In WDM systems, the solution for the XPM effect has the same form as Eq. (2.23) and the XPM induced phase shift on the channel $n$is given by:

$$\phi_{XPM}(t, L) = 2\gamma \sum_{i=,i\neq n}^{N} |u_n(t, 0)|^2 L_{eff} \tag{2.26}$$

where, N is the total number of the co-propagating channels. The second term is the pattern dependent nonlinear interference from the neighboring channels. It can be seen from Eq. (2.26), that the XPM induced phase shift is twice that of SPM when the optical power of all the channels are equal. XPM causes asymmetric spectral broadening of optical pulses, timing jitter and amplitude distortion in the time domain. Nonetheless, in the presence of chromatic dispersion, the walk-off effect between channels reduce the efficiency of the XPM. Hence, the channel suffers XPM mostly from its close neighboring channels.

The four wave mixing is another nonlinear effect that generates new frequency components. For WDM systems, with carrier frequencies of f_i, f_j and f_k, the signal at a new frequency $f_h = f_i + f_j - f_k$ can be generated by FWM, provided that the phase matching condition $\beta_{ijk} = \beta_i + \beta_j - \beta_k$ is satisfied. Here, β is the propagation constant. This leads to a serious performance degradation when the newly generated frequency components fall into other WDM channels.

In single-carrier systems, CD induced broadening results in the nonlinear mixing of overlapped optical pulses in neighboring time slots and intra-channel nonlinear effects, which is one of the dominant penalties for high bit rate (above 40 Gb/s) fiber optic systems [42]. As mentioned in the previous section, in the anomalous dispersion regime, the higher spectral components of an optical pulse travel faster than the lower spectral components. As a result, the lower spectral components of the leading pulse interact with the higher spectral components of trailing pulse, causing intra-channel four wave mixing (IFWM). The difference between FWM and IFWM is that echo pulses appear in time domain instead of in frequency domain.

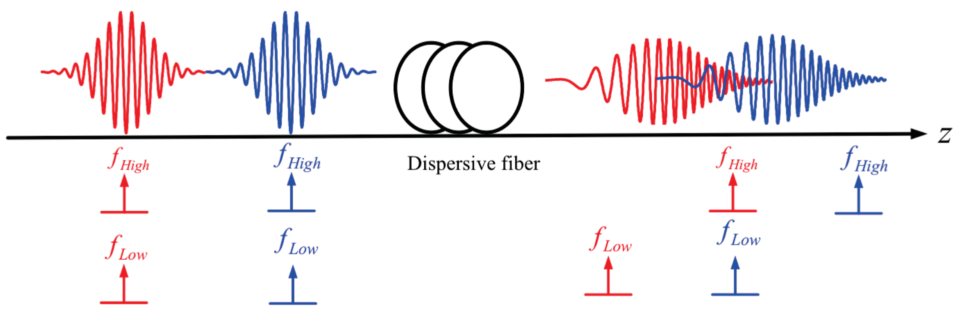

Fig. 2.2 Demonstration of the IFWM generation.

As far as transmission on fiber is concerned, the non-linear effects are nearly always undesirable. After attenuation and dispersion, they provide the next fundamental limitation on optical transmission [48, 50]. Specifically, they limit the maximum launch power into the fiber and thereby the achievable optical signal-to-noise ratio (OSNR). Kerr nonlinearities reduce the maximum transmission reach and system capacity. Following recent advances in high-speed digital signal processing technology, along with global adoption of coherent detection techniques, various intra-channel fiber nonlinearity compensation algorithms have been proposed. For instance, digital back-propagation (DBP) is an effective nonlinear compensation (NLC) technique, which has received considerable attention [51–57]. DBP normally requires multiple computation steps for each fiber span and at least two samples per symbol. This leads to high complexity [54]. Consequently, its application is limited to the transmission systems using offline signal processing. Alternatively, the perturbation-based nonlinear compensation (PB-NLC) technique compensates the accumulated nonlinearities with only one computation step and can be implemented with one sample per symbol [58–60]. However, practical implementation of this technique is limited due to the excessively large number of perturbation terms. This is especially true in dispersion-unmanaged links where numerous perturbation terms have to be considered due to the long dispersion induced delay spread of the pulses. Finally, both DBP and PB-NLC require the knowledge of the transmission links, such as transmission distance, dispersion and nonlinearity parameters, which are not always available in meshed optical networks. Therefore, it is desired to have a low computational cost adaptive nonlinearity mitigation/compensation scheme. This is the motivation for us to propose a novel nonlinear equalizer based on the first-order perturbation model with quantized perturbation coefficients.

2.2.6 Laser Phase Noise

Laser phase noise (PN) is another impairment in coherent optical communication system and is caused by spontaneous emission. PN broadens linewidth of the laser output and applies phase shift $\phi_{Tx}(t)$ and $\phi_{Rx}(t)$ from the transmit laser and the local oscillator (LO) laser to the optical signal, respectively. The evolution of the laser phase noise can be modelled as a Wiener process [61]:

$$\phi(t) = \int_0^t n(\nu) d\nu \tag{2.27}$$

where, $n(\nu)$ is a Gaussian variable. Laser phase noise is not an issue for non-coherent systems, since they either utilize no phase information or detect the phase difference between adjacent symbols where the laser phase noise is quasi-static. However, in coherent detection, the optical signal is linearly mapped to the electrical domain and the detected signal $r(t)$ becomes:

$$r(t) = s(t)e^{j[\phi_{Tx}(t)+\phi_{Rx}(t)]} \tag{2.28}$$

where $s(t)$ is transmitted symbols. Therefore, in single-carrier systems, for different symbols there will be a phase shift. thus we will observe constellations with random phase shifts with respect to the original constellation and it is impossible to decode the received symbol unless the carrier phase is recovered. As a result, carrier phase recovery is an indispensable procedure for single carrier systems.

2.3 Coherent Optical Transmission Systems

A coherent receiver linearly down-converts the complex-valued optical signal to the electrical domain by using homodyne or heterodyne detection. Therefore, amplitude, phase and frequency of the optical carrier can all be utilized to carry the information. There are several advantage for coherent detection over direct detection. The linearly detected signal enables the post digital signal processing and optical channel impairment compensation in the electrical domain at the receiver. A generic schematic of a coherent optical transmission system illustrated in Fig. 2.3.

At the transmitter, the bits are first encoded for forward error correction (FEC), and then binary data are split into two sequences to be transmitted in the X and Y polarization. Within each polarization, the bit sequence is first encoded with forward error correction overhead. It should be noted that FEC coding and decoding was not implemented in our DSP code, but the associated overhead was considered [62]. The coded bits are mapped to complex symbols based on the modulation format used such as quadrature phase-shift keying (QPSK). For the early single-carrier coherent systems, the modulated multi-level electrical signals were directly used to drive the electrical-to-optical (E/O) in-phase and quadrature (IQ) modulator [55]. These days, transmitter-side DSP and digital-to-analog converters (DACs) have become an indispensable part of coherent communication. In order to achieve better spectral efficiency and enhance the system performance and capacity, the pulse shaping, CD and fiber nonlinearity can be compensated at the transmiter [63–68]. Finally, pulse shaped signal are quantized and fed to the DAC to generate analog waveforms for driving the dual polarization in-phase and quadrature IQ modulators [69]. In this thesis, the system structure presented in Fig. 2.3 is the main focus, where the modulated symbols are processed in the digital domain. A finite impulse response (FIR) filter is needed to generate the high spectral efficiency Nyquist single-carrier signals [56], while an inverse fast Fourier transform (IFFT) is required to generate OFDM signals [70].

All of the research works in this thesis are focused on dispersion-unmanaged links with erbium-doped fiber amplifiers only. It has been show that the removal of the bulky and lossy inline optical CD compensating fibers not only reduces cost but also improves performance. Although, Raman amplification can achieve a lower noise figure, it was rarely deployed in commercial systems due to its high pump power requirement [57]. The other components such as wavelength selective switches (WSS), reconfigurable optical add-drop multiplexers (ROADMs) and optical filters are omitted for simplicity.

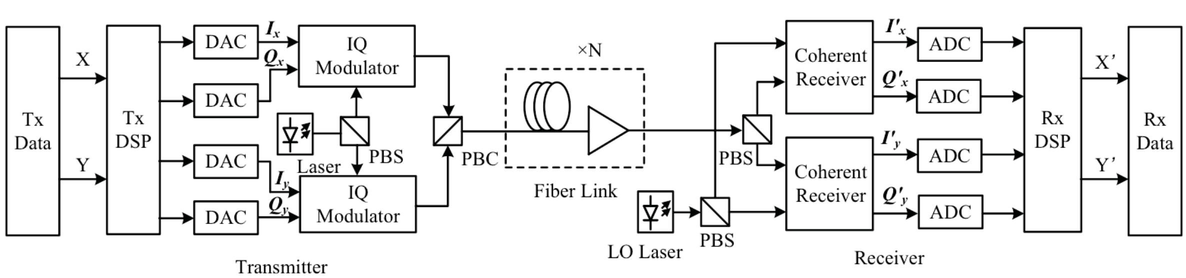

Fig. 2.3 Schematic of a coherent optical transmission system.

At the receiver, the optical signal is mixed with a local oscillator laser for the coherent optical-to-electrical (O/E) conversion. The DP signals are digitized using four analog-to-digital converters (ADCs) and then processed jointly. By doing so, the complex field of the received optical signal can be preserved, which allows for the digital compensation of optical channel impairments such as IQ mismatch, CD, frequency offset, timing jitter, polarization rotation, PMD and laser phase noise. This results in complicated receiver side DSP at those data rates. Finally, The processed signals are de-mapped back to bit sequences and after FEC decoding, the received binary data can be obtained.

2.3.1 Optical Coherent Receiver Structure

An optical coherent receiver is used to downconvert an optical signal to a baseband electrical signal. Figure 2.4 demonstrates schematic of a typical single polarization optical coherent receiver [71]. It comprises of a 90° optical hybrid and two balanced photodetectors (PDs) to improve the sensitivity.

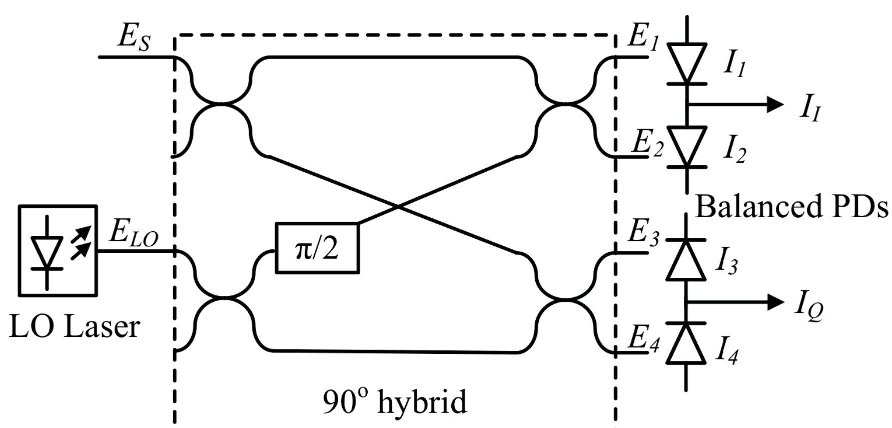

Fig. 2.4 Schematic of a single polarization coherent receiver.

The received optical signal after transmission in fiber can be expressed as:

$$E_{Rx}(t) = (I_s + Q_s)e^{j\omega t + \phi_{Tx}(t)} = s(t)e^{j\omega t + \phi_{Tx}(t)} \tag{2.29}$$

where, I_s and Q_s are the in-phase and quadrature components of the received signal,$s(t)$, respectively, ω and ϕ_{Tx} are the transmitter laser frequency and phase noise, respectively. In order to avoid large electrical bandwidth of the electronics and balanced PDs, the central frequency of the LO should be locked in the vicinity of ω. It should be noted that, there is a slight residual frequency offset ω_{FO}, between the LO and the transmitter laser frequency, if two independent free running laser sources are used. Hence, the LO complex envelope is given by:

$$E_{LO}(t) = \sqrt{P_{LO}} e^{j[(\omega + \omega_{FO})t + \phi_{LO}(t)]} \tag{2.30}$$

where, P_{LO} and ϕ_{LO} are the power and the phase noise of the LO signal, respectively. The output of the 90°optical hybrid after balanced detection is given by [71]:

$$I_I(t) = I_2 - I_1 = R \cdot \Re\{E_s E_{LO}\} \tag{2.31}$$

$$I_Q(t) = I_3 - I_4 = R \cdot \Im\{E_s E_{LO}\} \tag{2.32}$$

where, R is the responsivity of the PDs. It should be noted that the shot noise and thermal noise from PDs are omitted in Eqs. (2.31) and (2.32) since the major limiting noise source in long-haul transmissions is the ASE from the EDFA. Finally, by combining I_I and I_Q, the complex signal can be recovered as:

$$I = I_I - I_Q = R\sqrt{P_{LO}} s(t) e^{j[\phi_{Tx}(t) - \phi_{LO}(t) - \omega_{FO} t]} \tag{2.33}$$

where the local oscillator frequency offset, ω_{FO}, and signal phase noise, $\phi_{Tx}(t) - \phi_{LO}(t)$, are usually compensated in the receiver DSP.

2.3.2 Single-Carrier System

The research and development in optical fiber communication systems started in the first half of the 1970s. Such systems used employed intensity modulation/direct detection (IM/DD) or differential detection schemes, all of which modulate signals on one carrier [48]. Therefore, it is natural that single-carrier systems were the first candidate to be investigated when the technology migrated to coherent systems. For single-carrier systems, the transmitted baseband signal $S_{SC}(t)$ can be expressed as:

$$S_{SC}(t) = \sum_{i=-\infty}^{\infty} m_i h(t - iT) \tag{2.34}$$

where, m_i denotes the i$^{\text{th}}$ transmitted symbol, T is the symbol duration (the symbol rate equals $1/T$), and $h(t)$ represents the transmitted pulse shape. Fig. 2.5 (a) and (b) shows the digital domain building blocks of the single-carrier transmitter and receiver DSP, respectively.

The transmitter-side DSP is not necessary and simple electrical circuits can be used to generate the desired QAM formats with pulse shapes such as non-return-to-zero (NRZ) and return-to-zero (RZ). Digital pulse shaping filter, however, can be used to narrow the spectrum in order to achieve a higher spectral efficiency (SE) [56]. Furthermore, digital-to-analog converters and optical modulator can be digitally compensated by pre-emphasis techniques.

In optical communication, the root-raised-cosine (RRC) pulse shape is widely used for

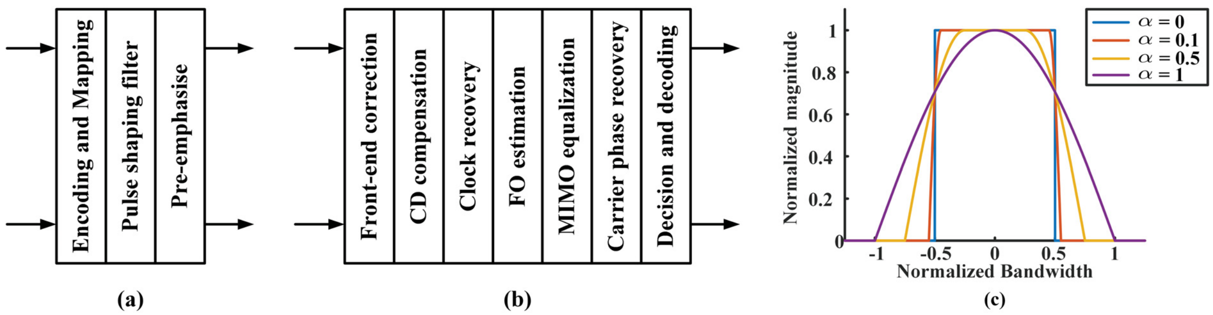

Fig. 2.5 The DSP of the single-carrier system at the (a) transmitter and (b) receiver, and (c) the spectra of raised cosine pulse shaping filter with various roll-off factors.

pulse shaping. The transfer function of RRC pulses can be expressed as:

$$H(f) = \begin{cases} \sqrt{T} & 0 \leqslant |f| \leqslant \frac{1-\alpha}{2T} \\ \sqrt{\frac{T}{2}\left(1+\cos\left[\frac{\pi T}{\alpha}\left(|f| - \frac{1-\alpha}{2T}\right)\right]\right)} & \frac{1-\alpha}{2T} \leqslant |f| \leqslant \frac{1+\alpha}{2T} \\ 0 & \frac{1+\alpha}{2T} \leqslant |f| \end{cases} \tag{2.35}$$

where, α is the roll-off factor and determines the signal bandwidth. Fig. 2.5(c) shows the spectrum of the RRC pulses for various roll-off factors.

It is observed that the RRC signal with $\alpha = 1$ has a bandwidth that is twice that of the RRC signal with $\alpha = 0$ (referred to as Nyquist pulse). In addition to an improved spectral efficiency, a narrower bandwidth signal also reduces the required sampling rates of DACs/ADCs at the expense of higher computational complexity and longer finite impulse response filter. The RRC signal, with a roll-off factor as small as 0.14 has been adopted in commercial products.

The receiver-side DSP includes:

1. **Front-end correction:** Ideally, the inphase and quadrature (IQ) components out of the 90° hybrid should be orthogonal to each other and sampled exactly the same

time at receiver. Therefore, to compensate for these imperfections, IQ-imbalance compensation schemes such as the well-known Gram–Schmidt orthogonalization [72] and the sampling skew compensation [73] should be applied.

2. **CD compensation:** In long-haul optical transmissions, the accumulated CD can be quite large. Although, CD can be compensated either in the time-domain using a FIR filter or in the frequency-domain [74, 75], an overlapped frequency-domain equalizer (OFDE) is preferred to accommodate such a large channel memory length [76]. In practical systems, the length of the fiber link might be unknown to the transceiver and blind CD estimation is typically implemented prior to the CD compensation equalizer [77, 78].

3. **Clock recovery:** Since the clocks in the transmitter and receiver are running independently, their sampling rates and phase deviate from each other. This deteriorates the signal quality. To obtain the correct sampling phase, many algorithms such as the Gardner algorithm [79], and the digital filter and square timing recovery [80] have been proposed.

4. **Frequency offset (FO) compensation:** The frequency offset is inevitable in coherent optical systems due to a difference in wavelengths of the free running transmitter and receiver lasers. FO rotates the received constellation ω_{FO} and can reach several GHz. FO can be estimated based on the periodogram of the 4th power of the symbols [81], and it can also be obtained by averaging the phase differences between neighboring symbols after removing their modulations [82]. It should be noted that since the FO is polarization independent, the FO in both polarizations can be compensated jointly for better estimation.

5. **Multiple-input and multiple-output (MIMO) equalization:** The optical channel with polarization diversity can be modeled as a 2×2 MIMO system. Therefore, an adaptive butterfly filter is employed to compensate for the ISI and polarization demultiplexing [8]. For the filter coefficients convergence, the training based and decision-directed least-mean square (LMS) algorithm can be used [83].

6. **Carrier phase recovery (CPR):** As mentioned previously, since coherently detected signals carry both amplitude and phase information, random phase shifts from the transmitter and LO laser should be removed before fully recovering the received symbols. Well-established CPR algorithms including the Viterbi&Viterbi algorithm [84] and the digital phase-locked loop (DPLL) [85] should be employed.

2.3.3 CO-OFDM System

OFDM is a well-known transmission technique and has become a standard for many communication systems [86]. In coherent optical OFDM, data is transmitted using multiple orthogonal subcarriers at lower data rate. The time domain transmitted OFDM signal $S_{OFDM}(t)$ can be expressed as [9]:

$$S_{OFDM}(t) = \sum_{i=-\infty}^{\infty} \sum_{K=1}^{N_c} c_{i,k} e^{j2\pi k \Delta f (t-iT_s)} . \Gamma(t - iT_s), \tag{2.36}$$

where, N_c is the number of subcarriers, $c_{i,k}$ is the mapped symbol transmitted on the k$^{\text{th}}$ subcarrier of the i$^{\text{th}}$ OFDM symbol, Δf is the subcarrier frequency spacing, and T_s is the symbol duration. $\Gamma(t)$ is defined as

$$\Gamma(t) = \begin{cases} 1 & -T_{CP} < t \leqslant T_s' \\ 0 & otherwise \end{cases} \tag{2.37}$$

where, T_{CP} and T_s' is the cyclic prefix (CP) length and observation length, respectively.

Fig. 2.6 (a) and (b) depicts the general DSP building blocks for the coherent optical OFDM (CO-OFDM) transmitter and receiver, respectively. At the transmitter, after FEC coding and symbol mapping, training symbols (TS) and pilot subcarriers (PS) are inserted for channel estimation and carrier recovery, respectively. The inverse fast Fourier transform (IFFT) is used for an efficient generation of OFDM signals. The spectrum of one OFDM symbol, which is composed of compactly packed sinc functions, is illustrated in Fig. 2.6(c). CP is added afterwards to prevent inter-symbol interference.

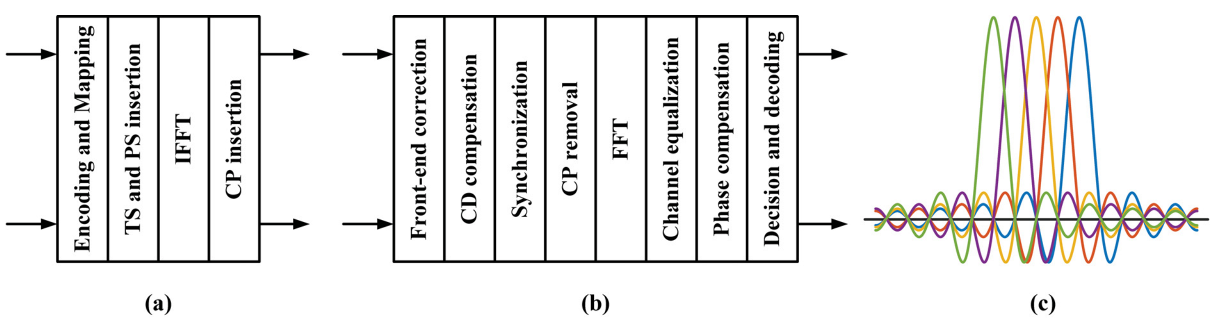

Fig. 2.6 The DSP of the CO-OFDM DSP at the (a) transmitter, (b) receiver and (c) illustration of OFDM spectrum.

The receiver-side DSP for OFDM systems includes:

1. **Front-end correction:** This is similar to the single carrier system.

2. **CD Compensation:** This block only exists in the reduced-guard interval(RGI) CO-

OFDM system to improve spectral efficiency by reducing the CP overhead [87,88]. In conventional OFDM systems, CD compensation is integrated in the OFDM channel equalization, which requires a very long CP to avoid the ISI [89].

3. **Frequency offset (FO) compensation:** FO offset is compensated using an RF pilot tone inserted at the center of the OFDM spectrum.

4. **Synchronization:** Many methods have been proposed to jointly synchronize the frame timing and carrier frequency by exploiting the periodic nature of the time-domain signal, for example, by sending training symbols with repeated parts or by calculating the auto-correlation between received samples and TS's if the CD and FO are already compensated [90, 91].

5. **Cyclic prefix removal:** After the cyclic prefix is removed, the packet data is sent to FFT.

6. **FFT:** FFT is used for sub-carrier demultiplexing.

7. **Channel equalization:** The optical fiber frequency response is quite flat. Therefore, zero-forcing equalization works very well and either training based time-domain [92] or frequency-domain [93] averaging can be used to refine the estimation.

8. **Phase compensation:** Since different subcarriers within each OFDM symbol are aligned in the time domain, they experience the same laser phase noise if the CD-induced walk-off is ignored. Therefore, pilot symbols are conventionally used to estimate the phase shift for the common phase error (CPE) compensation [94].

2.4 Conclusion

In this chapter, the background of optical communications was reviewed. Starting from the NLSE, the physical and mathematical basics of the fiber optic channel impairments, including fiber attenuation, ASE noise, CD, PMD, fiber nonlinearity and phase noise were presented. Then the architecture of coherent systems including optical modulation and coherent detection were discussed. Finally, the implementation of DSP and signal recovery, for both single carrier and OFDM systems, were explained.

Chapter 3

Low Complexity Multi-Sub-Band Transceiver for Reduced-Guard-Interval OFDM

ORTHOGONAL frequency-division multiplexing (OFDM) is a candidate for next generation optical transport systems. OFDM is a form of frequency-division multiplexing (FDM) in which multiple orthogonal subcarriers are used to transmit the data [95]. In coherent optical OFDM (CO-OFDM) systems, the serial data is divided into several parallel streams; one for each subcarrier. Each subcarrier is then independently modulated using a conventional modulation format at a relatively low symbol rate. The major advantage of OFDM over the single-carrier scheme is its ability to deal with severe channel impairments without complex equalization technique [96, 97]. This is due to the fact that an OFDM signal can be perceived as several low baud-rate narrowband signals rather than one high baud-rate wideband signal. To handle inter-symbol-interference (ISI) in dispersive fiber channel, cyclic prefix (CP) is inserted between consecutive OFDM symbols. Unfortunately, in conventional long-haul dispersion-uncompensated, a large CP overhead is required to endure the accumulated dispersion [98].

This chapter presents concepts and experimentally demonstrates a novel digital signal processing (DSP) structure for reduced-guard-interval CO-OFDM (RGI-CO-OFDM) systems. The concept introduced is based on digitally slicing optical channel bandwidth into multiple spectrally disjoint sub-bands, which are then processed in parallel. Each low bandwidth sub-band has a smaller delay-spread compared to a full-band signal. This enables compensation of chromatic dispersion (CD) using a simple time delay and a one-tap-per-symbol frequency domain equalizer with a very small CP overhead. In conventional RGI-CO-OFDM techniques, the system overhead is reduced by employing a full-band CD compensating equalizer prior to the OFDM signal processing. This enables a reduction of the guard-interval (i.e., CP) to accommodate most transmission effects with much shorter channel memory in the absence of CD-induced delay-spread [99]. Unfortunately, the computational complexity of the frequency domain equalizer (FDE) for CD compensation, which is traditionally implemented using an overlap-and-save method, becomes excessive for conventional long-haul links.

In terms of the DSP architecture, the proposed multi-sub-band (MSB) technique allows for a highly efficient parallelization of the DSP by deploying multiple independent processors running at a lower clock rate. It should be noted that this parallelization is performed in the frequency domain and allows for flexible optical receiver schemes. In this chapter, we test the system performance for different modulation formats (QPSK, 16QAM, and 32QAM) over various transmission distances and optical launch powers using only a 1.5% CP overhead. We also compare the proposed OFDM architecture performance against single carrier modulation formats. At the same total data rate, both systems have comparable performance and transmission reach, whereas the proposed method allows for a significant reduction of computational complexity due to removal of pre and post CD compensating equalizer.

3.1 Introduction

Digital signal processing has played an important role in supporting the recent expansion in the capacity of optical networks. Modern coherent optical communication systems has benefited from many powerful DSP techniques because of their access to the full optical field information at both transmitter and receiver.

In fiber optic communications, channel equalization can be efficiently realized by separately addressing slowly time-varying transmission effects, such as chromatic dispersion, from rapidly varying effects, such as phase noise (PN) and polarization-mode dispersion (PMD) [76]. At present, CD pre/post-compensation and forward error correction decoders are the main power consuming DSP blocks (more than 50%) of a conventional application-specific integrated circuits (ASIC) used in line cards [43, 44].

In order to reduce the DSP resources allocated to CD compensation, filter-bank (FB) based digital sub-banding has been proposed [100]. Using this approach, the transmitted signal bandwidth is divided into multiple sub-bands operating at lower baud rates. This bandwidth partitioning allows for compensation of CD on a per sub-band basis using elementary timing and equalization techniques, thus achieving higher DSP efficiency as well as a simplified parallelization. Moreover, lower symbol rates reduce hardware complexity. Since all sub-bands share the same optical transmission path, some of the channel properties are common to all the sub-bands. This fact allows for the utilization of more accurate and simplified impairment compensation techniques by jointly processing multiple sub-bands and taking advantage of information from other sub-bands. For example, we can estimate channel impairments for each sub-band individually and then by averaging the estimations, we can improve the performance. In addition, multi-sub-band signal processing can be applied in order to mitigate impairments such as linear and nonlinear crosstalk (i.e., inter-band interference (IBI) and inter-sub-band nonlinear effects) between adjacent transmitted sub-bands [101].

Finally, flexible smart optical transceivers (with reconfigurable rate and modulation format) can be efficiently realized using a FB based digital sub-banding approach. Specifically, the FB signal processing approach can be used to (i) change throughput by changing the constellation size of all or a subset of the sub-bands whilst maintaining a fixed frequency spectrum, or (ii) vary the number of sub-bands thus altering total spectral occupancy whilst maintaining a fixed reach [102]. The FB signal processing approach is also applicable in both long-haul and metro optical communication systems and may provide significant energy efficiency savings of 30%-50% in both the power consumption and the area of DSP ASICs [104].

Although each data sub-band may consist of single-carrier Quadrature amplitude modulation (QAM) or OFDM signal, CO-OFDM is an attractive 100 Gb/s modulation format [103], and is well suitable for multi-sub-band (MSB) FB-based multiplexing and detection [100]. To the best of our knowledge, all previously published papers presenting FB based multi-sub-band RGI-OFDM (MSB-RGI-OFDM) were purely based on simulations and the majority of fiber channel and modulation impairments (including Kerr nonlinearities, phase noise, local oscillator carrier frequency offset and optical front end imperfections) were omitted [100, 102, 104–106]. In the work presented here, digitally sub-banding RGI-OFDM is experimentally verified and its performance is compared against conventional coherent single carrier transmission.

3.2 Filter-Bank Based Communication Systems

In this section, the efficient implementation of the digital filter-bank based communications is reviewed. Figure 3.1 shows the block-diagram of a communication system employing filter-bank based MSB modulation and demodulation concepts [107, 108]. A set of M modulated symbols is fed in parallel into M discrete-time filters (with transfer functions $H_k(f)$, $k = 0, 1, \cdots, M$). This set of filters with common additive output represents a synthesis filter-bank. At the receiver, demodulation can be achieved by an analysis filter-bank (a set of M filters with common input). It is important to note that, at this point, each filter-bank output still runs at the high sampling rate of the analog-to-digital converter (ADC), which is M times faster than with sub-bands whose rate reduces to BW/M. Therefore, downsamplers may be placed (as described by arrow-down-K blocks) after each band-pass filter outputs. This will retain every K^{th} sample and discard the samples in between, thus reducing the sampling rate by a factor of K. Finally, the multiple outputs of the filter bank are taken at the decimator outputs [108].

In practice, filter bank systems are almost never directly implemented as shown in Fig. 3.1 (as band-pass filters). The reason is that, in this configuration, filters must operate at a rate that is M or K times faster than the symbol rate $1/T$. If the band-pass frequency responses are appropriately selected, it is possible to achieve quite efficient filter bank realizations. For example, in the critically sampled case (i.e., $K = M$), if the M receiver filters are selected as frequency-shifted versions of a single baseband filter $G(f)$, the so-called prototype filter, the system of Fig. 3.1 becomes equivalent to that shown in Fig. 3.2.

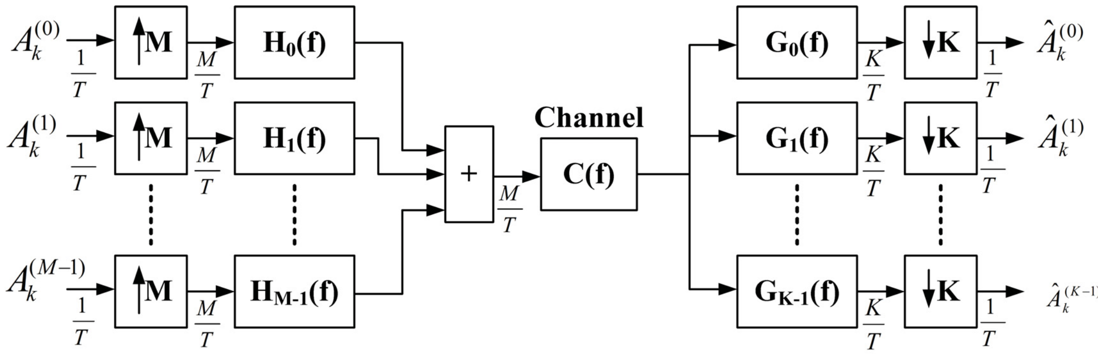

Fig. 3.1 A generic frequency-division multiplexed communication link based on a synthesis filter-bank in the transmitter and an analysis filter-bank in the receiver (notice that the usual combination of filter banks in DSP textbooks, for data compression purposes, has the opposite order of the analysis and synthesis filter banks).

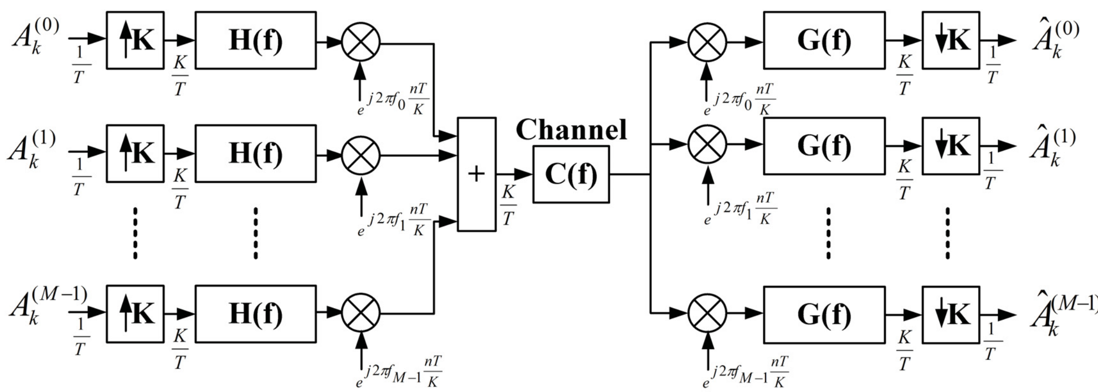

Fig. 3.2 Equivalent filter-bank representation of the frequency-division multiplexed communication link based on discrete-time up/down converters and baseband prototype filters.

The next step is to perform the discrete-time modulation with complex exponentials using an inverse discrete Fourier transform (IDFT) by applying linear time-invariant (LTI) filtering operations on the M branches (Fig. 3.3). This can be accomplished by inserting M filters corresponding to the so-called polyphase components of the prototype filter [108]. The i^{th} polyphase component of the prototype pulse shaping filter, where $i = 0, 1, , \cdots$, M-1 can be calculated as:

$$H^{(i)}[n] = H[nM + i] \tag{3.1}$$

The complexity of the resulting DFT and polyphase filters structure is very low [107].

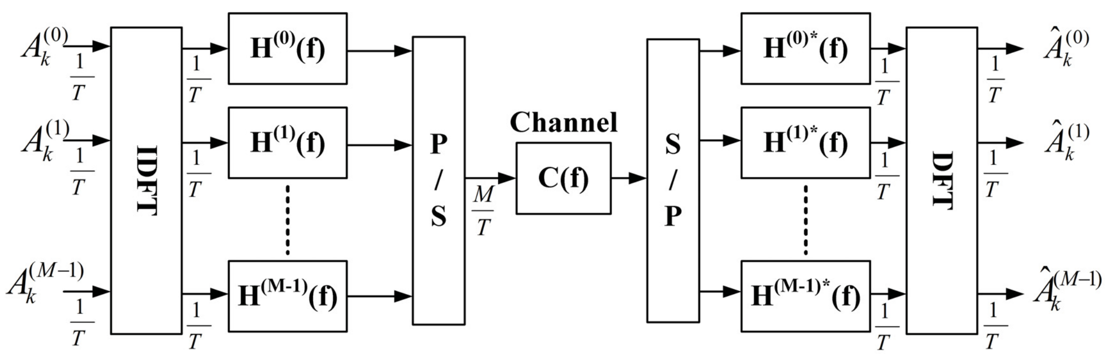

Fig. 3.3 Equivalent filter-bank representation of the frequency-division-multiplexed communication link based on M-points (I)DFT and M polyphase filters (corresponding to the uniform maximally decimated FBs). The receive filters were selected here to be matched filters relative to the transmit filters.

A mathematical description and design requirements of the DFT based polyphase filter structure is provided next. The transmit signal is an aggregate of the pulse-shaped and frequency-shifted sub-band signals, and is given by:

$$\begin{aligned} x(t) &= \sum_k \sum_{m=0}^{M-1} A^{(m)}[k] h[t - kT] e^{j2\pi(t-kT)f_k} \\ &= \sum_k \sum_{m=0}^{M-1} A^{(m)}[k] h_k[t - kT] \end{aligned} \tag{3.2}$$

where $h_k[t - kT]$ is defined as $h_k[t - kT] = h[t - kT]e^{j2\pi(t-kT)f_k}$, $A^{(m)}[k]$ and $1/T$ denotes transmitted symbol and sample rate, respectively. In an ideal channel, the transmitted signal can be reconstructed when:

$$\int_{-\infty}^{+\infty} h_k[t-mT]h_l[t-nT]dt = \delta_{kl}\delta_{mn}, \tag{3.3}$$

where, δ is the Kronecker delta function. A simple pulse shape which satisfies Eq. 3.3 is a rectangular pulse with time duration T. Other common pulse shapes are the raised-cosine and the square root-raised-cosine filters.

At time kT/M, the transmitted signal is given by:

$$x(k\frac{T}{M}) = \sum_{m=0}^{M-1}\sum_{n=-\infty}^{+\infty} A^{(m)}[n]h\left[(k-nM)\frac{T}{M}\right]e^{j2\pi mk/M}. \tag{3.4}$$

By changing the order of the summation and applying the change of variable $kT/M = lT + i(T/M)$, where $i = 0,\ 1,\ \cdots,\ M-1$, the output signal is given by:

$$x(lT + i\frac{T}{M}) = \sum_{n=-\infty}^{+\infty}\left(\sum_{m=0}^{M-1} A^{(m)}[nT]e^{j2\pi mi/M}\right)h[(l-n)T + i\frac{T}{M}]. \tag{3.5}$$

The inner summation in Eq. (3.5) is the IDFT of the sub-band symbols, and the term $h[(l-n)T + i\frac{T}{M}]$ is the i^{th} polyphase component of the transmitter pulse shaping filter. This suggests that the transmitter block diagram can be modified to perform the IDFT at the first step, followed by the pulse shaping filter on each output of the IDFT block, and then a serial-to-parallel conversion in order to transmit the symbols. The modified transmitter block diagram is shown in Fig. 3.3.

At the receiving side of the MSB system block diagram (Fig. 3.3), the signal for sub-band i is given by:

$$\hat{A}^{(i)}(nT) = \sum_{k=-\infty}^{+\infty} x(k\frac{T}{M})e^{j2\pi f_i kT/M}h[k\frac{T}{M} - nT] \tag{3.6}$$

Letting $kT/M = lT + i(T/M)$, where $i = 0, 1, \cdots, M-1$ which models polyphase sampling of the received signal, the sum in Eq. (3.7) can be broken down into two summations as follows:

$$\hat{A}^{(i)}(nT) = \sum_{m=0}^{M-1}\left(\sum_{n=-\infty}^{+\infty} x(lT + m\frac{T}{M})h[(n-l)T + m\frac{T}{M}]\right)e^{j2\pi mi/M}. \tag{3.7}$$

The preceding equation suggests modifying the receiver block diagram based on polyphase sampling as shown in Fig. 3.3, with polyphase samples filtered with the pulse shaping filters corresponding to different sub-bands, and then performing sub-band separation via the DFT block.

3.3 Underdecimated Filter Banks for Spectrally Efficient CO-OFDM Communication Systems

In CO-OFDM, the cyclic prefix is added (replicating a section of the OFDM symbol tail at the symbol head) in order to mitigate inter-symbol interference caused primarily by CD-induced delay-spread, denoted as $\Delta\tau_{CD}$. By introducing this overhead, within each OFDM frame, the channel linear convolution transforms into a cyclic-convolution as long as the channel memory does not exceed the length of the CP. Therefore, the CP length must be at least as long as the length of the CD-induced delay-spread, i.e.,

$$\Delta\tau_{CP} \geqslant \Delta\tau_{CD}. \tag{3.8}$$

As a consequence, a large accumulated CD translates into a large CP overhead, which reduces the transmission rate and spectral efficiency in long-haul and metro fiber optic networks. For example, for a 35 GHz channel transmitted over a $2,000$ km link of standard SMF, CP needs to be as long as 300 samples [104].

One possibility to reduce this CD-induced pulse broadening, and hence the required CP overhead, is to reduce the transmitted signal's bandwidth. However, reducing the bandwidth inevitably reduces the transmission bit rate. In order to retain the target high-speed bit rate, we propose parallel signaling over multiple narrowband sub-bands. Using this approach, the transmission scheme would consist of simultaneous transmission of multiple low-speed signals, each occupying different sub-bands. In fiber optic communication, CD can be modeled as a quadratic-phase all-pass (QP-AP) filter. Because our proposed transmission scheme breaks transmitted signals into multiple narrow-banded signals, this QP-AP filter can be approximated by the superposition of M different linear-phase band-pass filters. Since each band-pass filter has a different center frequency, the signal frequency components that fall within its pass-band propagate with different group velocities, and therefore CD-induced walk-off leads to successive time segregation of the individual frequency components. As a result, different sub-bands arrive at different times at the receiver, and each sub-band experiences minimal delay-spread internally due to its narrow bandwidth.

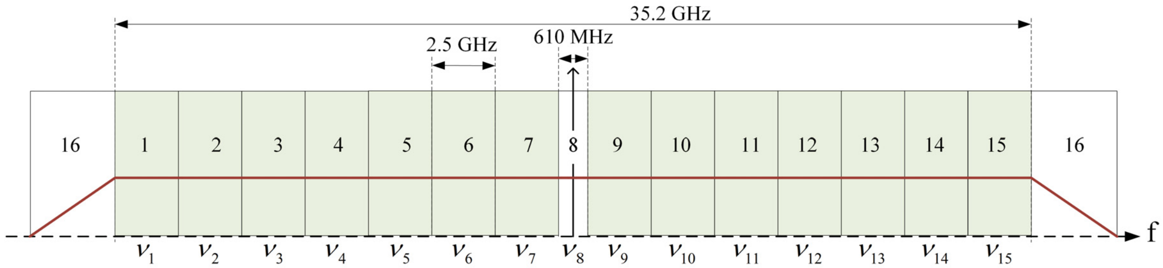

Fig. 3.4 Proposed digital multi-band data structure with an un-modulated (DC) RF pilot tone for carrier recovery: Each channel (assumed here 35.2 GHz) is digitally frequency-division de-multiplexed into M active sub-bands (here M=14). The extreme sub-band (partitioned into two wrapped-around halves) is dedicated for filtering the transition roll-off of DAC image-rejection filter, and the center sub-band is dedicated to the guard band for inserting a pilot tone.

Figure 3.4 illustrates the MSB-RGI-OFDM top-level data structure. Using the proposed scheme, the entire transmission bandwidth is divided into 16 sub-bands. Out of these 16 sub-bands, 14 sub-bands (SBs), each having identical bandwidths, are used for data. The remaining 2 auxiliary sub-bands have different bandwidths. The narrower of these two sub-bands is at the center of spectrum, and is used to transmit a pilot tone (PT) for carrier-recovery (CR) purposes. The outer and broader sub-band is used as a guard-band to support a larger roll-off transition band for the digital-to-analog converter (DAC) and ADC analog filters. As mentioned earlier, different sub-bands experience different time-offsets from the overall delay. These offsets, denoted as $\Delta\tau_i$, where $0 \leqslant i \leqslant 15$, are proportional to the central frequency ν_i of the pass-band of the i^{th} filter, the CD parameter β_2 and the transmission length L [106]:

$$\Delta\tau_i = -2\pi|\beta_2| \cdot L \cdot \nu_i \tag{3.9}$$

It should be noted that $\nu_{1\leqslant i\leqslant 7}$ are negative, resulting in positive $\Delta\tau_{1\leqslant i\leqslant 7}$ delays with respect to the transmitted data center frequency. Similarly, $\nu_{9\leqslant i\leqslant 15}$ leads to negative

$\Delta\tau_{9\leqslant i\leqslant 15}$ time shifts. This enables a very simple and accurate monitoring of the channel CD [109]. Once the timing per sub-channel is properly determined, small sub-band bandwidth significantly reduces the required CP overhead length as is shown in Fig. 3.5, which illustrates the required CP length for both conventional OFDM and MSB-RGI-OFDM.

(a) CO-OFDM (b) MSB-RGI-OFDM

Fig. 3.5 Comparison of required CP length for (a) conventional OFDM and (b) MSB-RGI-OFDM.

At the receiver, samples of the received optical field are filtered simultaneously using 15 digital band pass filters in parallel, where 14 filters are dedicated to the "data" sub-bands. An additional low-pass filter is used to filter out the PT for CR purposes. Next, the output of each filter is shifted by $[\Delta\tau_i]$ samples ($[\cdot]$ denotes the round to the nearest integer operation), decimated by a factor 8, followed by DFT-domain adaptive equalization, and then the constellation is sliced.

3.4 DFT Spread-OFDM for Sub-band Multiplexing

We used DFT Spread OFDM (DFTS-OFDM) transmitter for orthogonal sub-band multiplexing [110]. Figure 3.6 illustrates the DFTS-OFDM top-level structure. The benefits of this technique are narrowband frequency-flat bandwidth partitioning, flexible digital (de-)multiplexing with zero guard-bands and no inter-sub-band crosstalk [105]. Moreover, DFTS-OFDM mitigates peak-to-average power ratio (PAPR) and fiber nonlinear effects, which are substantial impairments afflicting conventional OFDM. The drawbacks of DFTS-OFDM is its increased susceptibility to phase noise and impairments due to carrier frequency offsets (CFO). Their mitigation is addressed in this work by the insertion of a pilot tone.

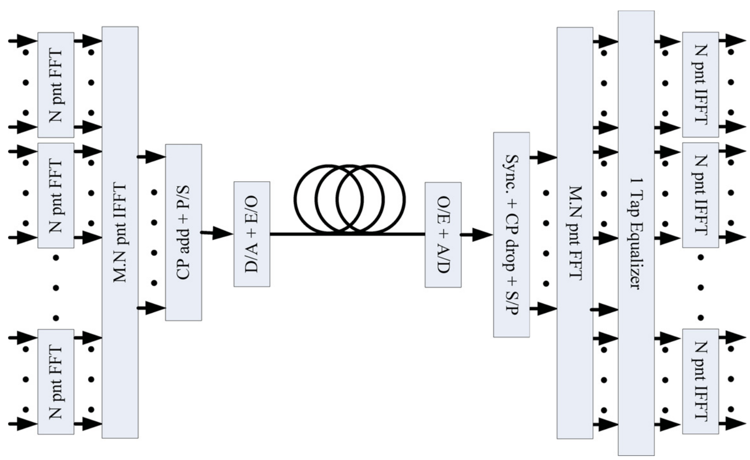

Fig. 3.6 Conventional DFTS-OFDM.

The DFT (de)spreading concept is based on introducing arrays of (IDFT) DFTs (after) before the main (DFT) IDFT in the OFDM (receiver) transmitter. Each DFT (de)spreading IDFT pair effectively defines a spectral sub-band, carrying a fraction of channel bandwidth. Moreover, upon placing the DFTS-OFDM transmitter and receiver back-to-back (as shown in Fig. 3.6), it is evident that the main inner IDFT cancels the DFT. This effectively brings each DFT spreading block back-to-back with its corresponding de-spreading IDFT and results in identity.

Figure 3.7 shows the transmitter structure of the MSB-RGI-OFDM used in this work. The encoding steps are as described next. First, data symbols are buffered into arrays of N symbols (in this case, N = 896). Then, each array is evenly divided into M sub-arrays (here, $M = 14$). This results in M sub-arrays, each having a length of N/M (64 for this case). Next, a N/M point fast Fourier transform (FFT) (64 points) is taken of each sub-array. The resulting 14 sub-arrays are combined into a new array of length 1024, where 16 subcarriers around DC are dedicated for a pilot tone, and 54 subcarriers on each side of the spectrum are set to zero to allow a larger roll-off transition for the analog DAC image-rejection filter. As per the conventional OFDM transmission scheme, each OFDM array undergoes a larger IFFT of length 1024, and a section of the "tail" (equal to CP length) of the obtained array is replicated at its "head". After the PT is digitally added, these arrays are un-buffered, quantized, converted to analog signals using a DAC, and then optically modulated.

As already mentioned, DFTS-OFDM is extremely sensitive to PN and CFO impairments; therefore, a PT was inserted at the DC sub-carrier for joint CFO compensation and CR. Both PT power, P_{pilot}, and data power, P_{signal}, contribute to total transmission power which is bounded due to fiber Ker nonlinearities. Therefore P_{pilot} is a design parameter and it has to be optimized. To characterize the performance, the well known measure called pilot-to-signal power ratio (PSR) was used. PSR is defined as:

$$PSR(\ dB) \ = \ 10log10\left(\frac{P_{pilot}}{P_{signal}}\right) \tag{3.10}$$

At a fixed total launch power, increasing P_{pilot} inevitably decreases P_{signal}, which in turn deteriorates the signal-to-noise ratio (SNR) at the receiver which leads to degraded performance. Therefore, there is a trade-off between SNR and performance of the PT based CR, which will be discussed in the next section.

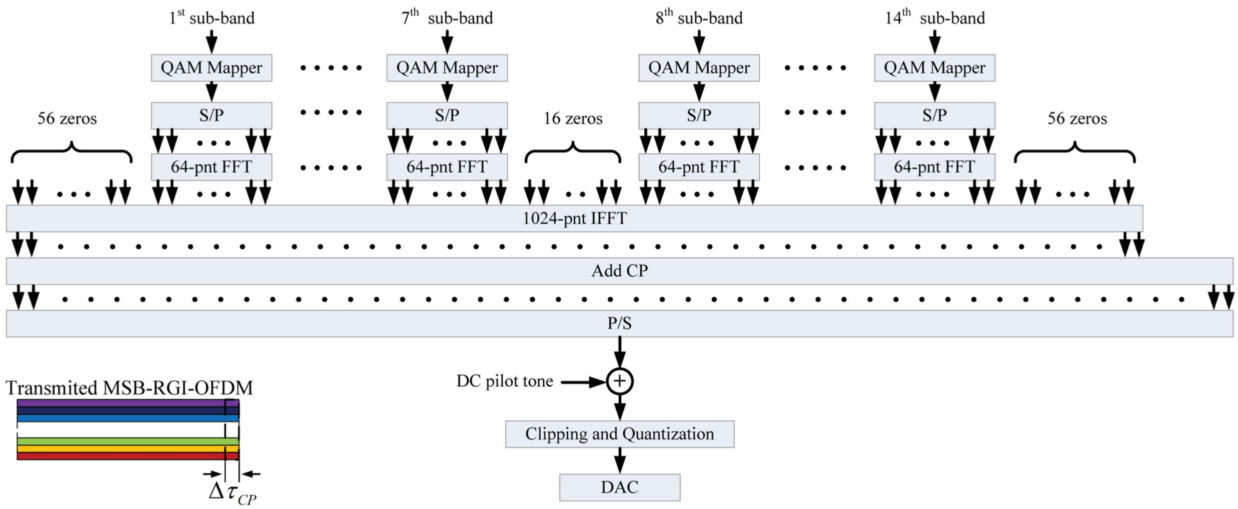

Fig. 3.7 MSB-RGI-OFDM Transmitter.

3.5 Receiver DSP Structure

At the receiver, for a more efficient implementation, we replaced the large FFT block used in a conventional DFTS-OFDM (shown in Fig. 3.6) with a filter-bank array, as depicted in Fig. 3.8. Each of the DFTS-OFDM sub-band receivers contains a de-spreading FFT. The filter-bank digitally extracts 2.5 GHz slices out of the 39.5 GHz bandwidth of the input signal over 14 parallel paths. The output of each filter is then down-sampled by a factor of 8, thus generating 14 twice-oversampled data streams (i.e., each sub-band is effectively sampled at a 5 GSa/s rate). The low sampling rate of the sub-bands significantly reduces the hardware complexity for the subsequent processing of these arrays. In addition, DSP algorithms function notably better in the narrow bandwidth environment. Indeed, optical OFDM receivers operated at relatively slow rates have been experimentally implemented and demonstrated [89,111]. However, the critical challenge that needs to be addressed is the design of an efficient implementation of a digital FB structure, which is capable of mutual and joint processing of samples obtained when utilizing both X and Y polarizations.

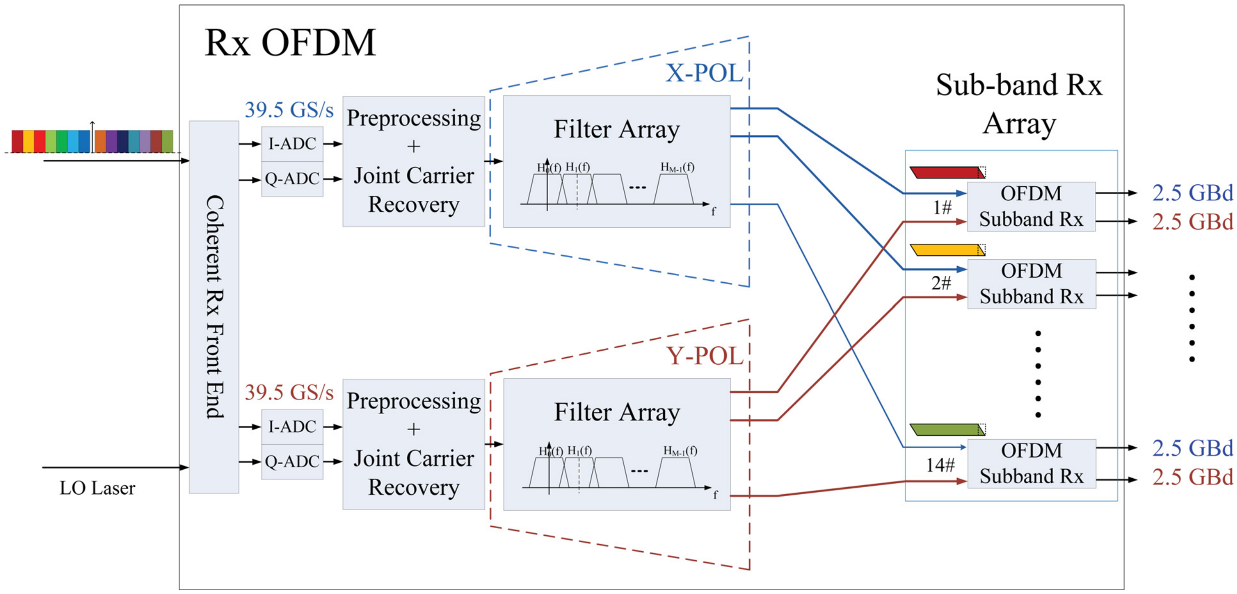

Fig. 3.8 filter-bank based MSB-RGI-OFDM Receiver.

Figure 3.9 presents a block diagram of a FB based receiver DSP tailored for MSB-RGI-OFDM transmission. The DSP code starts with optical front-end compensation, including the removal of DC, IQ imbalance compensation, and hybrid IQ orthogonalization using the Gram-Schmidt algorithm [109]. Next, the PT is filtered out and its phase is extracted under the assumption that the reference phase of the transmitted PT is known at the receiver and the extra phase shifts (due to laser PN and CFO) can be obtained and utilized for corrections of the received data. The PT is digitally filtered using an equiripple linear-phase low-pass filter (LPF). The bandwidth of this LPF has to be accurately determined, with the following trade-offs kept in mind. Since the PN, which is related to the transmitter laser line-width, broadens the spectrum of the PT, the LPF pass band has to be wide enough to capture and filter out this noise. On the other hand, the output of the LPF will be the PT in addition to some filtered amplified spontaneous emission (ASE) noise. An excessive LPF bandwidth will introduce (i) more ASE noise which will deteriorate the phase estimation, and (ii) will lead to crosstalk between the PT and the data sub-bands.

In this work, the optimal LPF bandwidth was empirically determined and its delay (which is inherent in any linear phase digital filter) was also considered.

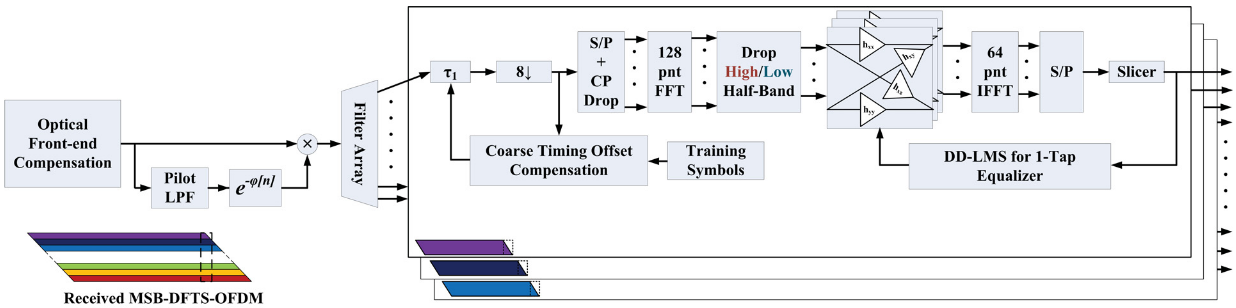

Fig. 3.9 Sub-band receiver processor for MSB-RGI-OFDM.

The key rationale for bandwidth partitioning is the transformation of the complex CD compensation task into elementary timing recovery performed independently per-sub-band. The quadratic phase profile that characterizes the CD impairment over the total bandwidth may be effectively approximated as linear phase segments over the narrow bandwidth of each sub-band [112]. Any linear phase filtering means a constant delay (which is equal to the slope of the phase in the frequency domain) [108]. As a result CD effect can be approximated by a constant group delay within each sub-band. Therefore, its compensation is possible by a regular timing recovery method, performed independently per sub-band. The coarse timing correction equal to integer sampling-interval time units may be corrected readily by a simple delay element or digital buffering of the received samples. However, delays equal to a fractional part of the sampling-interval as well as any other residual distortion and impairments may be corrected using conventional ISI equalization techniques. Since we opted for the OFDM dual-pol transmission structure in this work, the natural choice for mitigation of ISI and PMD impairments would be a 2×2 complex-butterfly DFT domain equalizer as indicated in Fig. 3.9. Similar to the conventional OFDM, the quality of ISI/PMD mitigation in our case is directly dependant on the CP length, which is significantly reduced due to the narrow bandwidth of each sub-band.

Furthermore, for a MSB-RGI-OFDM receiver, the timing recovery function is simplified relative to a full-band OFDM receiver. In conventional OFDM systems, the performance of delay and correlate (D&C) algorithms such as Schmidl–Cox are significantly degraded by the non-linear phase of the fiber CD frequency response. As a result D&C is not applicable for the full-band receivers without pre-compensation of dispersion. In our case, the frequency-flat-linear-phase channel response over each independent sub-band does not deteriorate timing recovery and yields improved D&C performance. Moreover, the complex parallelization of D&C algorithms is now simplified [112]. Therefore, the net result is more robust and simpler timing recovery.

As mentioned previously, the digitally sub-banded receivers do not require separate CD estimation, but there are additional advantages for per-sub-band optical channel equalization. Because channel frequency response is considerably flatter for each sub-band, this implies much smaller channel eigenvalue spread. Therefore, they allow much faster and more accurate convergence for their adaptive filter coefficients. This convergence speed-up will be manifested in every adaptive DSP algorithm. Consequently, rapid and accurate adaptive algorithms convergence means low data-aided overhead. Also, equalization-enhanced phase-noise (EEPN), i.e., the enhancement of local oscillator phase noise through the CD equalizer, is cut down by a factor of M and practically eliminated [106]. With the filter-bank method, as each sub-band is narrowband, its CD impulse response duration is M times shorter, therefore EEPN is reduced by a factor of M. In addition, IQ imbalance correction algorithms may be more effectively formulated in the filter-bank context. It will be seen that pairs of sub-bands (with center frequencies symmetric vs. the mid-band frequency) will be coupled in pairs in order to generate simple and rapidly converging IQ imbalance correction

3.6 Experimental Setup

Figure 3.10 shows the schematic diagram of the experimental setup. On the transmitter side, offline DSP fourteen 2-tuple independent pseudo-random bit sequences (PRBS) are mapped to QPSK/16QAM/32QAM symbols, followed by multi-sub-band OFDM multiplexing (outlined in Figs. 3.6 and 3.7) for each polarization. A Ciena WaveLogic 3 (WL3) transmitter card was employed, which contained four 39.5 GSa/s 6 bit DACs, a tunable frequency laser source, and a dual-polarization (DP) IQ modulator. The Tx laser was operated at 1554.94 nm. The electrical waveforms at the output of the DACs were applied to the IQ modulator to generate a true polarization multiplexed optical signal. The transmitter analog frequency response was compensated in the built-in DSP of the WL3. The DP QPSK/16QAM/32QAM MSB-RGI-OFDM optical signal is set to 23 dBm using a booster erbium-doped fiber amplifier (EDFA), and subsequently attenuated using a conventional variable optical attenuator (VOA) in order to get a desired optical launch power. The optical signal is then launched into a recirculating loop. The loop consists of four spans of 80 km of single-mode fiber (SMF-28e+LL) and four inline EDFAs. Each inline EDFA has a noise figure of 5.5 dB. A tunable bandwidth and tunable center wavelength band-pass filter (T-T BPF) was inserted after the 4th span. The gain of the last EDFA was adjusted (increased by 10 dB compared to the other EDFAs) in order to compensate for losses in the recirculating loop switches, couplers, and the T-T BPF.

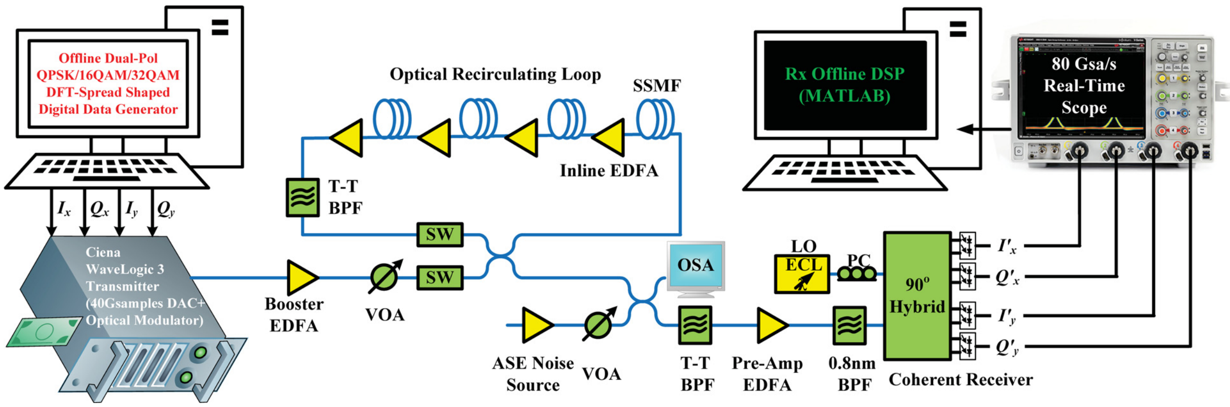

Fig. 3.10 Experimental setup. EDFA: Erbium-doped fiber amplifiers, BPF: band-pass filter, T-T BPF: Tunable bandwidth and tunable center frequency band-pass filter, LO: local oscillator, PC: polarization controller, SW: switch.

At the receiver side, a noise loading EDFA and a VOA were used to examine back-to-back system performance under different received optical signal to noise ratio (OSNR) scenarios. An optical spectrum analyzer (OSA) was used to measure the signal OSNR at 0.5 nm resolution, which was then converted to the 0.1 nm noise bandwidth. Another T-T BPF was employed to reject out-of-band ASE noise accumulated during transmission. The gain of the pre-amplifier EDFA was adjusted to ensure that the signal power reaching the coherent receiver was held constant at 5 dBm. A 0.8 nm BPF was used to filter out the out-of-band ASE noise generated by the pre-amplifier. At the polarization-diversity 90° optical hybrid, the signal was mixed with a 15.5 dBm LO from an external-cavity laser with a linewidth of 100 kHz. The beating outputs were passed through four balanced photodetectors. A 4-channel real-time oscilloscope sampled the signal at a sampling rate of 80 GSa/s and digitized it with 8 bit resolution. Finally, the digital received signals were resampled back to WL3 DACs sampling rate, and then processed offline using MATLAB.

3.7 Results and Discussion

The CP length used for all the experiments was 16 samples per 1024 samples of the OFDM frame, which was interpreted as 1 symbol overhead per sub-band and a CP overhead of 1.5%. The DAC was operating at a fixed rate of 39.5 GSa/s and only 14 out 16 sub-bands were used for the data. Thus, the symbol rate is calculated as GSym/s. Therefore, a total data rate for the transmission is 68 Gb/s, 136 Gb/s and 170 Gb/s for QPSK, 16QAM and 32QAM, respectively.

Compared to previously studied poly-phase filter-bank schemes in our group [105], the system tested here has an increased complexity, and also a 1.75% loss in spectral efficiency since the sub-carrier around DC were not used for data transmission. This is only because the prior work did not address CFO and PN impairments as its application was hardware implementation in an electrical back-to-back configuration, therefore omitting the optical channel, the optical-to-electrical, and the electrical-to-optical converters. Moreover, the DAC has a roll-off factor that is larger than a single sub-band. Therefore, instead of sacrificing 3 sub-bands (one for the pilot tone and two for the compensation of this large roll-off), and further reducing spectral efficiency, we decided to move 48 sub-carriers from the DC sub-band into the outer sub-band placing 24 on each side. This increased its width and allowed a larger roll-off, but this operation led to an uneven spectrum partitioning. The main experimental purpose was to demonstrate the reduced CP overhead without conventional CD compensation.

3.7.1 Back-to-Back Performance

In order to calibrate the experimental setup and find its optimal parameters in the absence of optical channel impairments, we started with a back-to-back performance analysis. We have investigated system performance under different pilot-to-signal power ratio values. Since BER was very small in back-to-back, the Q^2-factor was calculated from the scattering of the received constellation points (after equalization and before slicing) as $Q^2(in\,dB) = 20log_{10}\,(d_{\min}/2\sigma\ )$, where $d_{\min}$ is the minimum Euclidean distance of the constellation and σ is the estimated standard deviation of the noise in the in-phase or quadrature dimension [108]. For each modulation format, the PSR was swept with a 1-dB step and the optimum PSR corresponding to the maximum Q^2-factor was chosen.

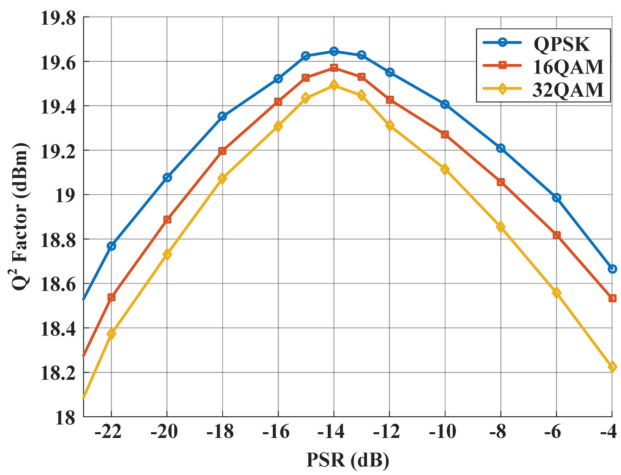

Fig. 3.11 Back-to-back performance of different modulation formats under different PSR.

Fig. 3.11 summarizes the relationship between the averaged Q^2-factor over all sub-bands versus PSR. We see that 14 dB leads to the best performance in all cases. After that, we optimized the bandwidth of the low-pass filter used at the receiver for digital filtering and removal of the pilot tone for carrier recovery purposes. We found that 300 MHz is a sufficient bandwidth for the pass-band. This is narrow enough to ensure no cross-talk between neighboring data sub-bands and PT. At the same time, it ensures that most of amplified spontaneous emission ASE noise around the PT is filtered out and its phase is not distorted.

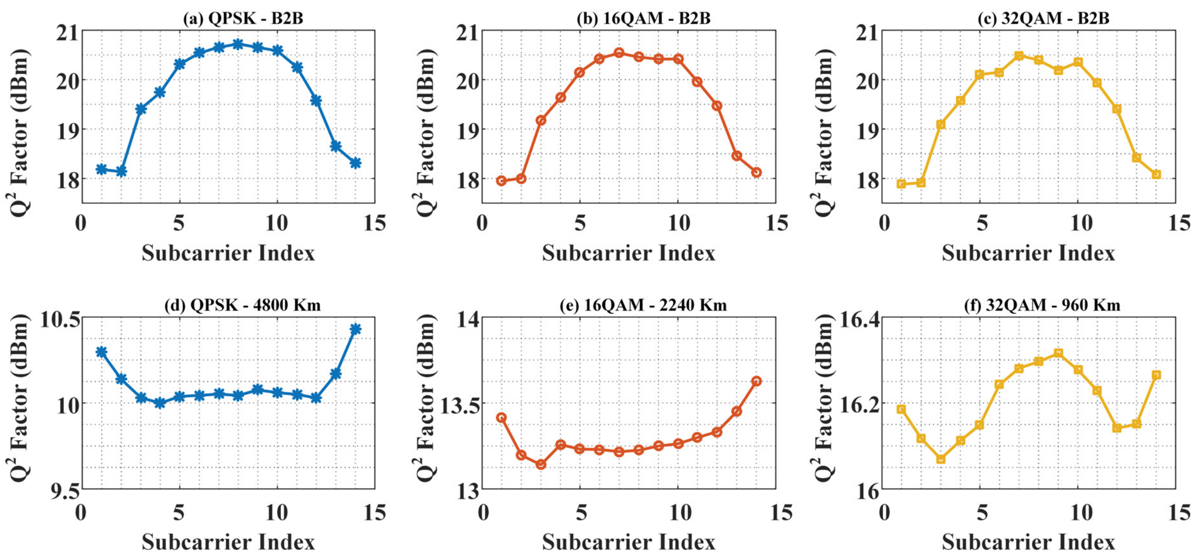

Fig. 3.12 Performance of each subcarrier for MSB-RGI-OFDM with different modulation formats in back-to-back and after transmission at optimum launch power and PSR.

Figure 3.12 demonstrates the performance of each sub-band in back-to-back and after transmission for different modulation formats at the optimum launch power. It is observed that in the back-to-back experiment, the sub-bands located at the center of the spectrum have better performance compared to sub-bands located at the edge. This can be due to the frequency response of the DAC's analog filter and its smaller effective number of bits at high frequencies. On the other hand, after transmission, sub-bands located at the center of the spectrum have worse performance. This is most likely due to the inter-sub-band nonlinear effects and linear cross-talk. The strength of inter-sub-band nonlinear effects become weaker for larger spacing and center sub-bands have more neighboring sub-bands at the smaller spacing on each side. Also, it seems sub-bands located on the right side of spectrum perform slightly better due to the inline EDFA gain profile. Here, since we have access to each sub-band at the transmitter, we can use water-filling algorithms, i.e., using different power, modulation format or coding for each subcarrier, in order to have the same performance for all sub-bands.

3.7.2 Transmission Performance and Comparison to Single Carrier Systems

This section presents measured Q^2-factor for different launch powers at the fixed transmission distance. The distances investigated were 5120 km, 2240 km and 960 km for QPSK, 16QAM, and 32QAM modulation formats, respectively.

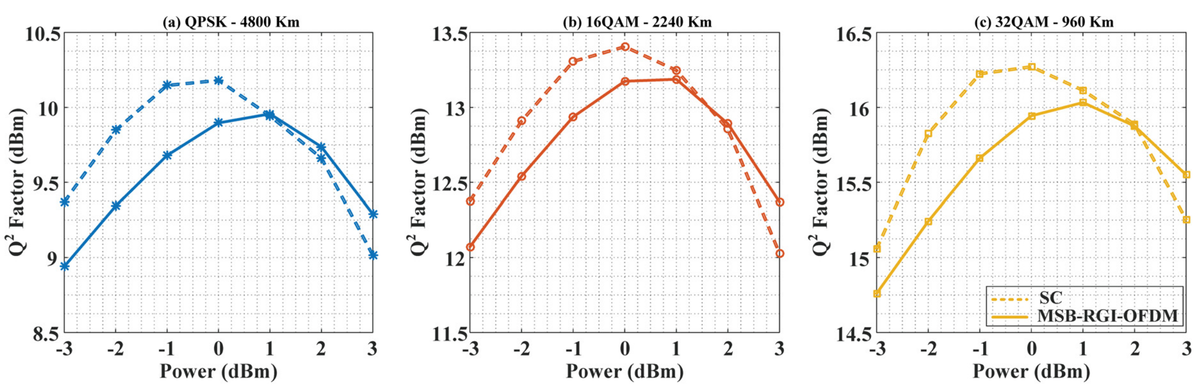

Fig. 3.13 Average Q^2-factor after transmission for different launch power. Solid line and dashed line corresponds to MSB-RGI-OFDM and SC, respectively.

Figure 3.13 shows the Q^2-factor versus different launch powers. If the power launched into the fiber is low, e.g., -3 dBm, the systems are mainly limited by linear impairments. However, as the launch power increases, fiber nonlinearities become more significant. For reference, we compared the performance against a standard single carrier (SC) modulation format at the same total data rate. A root-raised-cosine pulse shape with a roll-off factor 0.07 was used in order to have the same total bandwidth for both SC and MSB-RDI-OFDM systems. We used standard training based equalization DSP for the SC experiment. The DSP began with optical front-end compensation, followed by CFO and CD compensation using a frequency domain equalizer, and then polarization de-multiplexing and compensation of other linear channel impairments with a multi-tap time-domain butterfly filter and a phase locked loop [113]. It is observed that for all modulation formats, the optimum launch power is 1 dBm for MSB-RGI-OFDM and 0 dBm for the SC system. Both systems have similar performances, and the difference between the best Q^2-factor for both systems is only less than 0.5 dB.

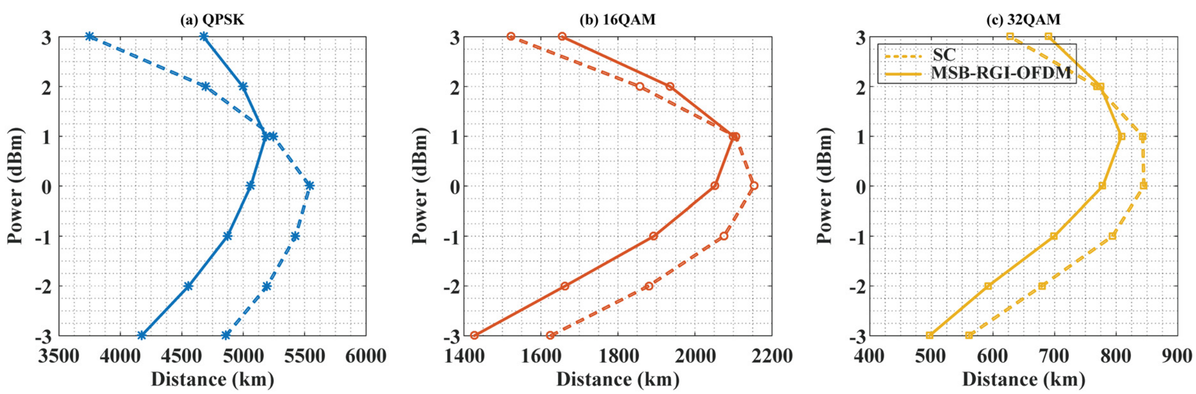

Fig. 3.14 Maximum transmission distance for different modulation formats. Solid line and dashed line corresponds to MSB-RGI-OFDM and SC, respectively. (a) QPSK transmission with BER threshold of 3.8×10^{-2}, (b-c) 16QAM and 32QAM transmission with BER threshold of 2×10^{-2}.

Next, we compare the achievable transmission distance for different modulation formats with a pre-set BER threshold for both SC and MSB-RGI-OFDM systems. These results are plotted in Fig. 3.14(a) for QPSK transmission with a BER threshold of 3.8×10^{-3} and in Fig. 3.14(b-c) for 16QAM, and 32QAM, respectively with a BER threshold of 2×10^{-2}.

Even though we can only transmit signals for integer number of loops in the experiments, the achievable transmission distance in Fig. 3.14 is estimated using interpolation at the BER threshold when necessary. Both systems achieve a similar transmission distance. SC systems requires CD compensation equalizers and multi-tap butterfly filters (here, 17 taps at two sample per symbol were used) in order to compensate for the channel impairments and reconstruct transmitted signal. In contrast to SC, MSB-RGI-OFDM requires maximum 1.5% CP overhead for long transmission distances. It should be noted that electronic CD pre-compensation is not necessary and all channel impairments were compensated via a simple one-tap-per-symbol equalizer. It should be noted that CP overhead can be further reduced for 16QAM and 32QAM due to smaller maximum transmission distances.

3.8 Conclusion

In this section of the thesis, we revised and experimentally verified a digital sub-band (de)multiplexing strategy, i.e. partitioning digitally the wideband spectrum of an optical channel into multiple sub-bands, to be separately processed. Each sub-band is narrowband, and therefore experiences a nearly flat frequency response of the end-to-end transmission environment along with negligible CD and PMD. MSB-RGI-OFDM maintains much faster and more accurate convergence for its adaptive filter coefficients in comparison to conventional OFDM and SC systems. Consequently, rapid and accurate adaptive algorithm convergence means low data-aided overhead. Therefore, channel estimation becomes much simpler for each sub-band. In comparison to conventional OFDM, receiver synchronization (timing recovery) is substantially simpler and more accurate on per-sub-band basis. In particular, the delay and correlate algorithm, which does not work for full-band signals due to CD, can be used for each narrow bandwidth frequency flat sub-band without any signal pre-equalization. Also, the EEPN is cut down by a factor of M, and practically eliminated as this method removes the need of a conventional CD compensating equalizer. To summarize, this technique reduces the computational complexity and in comparison to conventional OFDM, it simplifies almost every aspect of signal processing at the receiver. Moreover, it requires negligible CP overhead and a smaller training sequence. Furthermore, it is highly amenable for parallelization and can achieve comparable performance with commercially deployed SC at a lower computational cost.

Chapter 4

Chromatic Dispersion Mitigation Based on Multi-Sub-Band Single Carrier

This chapter presents concepts and experimentally demonstrates a novel sub-band multiplexed data architecture for chromatic dispersion (CD) mitigation. We are able to transmit a 32 Gbaud multi-sub-band (MSB) dual-polarization (DP) 16QAM over 2400 km. Using this approach, the transmitted signal bandwidth is divided into multiple narrow-bandwidth sub-bands, each operating at a low baud rate. Within each sub-band, the CD frequency response can be approximated as a linear-phase band-pass filter, which can be considered as an analog delay that does not require compensation. Therefore, the digital signal processing (DSP) required at the receiver is simplified by the removal of the CD compensating equalizer. In addition, this leads to efficient parallelization of DSP tasks by making it possible to use multiple independent sub-band processors running at a lower clock rate. The proposed system reduces receiver computational complexity and offers 1 dB higher Kerr-nonlinearity tolerance and 2% extended transmission reach in comparison to the conventional single carrier systems.

4.1 Introduction

To satisfy the ever-increasing demand for capacity in optical fiber communications, both the spectral efficiency and the data rate carried by individual wavelength-division multiplexed channels have to be increased. Currently, CD equalizer's high power and area requirements in long-haul and metro line-card application-specific integrated circuits (ASICs) [43, 44] is one of the major obstacles for implementing advanced DSP techniques such as nonlinearity compensation.

Coherent optical orthogonal frequency-division multiplexing (CO-OFDM) is an attractive 100 Gb/s modulation format [89] that is also well suited for multi-sub-band (MSB) filter-bank (FB) based detection [100]. It enables compensation of all linear channel impairments, including CD, via one-tap equalizers [89]. OFDM, however, is not spectrally efficient due to the large overhead required. The main overhead arises from the long cyclic prefix (CP) required to accommodate the accumulated CD. Dispersion-induced delay spread scales quadratically with the signal bandwidth [100]. A subbanded OFDM receiver architecture has been proposed to significantly reduce CP-overhead (i.e., guard interval between OFDM frames) [100, 105]. Using this approach, the transmitted signal bandwidth is divided into multiple narrow bandwidth OFDM sub-bands. This bandwidth partitioning allows for CD compensation on a per sub-band basis and achieves higher DSP efficiency as well as a simplified parallelization.

Previously, we experimentally demonstrated multi-sub-band reduced guard interval OFDM (MSB-RGI-OFDM) communication [114] and it was observed that the transmission reach reduced in comparison to conventional single carrier systems. This is due to the higher sensitivity of OFDM systems to local oscillator frequency offset and phase noise. Furthermore, because of the optical modulator imperfect biasing and carrier leakage center subcarriers were not used for data transmission and the data sub-carrier allocation was modified. This complicates the filter-bank polyphase implementation and reduces the spectral efficiency.

X. Liu et. al. proposed a novel multi-sub-band DFT-spread OFDM (MSB-DFTS-OFDM) equalizer that combines CD pre-compensation with OFDM equalization and sub-band demultiplexing in order to significantly reduce DSP complexity [115].

In the work presented in this chapter, the multi-sub-band processing architecture for single carrier (SC) systems is further investigated. We use an array of low rate SC sub-bands combined with polyphase channelizer to improve the system tolerance to phase noise and local oscillator frequency offset. In addition, we used a conventional time-domain SC equalizer applied to each sub-band individually rather than using the frequency-domain OFDM channel equalization technique. This approach allowed us to eliminate the CP overhead and improve the spectral efficiency. The partitioning and assembly of the sub-bands can be performed efficiently in the digital domain [107, 108]. In this work, we utilized an underdecimated uniform discrete Fourier transform (DFT) filter-banks based transmitter and receiver with a non-trivial prototype filter (i.e., overlapping sub-bands) [108]. For a 32 GHz channel, the number of sub-bands at different transmission distances required to fully mitigate the effects of CD and remove the CD compensation equalizer at the receiver were also determined. This method allows for a significant reduction of the receiver DSP computational complexity and it offers a simplified implementation for flexible optical transceivers. Finally, the performance and transmission reach of the proposed method against conventional single carrier systems are compared.

4.2 Chromatic Dispersion Mitigation by Multi-Sub-Band Single Carrier Transmission

Digital signal processing has played an important role in supporting the recent expansion in capacity of optical networks. Modern coherent optical communications has benefited from many powerful DSP techniques because of the access to the full optical field information (phase and amplitude) at both transmitter and receiver. In the absence of Kerr nonlinearity, the fiber can be regarded as a linear system. In principle, all the linear impairments can be fully compensated by digital filters [108]. In conventional single carrier systems, fiber CD is modeled as a quadratic-phase all-pass filter. Fiber CD is a time-invariant distortion and the CD accumulated upto the receiver could exceed several thousands of ps/nm. Therefore, it is desirable to use a non-adaptive filter with fixed taps for CD compensation [8]. On the other hand, the polarization-mode dispersion (PMD) may be modeled by the Jones matrix, and varies rapidly due to the fiber birefringence [61]. As a result, the compensation of PMD should be adaptive to continuously adjust the filter tap coefficients. Consequently, channel equalization can be realized more efficiently by separately addressing slowly time-varying transmission effects such as CD (by a long fixed-tap frequency-domain filter), from rapidly varying effects such as PMD, inter-symbol interference and other time-varying fiber impairments (by a short time-domain adaptive butterfly filter) [8]. As mentioned in the previous chapter, in a multi-sub-band transmission scheme, the CD frequency response can be approximated as a bank of M narrow-bandwidth linear-phase band-pass filters, each having a different but constant group delay. As a result, the bandwidth partitioning technique transforms CD into different analog delays for each sub-band.

Fiber CD results in temporal optical pulse broadening [61]. Therefore, transmitted data is received with a delay spread (normalized in units of discrete-time sampling intervals, Ts, at the receiver), which is given by [105]:

$$\Delta\tau_{CD} = \frac{2\pi\,|\beta_2| \cdot L \cdot BW}{T_s}. \tag{4.1}$$

where β_2, BW, and L are fiber group velocity dispersion parameter, signal bandwidth, and transmission distance, respectively. At the receiver, the sampling rate is also proportional to the signal bandwidth as ${T_s}^{-1} = \eta \cdot BW$, where η is a factor related to the spectral efficiency and the oversampling ratio. Therefore, the delay spread caused by CD is given by:

$$\Delta\tau_{CD} = 2\pi\,|\beta_2| \cdot \eta \cdot L \cdot BW^2. \tag{4.2}$$

It is evident that the delay-spread (i.e., temporal pulse broadening) is quadratic in bandwidth. This implies that it would be advantageous to decrease the bandwidth of the transmitted signal in order to significantly reduce the CD-induced delay spread. The complexity cost, C, for a finite impulse response time domain implementation of the CD compensation equalizer is $O(\Delta\tau_{CD})$. When the CD equalizer is implemented in frequency domain with the fast Fourier transform (FFT) algorithm, the complexity cost can be as low as $C = O(\log(\Delta\tau_{CD}))$ [105]. Therefore, dividing the total channel bandwidth into M sub-bands allows for per-sub-band compensation of CD while the delay spread in each sub-band is dramatically reduced by a factor of M^2. For example, for a 32 GHz channel transmitted over a $2,000$ km link of standard single-mode fiber, CD compensation of the un-partitioned BW transmission requires 250 taps per symbol, while dividing the BW into $M = 8$ sub-bands reduces this number to $\lceil 250/8^2 \rceil = 4$ taps per symbol for each sub-band [105]. Therefore, the CD memory length decreases dramatically for each sub-band and is comparable to other time-variant transmission effects such as PMD. As a result, a multi-sub-band processing architecture allows for compensation of all channel linear impairments including CD and PMD by a short time-domain adaptive butterfly equalizer. Therefore, it achieves higher DSP efficiency as well as simplified parallelization [100, 105, 116]. In addition, flexible optical transceivers (with reconfigurable rates and modulation formats) may be efficiently realized using this filter-bank based digital sub-banding approach [102]. For example, it allows flexible spectral occupancy by turning on and off certain sub-bands. Also, when operating with a fixed spectral occupancy, this allows changing the constellation size of all or a sub-set of the sub-bands in order to engineer the desired data throughput. Moreover, all sub-bands share the same optical transmission path therefore they experience common channel properties. This fact allows for the utilization of more accurate and efficient impairment compensation techniques by jointly processing multiple sub-bands and taking advantage of information from other sub-bands [101]. Additionally, each sub-band is considerably flatter in its frequency response due to its narrow bandwidth, which implies smaller channel eigenvalue spread. Therefore, they maintain faster and more accurate convergence for their adaptive filter coefficients in comparison to full-band conventional single carrier systems. This convergence speed-up will be manifested in every adaptive DSP algorithms. Consequently, rapid and accurate adaptive algorithms convergence means low data-aided overhead [105].

4.2.1 Transmitter and Receiver DSP Structure

Figure 4.1 illustrates a block diagram of the transmitter-side DSP. The multi-sub-band (MSB) signal was efficiently generated by utilizing a DFT-based synthesis filter-bank architecture [102]. The root-raised-cosine (RRC) pulse shape was chosen as a prototyping filter and calculated its polyphase coefficients required for the implementation. Next, each sub-band power was adjusted in order to achieve similar performance for all sub-bands in back-to-back configuration.

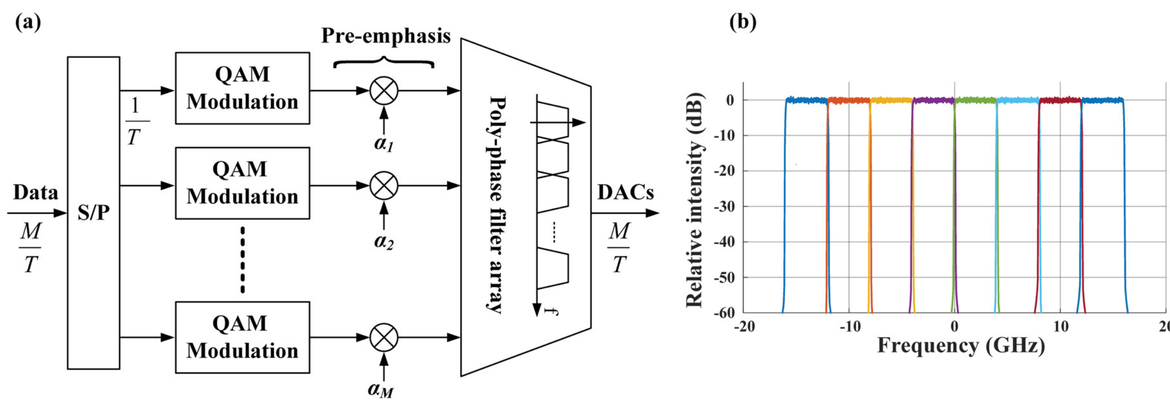

Fig. 4.1 (a) Transmitter-side DSP based on an M-point IDFT and M polyphase filters (corresponding to the M polyphases of the prototype pulse-shaping filter), (b) optical spectra of transmitted multi-sub-band signal.

Figure 4.2 shows the top-level block diagram of multi-sub-band receiver. The DSP code starts with front-end compensation, including the removal of the DC component, IQ imbalance compensation, and optical hybrid IQ orthogonalization [8]. Next, local oscillator (LO) laser frequency offset is compensated based on the DFT of the signal [8]. For sub-band demultiplexing, the key element is a bank of M parallel digital band-pass filters, each handling $1/M$ of the channel bandwidth. This is implemented by a twice-underdecimated DFT-based filter-bank structure. The receiver prototype filter was selected to be matched to the pulse-shaping filter [105]. According to Fig. 4.2, each of the M filter-bank output feeds a corresponding sub-band receiver processor. As a result, we have an array of M low-speed sub-band receivers working simultaneously in parallel. The rationale for this approach is that while we have invested some computational overhead in partitioning the spectrum into M sub-bands at the transmitter, this allows operating each sub-band receiver at a rate that is M-times slower (compared to un-partitioned twice-oversampled single-carrier detection). In addition, this facilitates the realization of the receiver since each sub-band DSP processor does not require a conventional full-band CD compensation equalizer.

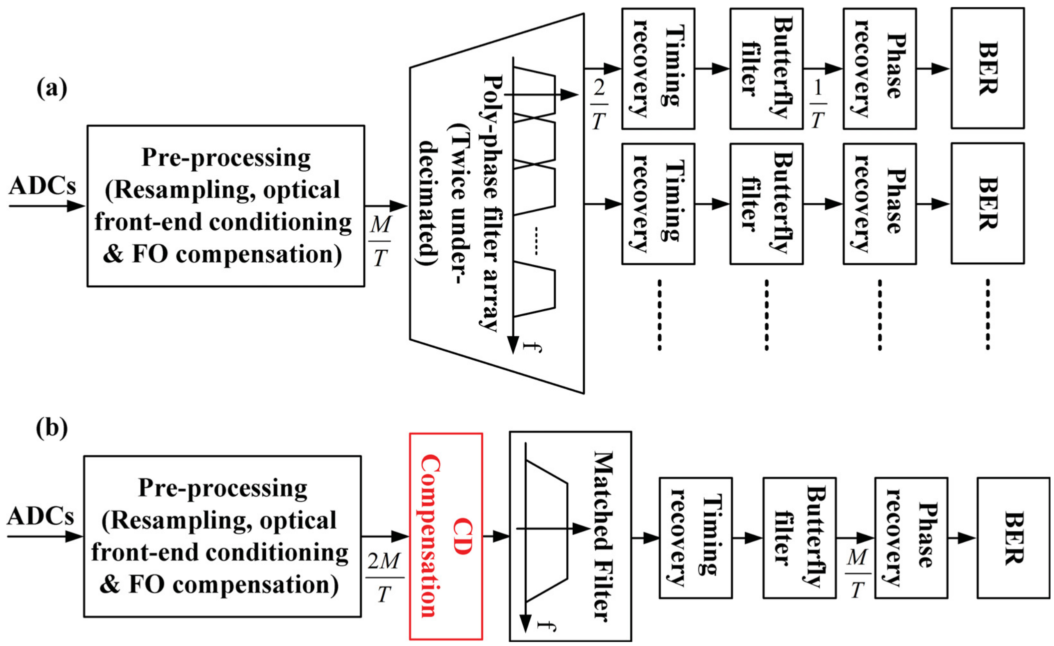

Fig. 4.2 (a) Receiver-side DSP based on twice under-decimated M-points DFT and polyphase filters (The M receive polyphase filters were selected to be matched to the transmit filters). (b) Conventional singe carrier receiver DSP.

Each sub-band DSP code starts with synchronization and timing recovery in order to facilitate data-aided modulation-transparent equalization. For synchronization, the integer part of each sub-band delay (measured in units of sub-band sample rate) may be readily corrected by conventional correlate and delay algorithms such as Schmidl–Cox [8] and using a simple digital buffer without any CD pre-equalization. In the next step, the fractional part of the delay, as well as any additional channel linear impairments, are corrected blindly by the low complexity multi-tap butterfly equalizer. This adaptive equalizer is implemented in the time domain and operated at 2 samples per symbol [8]. The carrier phase is recovered using the superscalar parallelization based phase locked loop (PLL) [117]. Finally, the symbols were mapped to bits and the bit error rate (BER) was counted over $100,000$ bits and a soft-decision forward error correction (20% overhead) BER threshold of 2×10^{-2} was considered.

The results obtained were also compared with a conventional single carrier transmission system. To achieve this, the FFT-based filter-bank multi-sub-band encoder at the transmitter was removed. At the receiver, the poly-phase filter-bank array was replaced with the overlap-and-save frequency domain CD equalizer. This was followed by matched filtering (as shown in Fig. 4.2(b). The remaining DSP blocks and other parameters are identical for both transmission schemes.

4.2.2 Experimental/Simulation Setup

Figure 4.3 shows the schematic diagram of the experimental and simulation setup. For the transmitter side offline DSP, four 2-tuple independent pseudo-random bit sequences (PRBS) with a length of 217 are mapped to 16QAM symbols, followed by multi-sub-band multiplexing (outlined in Fig. 4.1.(a)) for each polarization. A Ciena WaveLogic 3 (WL3) line card was employed, which contains four 39.5 GSa/ 6 bit digital-to-analog converter (DACs), a tunable frequency laser source, and a dual-polarization (DP) IQ modulator. The transmitter laser was operated at 1554.94 nm. The transmitter analog frequency response was compensated using the on-board built-in DSP of the WL3. The output optical signal is then boosted to 23 dBm using an erbium-doped fiber amplifier (EDFA), and subsequently attenuated using a conventional variable optical attenuator (VOA) in order to get a desired optical launch power. The optical signal is then launched into a recirculating loop. This loop consists of four spans of 80 km of single-mode fiber (SMF-28e+LL) and four inline EDFAs. Each inline EDFA has a noise figure of 5.5 dB. A tunable bandwidth and tunable center wavelength band-pass filter (T-T BPF) is inserted after the 4th span in order to reject out-of-band amplified spontaneous emission (ASE) noise accumulated during transmission. The gain of the last EDFA is adjusted (increased by 10 dB compared to the other EDFAs) in order to compensate for losses occurring inside the recirculating loop, including switches, couplers and the band-pass filter.

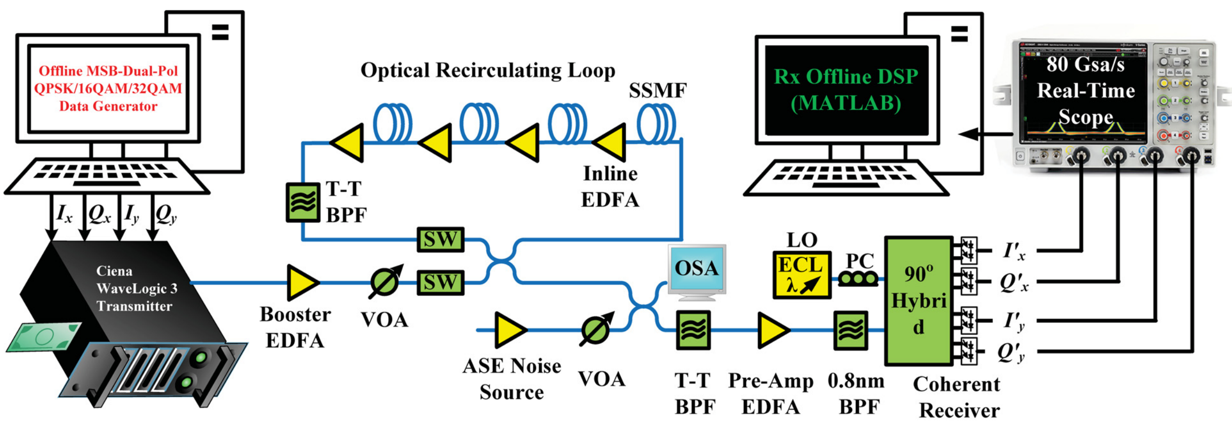

Fig. 4.3 Experimental setup. EDFA: erbium-doped fiber amplifiers, BPF: band-pass filter, T-T BPF: Tunable bandwidth and tunable center frequency band-pass filter, LO: local oscillator, PC: polarization controller, and SW: switch.

At the receiver side, an optical spectrum analyzer (OSA) was used in order to measure the optical signal-to-noise ratio (OSNR) at 0.5 nm resolution bandwidth which was then converted to a 0.1 nm noise bandwidth. The gain of the pre-amplifier EDFA was adjusted to ensure that the signal power reaching the coherent receiver was held constant at 5 dBm. Finally, a 0.8 nm BPF was used to filter out the out-of-band amplified spontaneous emission (ASE) noise generated by the pre-amplifier. At the polarization-diversity 90° optical hybrid, the signal was mixed with 15.5 dBm local oscillator (LO) light from an external-cavity laser (ECL) with a linewidth of 100 kHz. The beating outputs were passed through four balanced photodetectors. A 4-channel real-time oscilloscope sampled the signal at a sampling rate of 80 GSa/s and digitized it with 8-bit resolution.

For the simulation model, the DACs, optical modulator, fiber optic recirculating loop, and the coherent receiver were assumed to be ideal and were implemented in OptiSystem™ v13. In addition, the LO frequency offset and fiber nonlinearity parameters were set to zero.

4.2.3 Results and Discussion

In this section, we investigate the performance of multi-sub-band (MSB) architecture against conventional single carrier (SC) systems. Unlike conventional SC systems, the MSB technique does not require a CD compensation equalizer, but other DSP blocks and parameters are identical for both schemes (also demonstrated in Fig. 4.2). For all measurements, a root-raised-cosine filter with a roll-off factor equal to 0.01 is chosen as a pulse-shaping filter for 32-Gbaud DP-16QAM transmission. A nontrivial DFT filter-bank (i.e., overlapping sub-bands) structure was used for a more efficient implementation, therefore, a small roll-off factor reduces the linear cross-talk between overlapped neighboring sub-bands and maximizes the spectral efficiency. Also, the butterfly filter has 15 adaptive taps at 2 Sa/symbol in both techniques.

4.2.4 Simulation Results

Figure 4.4 demonstrates the Q-factor penalty vs. number of sub-bands obtained at different transmission lengths, when the multi-sub-band signal architecture has been employed exclusively (i.e., no CD compensation). It was observed that for 960, 1760, 2560, and 3360 km transmission 6, 8, 9, and 10 sub-bands are sufficient in order to reduce the Q-factor penalty to below 0.5, 0.35, 0.2, and 0.1 dB, respectively. This residual penalty originates from the linear cross-talk between overlapped neighbouring sub-bands. It should be noted that this Q-factor penalty due to linear cross-talk decreases for smaller roll-off factors, and for longer transmission distances when the ASE noise becomes the dominant impairment.

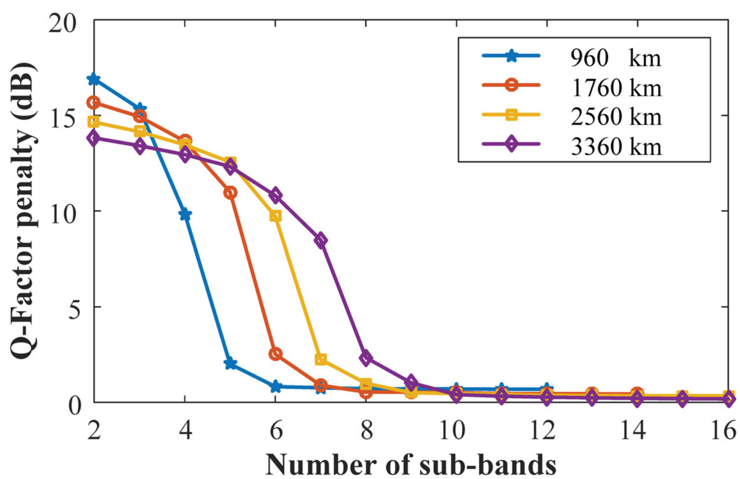

Fig. 4.4 Simulated Q-factor penalty versus number of sub-bands at different transmission distance for 32 Gbaud MSB-DP-16QAM.

Figure 4.5 shows minimum number of required sub-bands, in order to fully mitigate the effects of CD for different distances (when no other impairments exist). According to Eq. (4.2), the CD-induced delay-spread decreases quadratically when decreasing the bandwidth of the transmitted data. Based on Fig. 4.5, it is evident that applications with transmission reach between metro (typically less than 500 km) and long-haul (less than 5000 km) distances only require a few sub-bands (less than 12) in order to mitigate CD. In addition, this can be efficiently implemented using a polyphase FFT-based filter-bank structures. This enables a highly efficient parallelization of DSP tasks by deploying multiple processors running at a lower clock rates. We want to point out that this multi-sub-band processing is essentially a parallelization of the DSP in the frequency domain rather than the time domain.

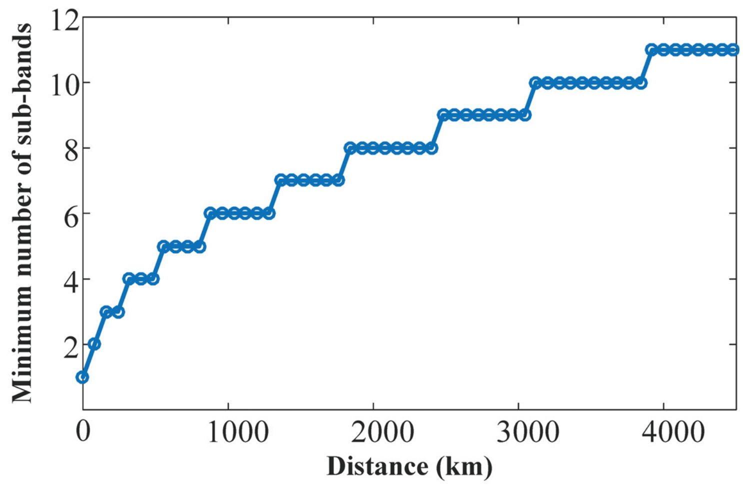

Fig. 4.5 Simulated number of required sub-bands versus different transmission distance for 32 Gbaud MSB-DP-16QAM to fully mitigate the effects of CD.

4.2.5 Experimental Results

During this experiment, the back-to-back performance was first investigated. Figure 4.6 summarizes the BER versus OSNR (at 0.1 nm noise bandwidth) curves for different numbers of sub-bands for 32 Gbaud MSB-DP-16QAM. The OSNR is swept by using receiver-side noise loading and controlling the noise power using a VOA. As shown in both figures, small penalties are observed when we increase the number of subcarriers. It demonstrates that in the high OSNR regime, the MSB architecture suffers from linear cross talk due to overlapping neighboring sub-bands. At low OSNRs, both systems have similar performance. However, as the OSNR increases, MSB signal performance degrades due to the cross-talk between neighboring sub-bands. The penalty at the soft forward error correction (FEC) BER threshold of 2×10^{-2} is less than 0.4 dB for all cases of 4, 6, and 8 sub-bands partitioning.

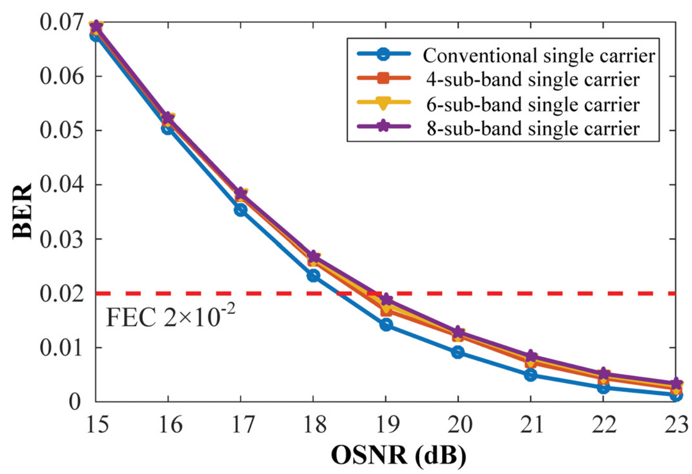

Fig. 4.6 Experimental back-to-back performance of 32 GBaud conventional SC-DP-16QAM and different MSB-DP-16QAMs.

Next, the BER under different launch powers was investigated for fixed transmission distance of 2240 km. As shown in Fig. 4.7, if the power launched into the fiber is low, both systems are mainly limited by linear impairments and the BER is approximately the same. However, as the launch power increases, fiber nonlinearities become more significant and MSB signaling obtains a lower BER than the conventional single carrier signal. As demonstrated in Fig. 4.6, MSB signaling suffers from linear-crosstalk between neighboring sub-bands, however, the overall system performance improves after transmission due to the higher nonlinearity tolerance of the MSB technique. The improvement is particularly significant when the launch power is greater than 1 dBm and it has been investigated and demonstrated previously in [117].

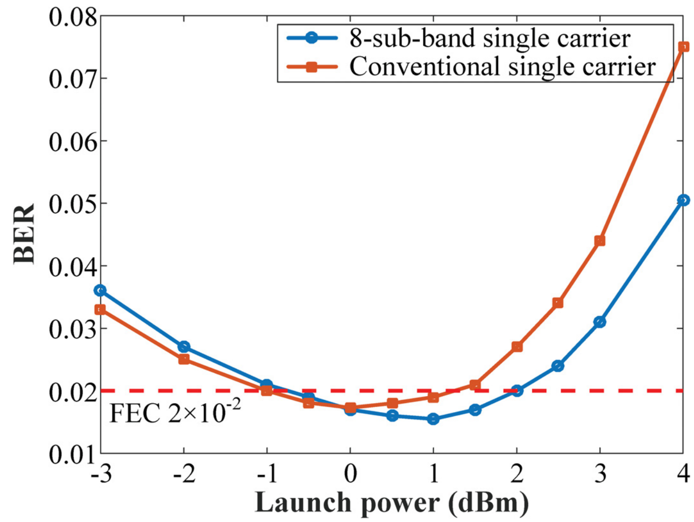

Fig. 4.7 Experimental BER versus launch power for 32 Gbaud conventional SC-DP-16QAM and 8-MSB-DP-16QAM after 2240 km.

Finally, we compare the achievable transmission distance for different launch powers with a pre-set BER threshold of 2×10^{-2}. The results are summarized in Fig. 4.8. In accordance with the results in Fig. 4.7, the achievable transmission distances of SC signals is slightly larger in comparison to MSB signals in the linear regime with low launch powers due to absence of crosstalk between neighboring sub-bands. However, when considering the maximum transmission distance of the two signals at their respective optimum launch powers, it is seen that the achievable reach is extended for the multi-sub-band signals by 2% due to its higher tolerance to nonlinearity. All the while, the complexity of the receiver significantly decreases due to the elimination of the CD compensation equalizer and the reduced data rates of each sub-band receiver.

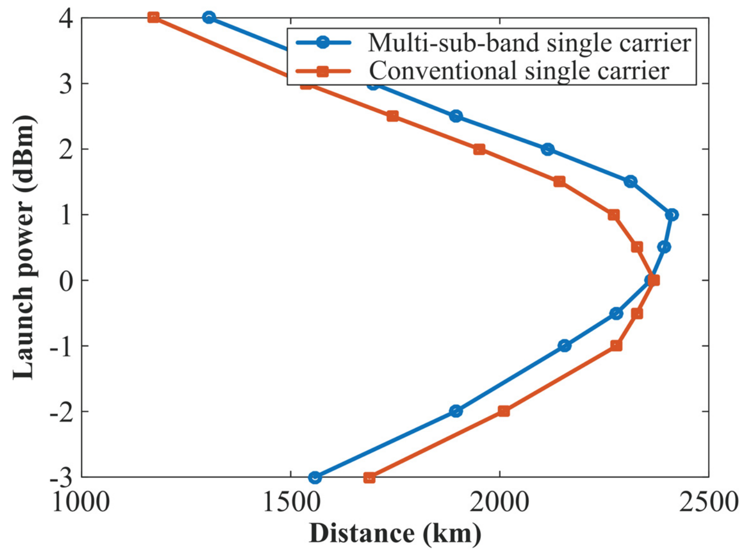

Fig. 4.8 Experimental maximum transmission distance versus launch power for 32 Gbaud conventional SC-DP-16QAM and MSB-DP-16QAM at soft FEC BER threshold of 2×10^{-2}.

4.3 Multi-Band Equalization

As internet traffic grows rapidly, it is necessary to upgrade conventional communication networks to be more scalable and spectrally efficient. To this end, the ultradense wavelength-division multiplexing (UD-WDM) and super channel communication have been studied extensively [118]. Our proposed technique, similar to other Nyquist pulse shaped communication systems, requires filters with very small roll-off factors to limit the linear cross-talk between neighboring bands. In this section, the adoption of low complexity non-iterative inter-band interference (IBI) compensation technique to relax this requirement is briefly investigated.

In this work, the sub-band spacing was chosen to be equal to the baud rate. Therefore, the samples of the received signals for each sub-band can be treated as linear combination of the modulated symbols of the other sub-band with constant coefficients [119]. Therefore, crosstalk of each sub-band can be canceled out by use of the sampled value of adjacent sub-bands.

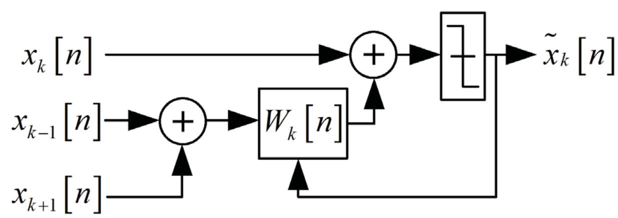

Fig. 4.9 Inter-band interference equalizer.

This work used a pulse shaping filter with a large roll-off factor (ROF) and an IBI compensating equalizer, as depicted in Fig. 4.9, after the conventional linear DSP to reduce the computational complexity.

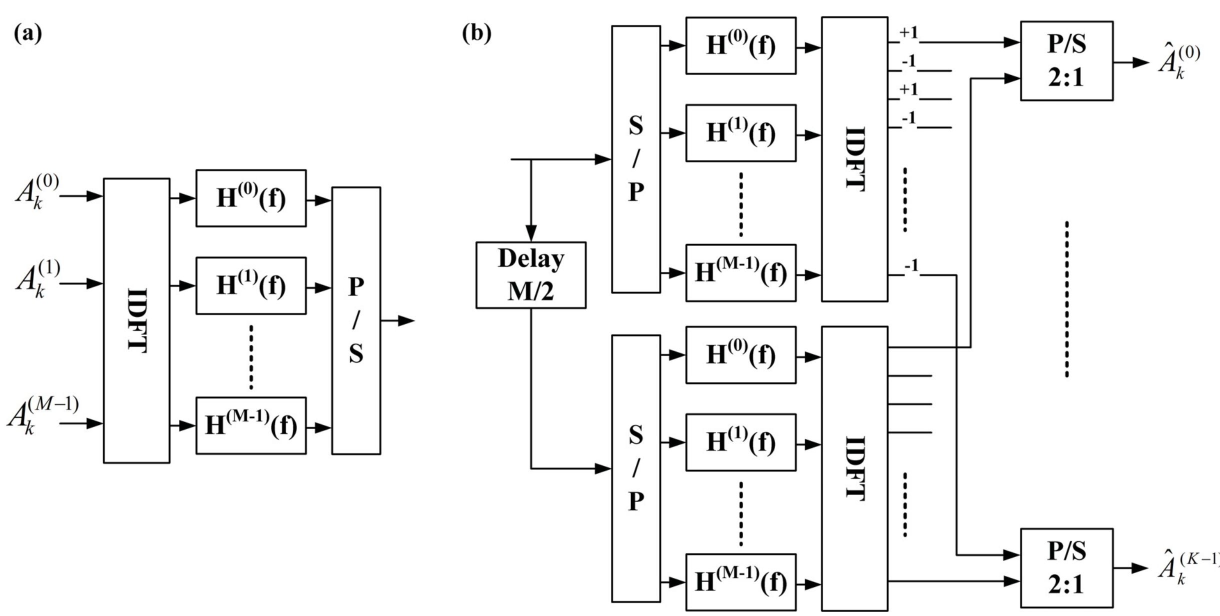

Fig. 4.10 Block diagram of (a) transmitter and (b) receiver polyphase channelizer.

Figure 4.10 shows the block diagram of a transmitter and receiver polyphase channelizer. From the diagram, the number of complex multipliers required for transmitter and receiver polyphase channelizer per sub-band can be determined as:

$$3 \cdot \log(M) + 3 \cdot N_{FB} + N_{IBI} \tag{4.3}$$

where, M is number of sub-bands, N_{FB} and N_{IBI} are the lengths of the prototyping filter and the number of IBI compensation equalizer adaptive taps, respectively.

4.3.1 Simulation Results

In this section, the performance of multi-band signal processing scheme against independent equalization of each sub-band is investigated. All DSP blocks, simulation parameters, and transmission setup are identical to that used in Section 4.2.2.

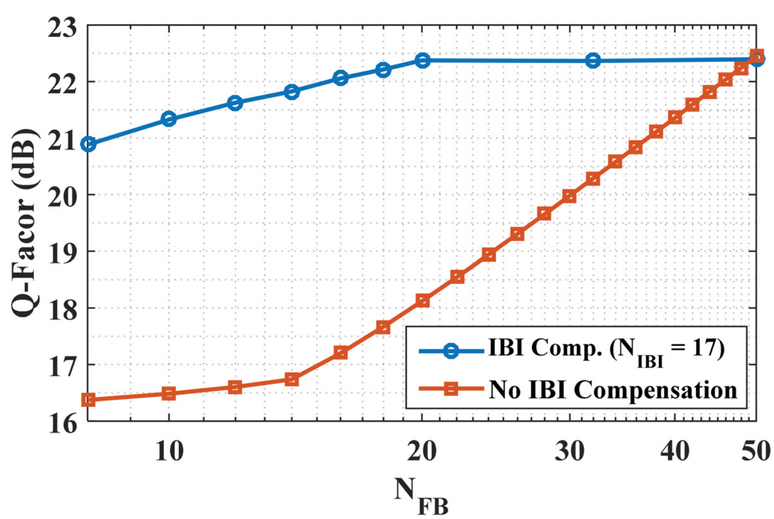

Fig. 4.11 Q-factor versus prototyping filter length for 8 sub-bands 32 Gbaud DP-16QAM in back-to-back.

Figure 4.11 demonstrates simulated Q-factor versus number of polyphase coefficients in each branch for a 8 sub-band conventional MSB system (with ROF = 0.01) and for the proposed scheme (with ROF = 0.1). The results show that the prototyping filter length can be reduced from 48 to only 20 for IBI compensation with 15 adaptive taps. This reduces the number of complex multiplier of polyphase structure by

$$\frac{3 \cdot \log(8) + 3 \cdot 20 + 15}{3 \cdot \log(8) + 3 \cdot 48} = 45\%.$$

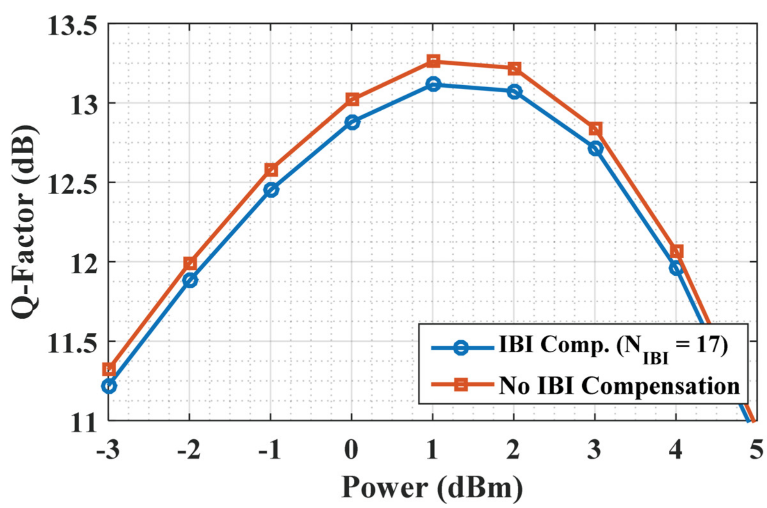

Fig. 4.12 Q-factor versus launch power for 8 sub-bands 32 Gbaud DP-16QAM at 3120 km.

Next, the transmission distance was kept fixed to 3120 km and the Q-factor was simulated for different launch powers. Eight sub-bands were multiplexed and simulations were done for the conventional MSB system (with ROF = 0.01) and this proposed system with the cross talk cancellation technique (with ROF = 0.1). The BER for both system were slightly below the 20% soft-decision FEC threshold. Figure 4.12 shows that the optimum launch power is 1 dBm and both systems have similar performances. The difference between the best Q-factors for both systems is only less than 0.2 dB.

4.4 Conclusion

In this chapter, a novel DSP structure for the mitigation of CD was demonstrated numerically and experimentally. The proposed concept is based on digitally partitioning the optical channel bandwidth into multiple sub-bands in order to process data in parallel and mitigate CD. It should be noted that this parallelization is performed in the frequency domain. Each narrow-bandwidth sub-band is characterized by a flatter frequency response and a smaller CD-induced delay-spread, compared to the full-band SC signal. This enables per-sub-band compensation of CD by elementary timing recovery and minimal equalization. In terms of the DSP architecture, this approach allows for a highly efficient receiver implementation by deploying multiple processors running at a lower clock rate. Finally, it was experimentally demonstrated that filter-bank based multi-sub-band signaling offers longer transmission reach, better nonlinearity tolerance, and simplifies the realization of flexible optical transceivers. All this while lowering the computational complexity by the elimination of the CD compensation step at the receiver DSP. The work presented in this chapter demonstrates the potential of multi-sub-banding for next generation flexible data-rate adaptive and spectrally efficient high-speed communication systems.

Chapter 5

Efficient Adaptive Nonlinear Equalizer for Intra-channel Nonlinearity Compensation for Agile Optical Networks

THIS chapter presents the concepts and experimental results of two novel low-complexity technique for fiber nonlinearity compensation. In the first work, we propose and experimentally verify the adoption of a decision-directed least mean square (DD-LMS) algorithm for the optimization and reduction in complexity of a perturbation based nonlinearity compensation (PB-NLC) equalizer. We show that for 32 Gbaud dual polarization (DP) 16 Quadrature amplitude modulation (16QAM) propagated for 2560 km in single-mode fiber (SMF), the proposed scheme further reduces the computational terms compared to the conventional PB-NLC with uniform quantization of perturbation coefficients for the same improvement in Q-factor. In the second work, an all adaptive nonlinear equalizer based on a first-order perturbation model with quantized perturbation coefficients is proposed. This novel technique does not require any prior calculations or detailed knowledge of the transmission system. Transmission up to 2818 km for a 32 Gbaud DP 16QAM signal was achieved. For efficient implementation, and to facilitate integration with conventional digital signal processing (DSP) approaches, we compensate fiber nonlinearities independently and after the equalization of linear impairments. Therefore, this algorithm can be easily implemented in currently deployed transmission systems following the conventional linear DSP. The proposed equalizer operates at one sample per symbol and requires only one computation step. In addition, unlike previously proposed adaptive nonlinear equalization techniques, this technique identifies common symmetries between perturbation coefficients to avoid duplicate operations. Furthermore, by grouping multiple nonlinear terms and dedicating only one adaptive nonlinear filter coefficient to each group, only a few adaptive filter coefficients are used. Finally, the complexity of the proposed algorithm is lower than previously studied nonlinear equalizers by more than one order of magnitude.

5.1 Overview

To satisfy the ever-increasing demand in capacity of optical fiber communications, both the spectral efficiency (SE) and the data-rate carried by each wavelength-division multiplexed channel has to increase. According to Shannon's theory of linear communication systems, the channel capacity is logarithmically proportional to the signal-to-noise ratio (SNR). Therefore, the capacity can be increased by using a larger signal power. However, because of fiber Kerr nonlinearities, there is a limit imposed on the optical launch power. Further increases in input signal power beyond an optimum power level degrades transmission performance. Consequently, fiber nonlinearities are one of the major impairments remaining to be addressed for the next generation coherent optical fiber communication systems that ultimately limit the achievable transmission distance [120]. Following recent advances in high-speed digital signal processing technology, along with global adoption of coherent detection techniques, various intra-channel fiber nonlinearity compensation algorithms have been proposed [121]. A few selected techniques are descirbed below.

Digital back-propagation (DBP) is an effective nonlinear compensation (NLC) technique which has received considerable attention [122–124]. dBP is based on numerically solving the inverse of the nonlinear Schrödinger equation (NLSE). Therefore, it normally requires (a) multiple computation steps per each fiber span, (b) at least two samples per symbol, and (c) prior knowledge of fiber optic transmission system parameters. This results in a high complexity [55]. Consequently, its application is limited to the transmission systems using offline signal processing. There are also reports of nonlinear frequency-domain equalizers based on closed form analytical approximations of fiber third-order Volterra kernels. These techniques simultaneously compensate both nonlinear and linear impairments. However, their major drawback is their high complexity [125, 126].

Wiener-Hammerstein equalization and modified nonlinear decision feedback equalizer were proposed as a simpler alternative for orthogonal frequency-division multiplexing (OFDM), and single carrier transmissions, respectively [127, 128]. These algorithms adaptively compensate for all fiber impairments according to the following formulas (presented in time-domain):

$$A_{0,x}^{\text{Out}} = \sum_{l=-n_L}^{+n_L} H_{l,xx} A_{n,x} + \sum_{l=-n_L}^{+n_L} H_{l,xy} A_{n,y} + \sum_{m,n,k=-n_{NL}}^{+n_{NL}} C_{m,n,k}^{1} A_{n,x} A_{k,x}^{*} A_{m,x} + \sum_{m,n,k=-n_{NL}}^{+n_{NL}} C_{m,n,k}^{2} A_{n,y} A_{k,y}^{*} A_{m,x} \quad (5.1)$$

$$A_{0,y}^{\text{Out}} = \sum_{l=-n_L}^{+n_L} H_{l,yy} A_{l,y} + \sum_{l=-n_L}^{+n_L} H_{l,yx} A_{l,x} + \sum_{m,n,k=-n_{NL}}^{+n_{NL}} C_{m,n,k}^{3} A_{n,y} A_{k,y}^{*} A_{m,y} + \sum_{m,n,k=-n_{NL}}^{+n_{NL}} C_{m,n,k}^{4} A_{n,x} A_{k,x}^{*} A_{m,y} \quad (5.2)$$

where n_L and n_{NL} are linear and nonlinear equalizer memory lengths, respectively. $H_{l,\{xx,xy,yy,yx\}}$ and $C_{m,n,k}^{\{1,2,3,4\}}$ are linear and nonlinear adaptive filter coefficients. Their nonlinear filter computational complexity grows as ${n_{NL}}^3$ and they require a long training sequence for their $4 \cdot {n_{NL}}^3$ adaptive nonlinear filter coefficients. Therefore, their performance was investigated for single polarization systems with in-line dispersion compensation and a short channel nonlinear memory length (i.e., fiber with small dispersion parameter) [127, 128].

Perturbation-based nonlinear pre-compensation and post-equalization techniques compensate the accumulated nonlinearities with only one computation step and can be implemented at one sample per symbol [58–60]. Typically, perturbation based NLCs have lower computational complexity than blind nonlinear equalization algorithms [125–128]. However, perturbation based NLC algorithms requires prior knowledge of fiber optic transmission system parameters in order to calculate the perturbation coefficients [58] and 50% chromatic dispersion (CD) pre-compensation at the transmitter for efficient implementation [59, 60].

Development of wavelength-selective switching (WSS) technologies and flexible optical transceivers (with reconfigurable rates and modulation formats) is enabling the next generation of transparent optical networks. Remote reconfiguration of a mesh network (i.e., dynamic networking) and adaptation of the flexible optical transceivers provide optimal network utilization and agility [29, 129]. Thus, many sets of perturbation coefficients (depending on different transceiver configuration, CD pre-compensation, and selected transmission route) have to be stored in the memory of the line card. In addition, considering all the possible network parameters, the identification of a correct set of perturbation coefficients becomes a very difficult task. Furthermore, for certain scenarios, the exact transmission route is unknown at the transmitter or at the receiver. Therefore, perturbation based NLC (PB-NLC) cannot be easily deployed in dynamically reconfigurable meshed optical network architectures, and its application is restricted to point-to-point systems with well-studied parameters.

Therefore, low-complexity adaptive nonlinear equalization algorithms are highly desirable for the next generation agile and flexible high-data rate fiber optic communication systems. In addition, such equalization techniques should not require accurate knowledge of transmission link and transceiver parameters.

5.2 Principles of Perturbation Based Nonlinearity Compensation

The evolution of the optical field envelope in a fiber optic link is described by the nonlinear Schrödinger equation [61]:

$$\frac{\partial}{\partial z}u(t,z) + j\frac{\beta_2(z)}{2}\frac{\partial^2}{\partial t^2}u(t,z) = j\gamma(z)|u(t,z)|^2 u(t,z) \tag{5.3}$$

where, $u(t,z)$ is the optical field, $\beta_2(z)$ is the group velocity dispersion, and $\gamma(z)$ is the nonlinear coefficient. The nonlinear term in Eq. (5.3) can be treated as a small perturbation by denoting $u(t,z) = u_0(t,z) + j\Delta u(t,z)$, where, $u_0(t,z)$ is the solution of linear propagation, and $\Delta u(t,z)$ is the perturbation due to the nonlinear effects. With a first order approximation and assuming phase-matching condition, among all possible symbol triplets (with indices m, n, and k) that cause intra-channel nonlinear impairments, only the triplets that hold the $k = m + n$ property play a significant role. Therefore, the intra-channel four-wave-mixing (IFWM) and intra-channel cross-phase-modulation (IXPM) nonlinear-induced distortions on the transmitted symbol can be expressed as (the triplets which result in phase rotation have been removed here) [125]:

$$\Delta A_{0,x} = P^{3/2}\left[\sum_{\forall m\neq 0, n\neq 0} C_{m,n}A_{n,x}A^*_{m+n,x}A_{m,x} + \sum_{\forall m\neq 0, n} C_{m,n}A_{n,y}A^*_{m+n,y}A_{m,x}\right] \tag{5.4}$$

$$\Delta A_{0,y} = P^{3/2}\left[\sum_{\forall m\neq 0, n\neq 0} C_{m,n}A_{n,y}A^*_{m+n,y}A_{m,y} + \sum_{\forall m\neq 0, n} C_{m,n}A_{n,x}A^*_{m+n,x}A_{m,y}\right] \tag{5.5}$$

Here, x and y subscripts denote the two polarizations, P is the optical signal power, $C_{m,n}$ are the perturbation coefficients with m and n denoting the symbol index relative to the current symbol, and $A_{k,x/y}$ is the transmitted symbol. Equations (5.4) and (5.5) imply that the nonlinear field is a linear combination of triplets consisting of transmitted symbols, weighted by coefficients $C_{m,n}$. The perturbation coefficients can be numerically calculated as [126]:

$$C_{m,n} = ik \int_{o}^{L} dz\gamma(z) f(z) \\ \times \int dt g^{(0)*}(z,t) g^{(0)}(z, t-mT) g^{(0)}(z, t-nT) g^{(0)*}(z, t-(n+m)T). \quad (5.6)$$

where, $\gamma(z)$ denotes the fiber nonlinear coefficient, k is the scaling factor, $f(z)$ describes the power distribution profile along the link, T is the symbol period, $g^{(0)}(0,t)$ is the pulse shape with zero accumulated dispersion ($i.e.$, $z=0$), and $g^{(0)}(z,t)$ is the dispersed pulse shape corresponding to a fiber length z, which is calculated according to:

$$g^{(0)}(z,t) = ifft\left\{fft\left[g^{(0)}(0,t)\right] \times \exp\left[-i\beta_2 (2\pi f)^2 z/2\right]\right\}. \quad (5.7)$$

where, $(i)fft[\cdot]$ denotes the (inverse) Fourier transform, f is the frequency, and β_2 is the first-order group velocity dispersion [126]. Figure 5.1 demonstrates the normalized perturbation coefficients after 480 km of single-mode optical fiber (SMF).

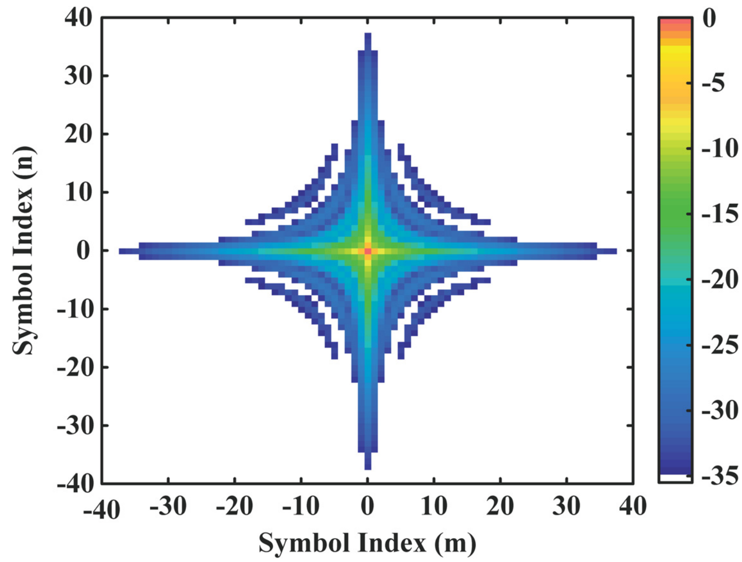

Fig. 5.1 Normalized perturbation coefficients after 480 km of SMF ($|C_{m,n}|/C_{0,0} \leq -35\ dB$), with a span length equals of 80 km with lumped amplification and 32 Gbaud root-raised-cosine pulse shaped with a 1% roll-off factor.

Assuming Gaussian pulses and ignoring attenuation, analytical expressions for the nonlinear coefficients in terms of the exponential integral function exist [58]:

$$C_{m,n} = j\frac{8}{9}\frac{\gamma\tau^2}{\sqrt{3}\,|\beta_2|}\frac{1}{2}E_1\left(\frac{(m-n)^2T^2\tau^2}{3|\beta_2|^2L^2}\right) \quad m\,\mathrm{or}\,n = 0 \tag{5.8}$$

$$C_{m,n} = j\frac{8}{9}\frac{\gamma\tau^2}{\sqrt{3}\,|\beta_2|}E_1\left(-j\frac{mnT^2}{\beta_2 L}\right) \quad m,n \neq 0 \tag{5.9}$$

where, τ is the pulse-width, T is the symbol period, L is the transmission distance, m and n are the symbol indices, and $E_1(\centerdot)$ is the exponential integral function [130]. It can be seen that for all $m,n \neq 0$:

$$C_{m,n} = C_{n,m} = C_{-m,-n} = C_{-n,-m} \tag{5.10}$$

$$C_{m,n} = C_{n,m} = -C^*_{m,-n} = -C^*_{-n,m} \tag{5.11}$$

Here, it is evident that $C_{m,n}$ varies with only a single parameter $q = m \cdot n$, and thus all pairs of (m,n) could share the same coefficient C_q as long as their product equals a unique q. It should be noted that in the case of other symmetric pulses the perturbation coefficients still satisfy the properties stated in Eqs. (5.10) and (5.11). We also verified Eqs. (5.10) and (5.11) by numerical integration of Eq. (5.6) for a root-raised-cosine (RRC) pulse shaping filter. For a more efficient implementation of the algorithm, quantization of the coefficients (i.e., combining multiple terms with similar perturbation coefficients) can be used to reduce the number of complex multiplications [59, 60]. However, there is an expected trade-off: fewer quantization levels lead to lower complexity, at the expense of reduced performance. In this case, Eqs. (5.4) and (5.5) can be simplify as:

$$\Delta A_{0,x} = P^{3/2} \sum_{k=1}^{N_k} C_k \left(\sum_{\forall m,n \in C_k} A_{n,x} A^*_{m+n,x} A_{m,x} + \sum_{\forall m,n \in C_k} A_{n,y} A^*_{m+n,y} A_{m,x} \right) \tag{5.12}$$

$$\Delta A_{0,y} = P^{3/2} \sum_{k=1}^{N_k} C_k \left(\sum_{\forall m,n \in C_k} A_{n,y} A^*_{m+n,y} A_{m,y} + \sum_{\forall m,n \in C_k} A_{n,x} A^*_{m+n,x} A_{m,y} \right) \tag{5.13}$$

where, N_k is the total number of quantization levels and the range of C_k was obtained using the following formula:

$$\begin{gathered} m,n \in C_k \qquad \text{if} \qquad C_{k,lower} \leq C_{m,n} \leq C_{k,upper} \\ C_k = \frac{C_{k,upper} + C_{k,lower}}{2}. \end{gathered} \tag{5.14}$$

Unfortunately, conventional uniform quantization does not provide optimum performance [130], and optimized quantization levels and quantized values of C_k, have to be determined. The exhaustive search method with minimum mean square error (MMSE) as criteria for the level estimation has been proposed for offline calculation of optimum quantized perturbation coefficients and the corresponding quantization levels [131].

In cases where a single fiber type is deployed throughout the transmission path, and assuming a symmetric power profile and dispersion map (which can be readily obtained by 50% CD pre-compensation at the transmitter), it can be shown that perturbation coefficients become purely imaginary-valued [58–60]. This reduces the computational complexity by replacing the complex multipliers with real multipliers and by reducing the nonlinear channel memory. However, this approach has a limited practical use when it comes to reconfigurable mesh optical networks. In addition, most of the fibers in optical networks come from legacy networks, which contain different fiber types (ITU-T G.652, G.653, and G.655) with widely varying characteristics [132]. Therefore, a symmetric dispersion map cannot be obtained by only performing 50% CD pre-compensation at the transmitter. In addition, for long-haul fiber optic transmissions, CD pre-compensation would largely enhance the signal's peak-to-average power ratio (PAPR), which would not only enhance the nonlinear impairment, but also inevitably increase DAC quantization noise and distortion from clipping noises [133].

5.3 Optimization of Quantized Perturbation Coefficients

In this work, we further investigate the quantization of perturbation coefficients and propose a novel nonlinearity compensator/equalizer based on adaptive quantization of perturbation coefficients instead of using the average value for each quantization region as per Eq. (5.14). For this purpose, we use the DD-LMS algorithm to refine these values, which improves the performance. Rearranging to Eqs. (5.12) and (5.13), equalized symbols can be express as:

$$A_x^{out} = A_x + C_1\Gamma_{x,1} + C_2\Gamma_{x,2} + \cdots \tag{5.15}$$

$$A_y^{out} = A_y + C_1\Gamma_{y,1} + C_2\Gamma_{y,2} + \cdots \tag{5.16}$$

where, we define:

$$\Gamma_{x,k} = \sum_{m,n\in C_k} \left(A_{n,x}A^*_{m+n,x}A_{m,x} + A_{n,y}A^*_{m+n,y}A_{m,x}\right) \tag{5.17}$$

$$\Gamma_{y,k} = \sum_{m,n\in C_k} \left(A_{n,y}A^*_{m+n,y}A_{m,y} + A_{n,x}A^*_{m+n,x}A_{m,y}\right) \tag{5.18}$$

Each C_k is continuously updated based on the stochastic gradient algorithm using the following set of equations:

$$C_{k,x}(p+1) = C_k(p) + \mu\varepsilon_{k,x}(p)\Gamma^*_{x,k}(k) \tag{5.19}$$

$$C_{k,y}(p+1) = C_k(p) + \mu\varepsilon_{k,y}(p)\Gamma^*_{y,k}(k) \tag{5.20}$$

Here, μ is the algorithm step size, p denotes the update step index and $\varepsilon_{k,x/y}$ is the error at p^{th}-step, given by

$$\varepsilon_{x/y}(p) = A^{out}_{x/y}(p) - decision\left\{A^{out}_{x/y}(p)\right\}. \tag{5.21}$$

We point out in the absence of fiber birefringence and noise based on Eqs. (5.4) and (5.5), we have

$$C_{k,x} = C_{k,y} \tag{5.22}$$

Therefore, Eqs. (5.19) and (5.20) can be averaged over two polarizations for better estimation and higher noise rejection. Alternatively, for a more efficient implementation, the adaptation process can be divided between two polarizations where half of the coefficients are updated using the X-polarization, and the remaining coefficients are calculated using the Y-polarization.

5.3.1 Receiver DSP Structure

Figure 5.2 shows the top-level block diagram of the receiver. The DSP code starts with front-end compensation, including the DC removal, inphase quadrature (IQ) imbalance compensation, and optical hybrid IQ orthogonalization using the Gram-Schmidt orthogonalization procedure [8]. Next, the signal was resampled to two samples per symbol and then passed through the overlap-and-save frequency domain CD compensation and laser frequency offset compensation based on the FFT of the signal at the 4th power. Matched filtering was performed in the frequency domain using the same pulse-shaping filter used at the transmitter. Sampling frequency-offset compensation and timing recovery were carried out using a non-data-aided feed-forward symbol-timing estimator [134]. Next, synchronization was performed in order to facilitate data-aided modulation-transparent equalization by conventional correlate and delay algorithms (i.e., Schmidl-Cox) [135]. A training-symbol-aided decision-directed least radius distance (TS-DD-LRD) [136] based fractionally spaced linear equalizer was employed. The equalizer used had 15 taps for fast convergence of the coefficients. The carrier phase was recovered using the superscalar parallelization based phase locked loop (PLL) combined with a maximum likelihood phase estimation [137]. Afterwards, the fiber nonlinearity was compensated using either our novel adaptive nonlinear equalizer or the traditional perturbation based post nonlinearity compensation [58]. The two methods were then compared. Finally, the symbols were mapped to bits and the bit error rate (BER) was counted over 100, 000 bits and a soft-decision forward error correction BER threshold of 2×10^{-2} with a 20% overhead was considered.

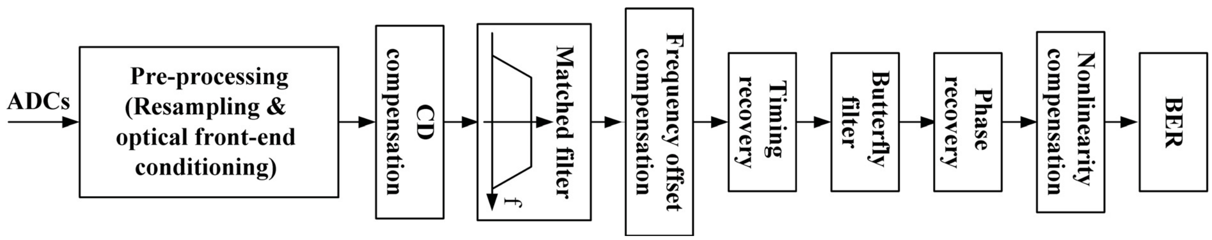

Fig. 5.2 Receiver DSP

5.3.2 Experimental Setup

Figure 5.3 shows the schematic diagram of the experimental setup. The offline DSP at the transmitter side began with four 2-tuple independent pseudo-random bit sequences (PRBS) mapped to 16QAM symbols, followed by pulse shaping at two samples per symbol for each polarization. A Ciena WaveLogic 3 (WL3) line card was employed, which contained four 39.5 GSa/s 6-bit digital-to-analog converter (DACs), a tunable frequency laser source, and a dual-polarization (DP) IQ-modulator. The transmitter laser was operated at 1554.94 nm. The transmitter analog frequency response was compensated using the on-board built-in DSP of the WL3. The output optical signal was then boosted to 23 dBm using an erbium-doped fiber amplifier (EDFA), and subsequently attenuated using a conventional variable optical attenuator (VOA) in order to get a desired optical launch power. The optical signal was then launched into a recirculating loop. This loop consisted of four spans of 80 km of single-mode fiber (SMF-28e+LL), and four inline EDFAs. Each inline EDFA has a noise figure of 5.5 dB. A tunable bandwidth and tunable center wavelength band-pass filter (T-T BPF) was inserted after the 4th span in order to reject the out-of-band amplified spontaneous emission (ASE) noise accumulated during transmission. The gain of the last EDFA is adjusted (increased by 10 dB compared to the other EDFAs) in order to compensate for losses occurring inside the recirculating loop including switches, couplers and the band-pass filter.

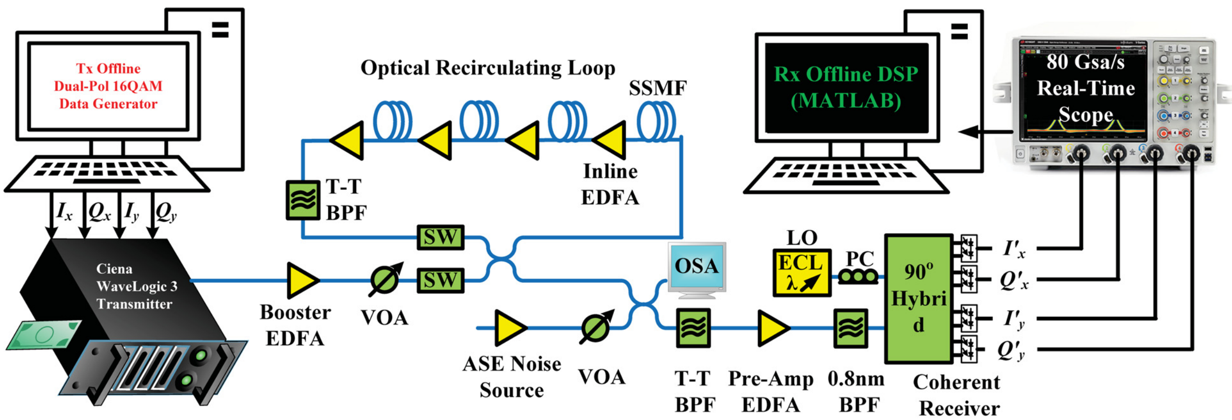

Fig. 5.3 Experimental setup. EDFA: Erbium-doped fiber amplifiers, BPF: Band-pass filter, T-T BPF: Tunable bandwidth and tunable center frequency band-pass filter, LO: Local oscillator, PC: Polarization controller, SW: Switch.

At the receiver side, an optical spectrum analyzer (OSA) was used in order to measure the signal optical signal-to-noise ratio (OSNR) at 0.5 nm resolution bandwidth which was then converted to a 0.1 nm noise bandwidth. The gain of the pre-amplifier EDFA was adjusted to ensure that the signal power reaching the coherent receiver was held constant at 5 dBm. Finally, a 0.8 nm BPF was used to filter out the out-of-band amplified spontaneous emission noise generated by the pre-amplifier. At the polarization-diversity 90° optical hybrid, the signal was mixed with a 15.5 dBm local oscillator (LO) light from an external-cavity laser (ECL) with a linewidth of 100 kHz. The beating outputs were passed through four balanced photodetectors. A 4-channel real-time oscilloscope sampled the signal at a sampling rate of 80 GSa/s and digitized it with 8-bit resolution.

5.3.3 Discussion and Results

In this section, the performance of proposed nonlinear equalizer against perturbation based nonlinear compensation at the receiver is investigated. All DSP blocks and parameters are identical for all schemes except for the nonlinearity compensation block. For all measurements, a root-raised-cosine (RRC) filter with a roll-off factor of 0.01 is chosen as a pulse-shaping filter for 32-Gbaud dual-polarization (DP) 16QAM transmissions.

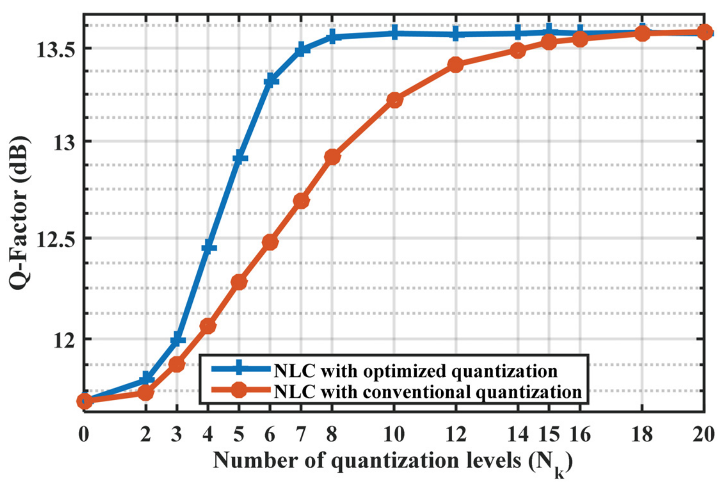

Fig. 5.4 Q-factor after nonlinearity compensation with optimized and conventional (linear) quantization of perturbation coefficients.

Figure 5.4 shows the Q-factor after 2560 km of SMF transmission for different numbers of quantization levels at the optimum nonlinear launch power of 2 dBm (as shown in Fig. 5.5). For 5 quantization levels, our optimized quantization method outperforms the conventional linear quantization by more than 0.5 dB in terms of

Q-factor improvement. With only 8-levels, the DD-LMS based quantization scheme reaches its maximum performance and the nonlinearity compensation gain increases only slightly with more quantization levels. On the other hand, the linear method requires 15 quantization levels for the same NLC gain, and the Q-factor shows a stronger dependence on the number of quantization levels.

Figure 5.5 shows the Q-factor after transmission of 2560 km for different launch powers. Here, the number of quantization levels equals was fixed to 8 for both the optimized and the linear quantization methods, and the optimum lunch power increases by 2 dBm for both nonlinearity compensation methods. Furthermore, the Q-factor improved by 0.85 and 0.3 dB, and the nonlinearity tolerance improved by 2.2 and 3.35 dBm for the cases of linear and optimized quantization of perturbation coefficients, respectively.

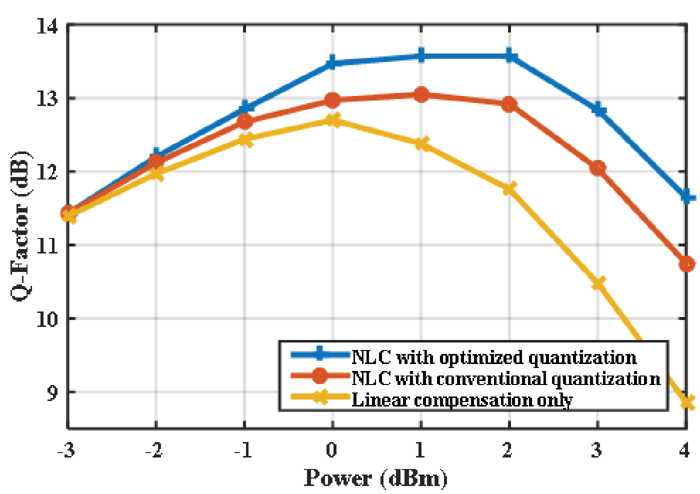

Fig. 5.5 Q-factor versus launch power for linear compensation and nonlinearity compensation with optimized and linear quantization of perturbation coefficients ($N_k = 8$).

Figure 5.6 shows convergence of optimized quantized perturbation coefficients over time, when the number of quantization levels is set to 8. It can be seen that rapid convergence can be achieved even in the extreme case of initializing the DD-LMS algorithm with zeros. We point out that the nonlinear effect is not a time-varying effect and therefore adaptation of perturbation coefficients can be terminated after convergence is obtained. Subsequently, the average steady state perturbation coefficient values can be used for nonlinear compensation and these optimum coefficients can be stored in memory for future use.

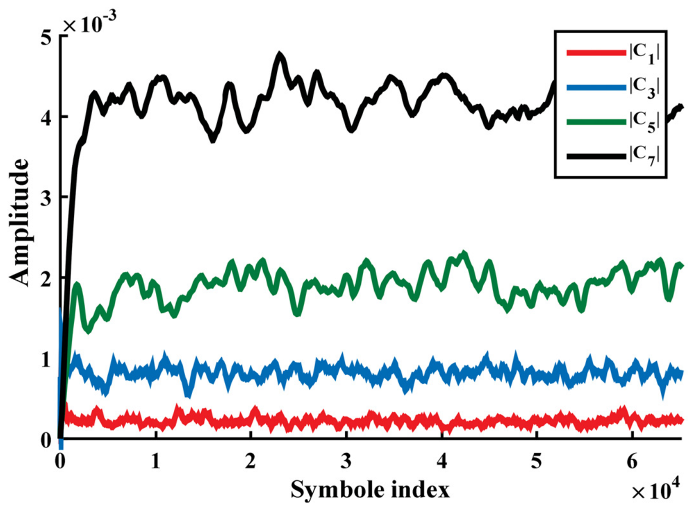

Fig. 5.6 Convergence of adaptive perturbation coefficients over time($N_k = 8$).

5.4 Adaptive Nonlinear Filter Equalization Technique

Assuming linear impairments are compensated by conventional single carrier DSP [8], the details of proposed equalizer are as follows. After rearranging Eqs. (5.1) and (5.2) with respect to Eqs. (5.12) and (5.13), the output of the nonlinear equalizer can be express as:

$$A_x^{out} = A_x + C_1\Gamma_{x,1} + C_2\Gamma_{x,2} + \cdots + C_1{}'\Gamma'{}_{x,1} + C_2{}'\Gamma'{}_{x,2} + \cdots \tag{5.23}$$

$$A_y^{out} = A_y + C_1\Gamma_{y,1} + C_2\Gamma_{y,2} + \cdots + C_1{}'\Gamma'{}_{y,1} + C_2{}'\Gamma'{}_{y,2} + \cdots \tag{5.24}$$

where we define:

$$\Gamma_{x,k} = \sum_{m,n \in C_k} A_{n,x} A^*_{m+n,x} A_{m,x} + A_{n,y} A^*_{m+n,y} A_{m,x} \quad \& \quad \Gamma'_{x,k} = \sum_{m \in C'_k} A_{0,y} A^*_{m,y} A_{m,x} \tag{5.25}$$

$$\Gamma_{y,k} = \sum_{m,n \in C_k} A_{n,y} A^*_{m+n,y} A_{m,y} + A_{n,x} A^*_{m+n,x} A_{m,y} \quad \& \quad \Gamma'_{y,k} = \sum_{m \in C'_k} A_{0,x} A^*_{m,x} A_{m,y} \tag{5.26}$$

Equations (5.25) and (5.26) imply that the nonlinear equalizer output can be expressed as a linear combination of symbol triplet sums i.e., $\Gamma_{x/y,k}$ $(m, n \neq 0)$ and $\Gamma'_{x/y,k}$ $(n = 0)$. The motivation to split the sums into two different linear combinations of $\Gamma_{x/y,k}$ and $\Gamma'_{x/y,k}$ lies in the fact that C'_k is always purely imaginary according to Eq. (5.6), whereas C_k is generally a complex number. Based on adaptive filter theory, each C_k and C'_k can be learned and continuously updated utilizing the stochastic gradient algorithm using the following set of equations:

$$C_{k,x/y}(p+1) = C_k(p) + \mu \varepsilon_{k,x/y}(p) \Gamma^*_{x/y,k}(k) \tag{5.27}$$

$$C'_{k,x/y}(p+1) = C'_k(p) + i \cdot imag\left\{\mu \varepsilon_{k,x/y}(p) \Gamma'^*_{x/y,k}(k)\right\} \tag{5.28}$$

Here, μ is the algorithm step size, p denotes the update step index and $\varepsilon_{k,x/y}$ is the error at pth step, given by

$$\varepsilon_{x/y}(p) = A^{out}_{x/y}(p) - decision\left\{A^{out}_{x/y}(p)\right\}. \tag{5.29}$$

Similar to what was shown in the previous section, C_k and C'_k are the same for both polarizations. Therefore, for a more efficient implementation, the adaptation process can be divided between two polarizations, where half of the coefficients are updated using x-polarization, and the remaining coefficients are calculated using y-polarization.

In order to identify indices of triplet symbols, which constitute the triplet sums (i.e., $\Gamma_{x/y,k}$ *or* $\Gamma'_{x/y,k}$), the nonlinear channel memory length has to be determined first. Pulse broadening induced by chromatic dispersion leads to multiple pulse collisions in an optical fiber. These pulses interact with each other due to fiber Kerr effect and induce nonlinear distortion on the transmitted symbols. Therefore, the maximum nonlinear memory of the fiber is highly related to the CD-induced pulse broadening (normalized by symbol length) expressed by [8]:

$$n_{\max}^{CD} = \frac{\Delta T}{T} = \frac{B_W \frac{c}{f_0^2} \cdot \int_0^{L_{tot}} D(z)dz}{T} \tag{5.30}$$

Here, $D(z)$and L_{tot} denote the dispersion parameters and total link length, respectively, and B_w, T, f_0 and c are the bandwidth of the signal, the symbol duration, the center frequency of the channel of interest, and the speed of light, respectively. At the launch point, accumulated dispersion and channel nonlinear memory are equal to zero. However, as a pulse propagates down the fiber, CD increases the linear and nonlinear channel memory. At the receiver, it equals to $n_{\max}^{CD}$. Therefore, we use half of the maximum pulse broadening as an approximation for the effective fiber nonlinearity memory i.e.,

$$n_{eff}^{NL} = \left\lfloor n_{\max}^{CD}/2 \right\rfloor . \tag{5.31}$$

where, $\lfloor . \rfloor$ denotes the floor operator. We point out that accumulated dispersion can be easily extracted from the CD compensation equalizer or any CD monitoring algorithms [138]. In addition, fiber nonlinearity memory can be set manually based on acceptable computational complexity and available DSP resources. Based on properties extracted from Eqs. (5.11) and (5.10), we uniformly group symbols into $N_1 + 2N_2$ sets of indices (N_1 sets for $n = 0$ corresponding to C_k and $2N_2$ sets for $m, n \neq 0$ corresponding to C'_k indices as follow:

$$\tau_i = \{(m,0)|m \in \mathbb{Z} - \{0\} \text{ and } m_i \leq |m| < m_{i+1}, \\ m_i = \left\lfloor \frac{i \cdot n_{eff}^{NL}}{N_1} \right\rfloor \text{ and } i = 0,1,....,,N_1\} \tag{5.32}$$

$$\tau'_i = \{(m,n)|m,n \in \mathbb{Z} - \{0\} \text{ and } q_i \leq m \cdot n < q_{i+1}, \\ q_i = \left\lfloor \frac{i \cdot n_{eff}^{NL}}{N_2} \right\rfloor \text{ and } i = -N_2, -N_2+1, ..., N_2\}. \tag{5.33}$$

where, $\lfloor . \rfloor$ denotes the floor operator. Note that, for τ'_i, in accordance with Eq. (5.9) the product of m and n (i.e. $q = m \cdot n$) is used for partitioning the symbols. The maximum value for q is n_{eff}^{NL}. Also for τ'_i and $i = -N_2, -N_2+1, \cdots, 0$ we have $m \cdot n < 0$ which corresponds to triplets with the first two indices in 1st and 3rd quadrature whereas $i = 0, 1, \cdots, N_2$ results in $m \cdot n > 0$ and similar sets of indices in 2nd and 4th quadrature. In this case and based on Eq. (5.11), for the corresponding perturbation coefficients, we have $C'_k = -C'^*_{N_2+k}$. We used this property and averaging to improve estimates of the perturbation coefficients. Figure 5.7 shows all symbol indices that have been used in our nonlinearity compensation algorithm and the perturbation based NLC when $max\{(|C_{m,n}|/C_{0,0})\} < -35$ dB. We observe that the proposed algorithm uses similar indices for adaptive perturbation nonlinearity compensation. Furthermore, we numerically integrated Eq. (5.6) for different system parameters, and observed that in all cases, our nonlinear equalizer uses a smaller set of triplet's indices in comparison to the perturbation based NLCs [59]. Therefore, the proposed algorithm should have similar computational complexity to the perturbation based NLCs [58, 59].

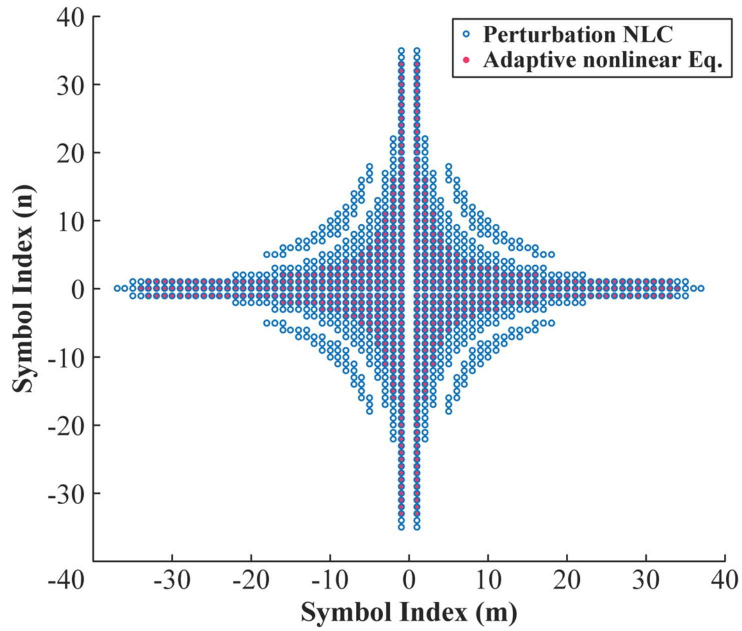

Fig. 5.7 Symbol indices for the perturbation based nonlinear compensation and the proposed adaptive nonlinear equalizer after 480 km of SMF.

We calculated the total number of total symbol triplets for our nonlinear equalizer as follow:

$$4 \cdot \sum_{n=1}^{n_{eff}^{NL}-1} \left\lfloor \frac{(n_{eff}^{NL}-1)}{n} \right\rfloor + 2n_{eff}^{NL} - 1 \approx (n_{eff}^{NL}-1) \cdot log(n_{eff}^{NL}-1) + 3n_{eff}^{NL} - 1. \tag{5.34}$$

In comparison to previously studied nonlinear equalizers [58–60], the total number of triplet indices is reduced from $\left(n_{eff}^{NL}\right)^3$ to $(n_{eff}^{NL}-1) \cdot log(n_{eff}^{NL}-1)$, which is smaller by more than an order of magnitude.

5.4.1 Discussion and Results

In this section, we investigate the performance of proposed nonlinear equalizer against perturbation based nonlinear compensation at the receiver. All DSP blocks, parameters and transmission setup are identical for all schemes except for the nonlinearity compensation block and details are discussed in Sections 5.3.1 and 5.3.2. Also, there are 25 adaptive coefficients for the nonlinear equalizer. Specifically, N_1 and N_2 are equal to 5 and 10 respectively. We have investigated the performance of the perturbation based NLC using two different implementations: 1) without quantization of coefficients and 2) with uniform quantization of perturbation coefficients into 15 coefficients. In the experiment, the performance is investigated at 1 dBm launch power after 2560 km of fiber.

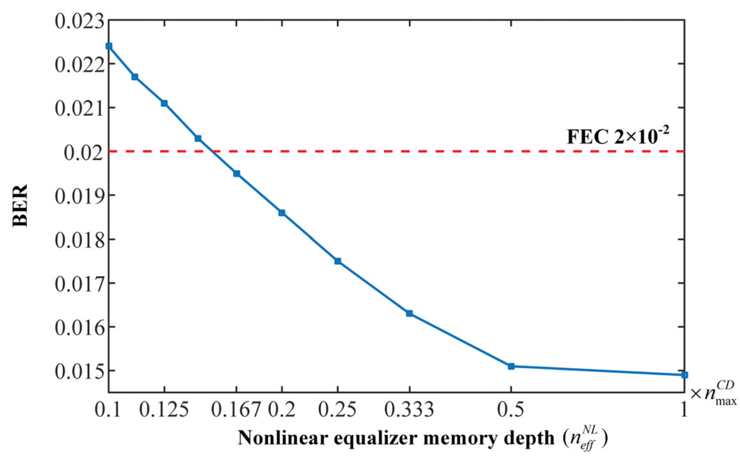

Fig. 5.8 Experimental BER versus nonlinear equalizer depth (normalized by maximum CD-induced pulse broadening) for 32 Gbaud SC-DP-16QAM after 2560 km and 1 dBm launch power.

Figure 5.8 summarizes the BER versus nonlinear equalizer memory depth curves for 32 Gbaud DP-16QAM. The equalizer memory, n_{eff}^{NL}, is normalized by the maximum CD-induced pulse broadening $n_{\max}^{CD}$. As shown in both figures, a negligible penalty is observed when $n_{eff}^{NL} = n_{\max}^{CD}/2$; and by further decreasing the memory depth the performance decreases significantly. This justifies our motivation for Eq. (5.31). In addition, it should be noted that in the case that $n_{\max}^{CD}$is unknown at the receiver, the equalizer memory can be set manually by starting from a small n_{eff}^{NL} and gradually increasing the value until the desired performance is reached.

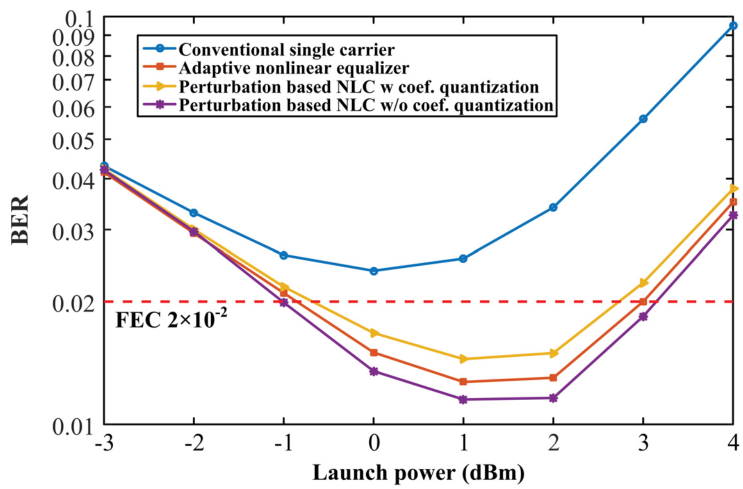

Fig. 5.9 Experimental BER versus launch power for 32 Gbaud SC-DP-16QAM after 2560 km.

Next, we investigated the BER under different launch powers. The investigated distance is 2560 km. As shown in Fig. 5.9, when the power launched into the fiber is low, transmission is mainly limited by linear impairments and the BER is approximately the same for all algorithms. However, as the launch power increases, fiber nonlinearities become more significant and nonlinear compensation enables a lower BER than the conventional single carrier signal. The improvement is particularly significant when the launch power is larger than 1 dBm. As demonstrated in Fig. 5.9, the performance of the proposed algorithm is better than (i) the perturbation based NLC with 25 uniform quantized coefficients, and (ii) comparable to more computationally complex perturbation based NLCs without coefficient quantization.

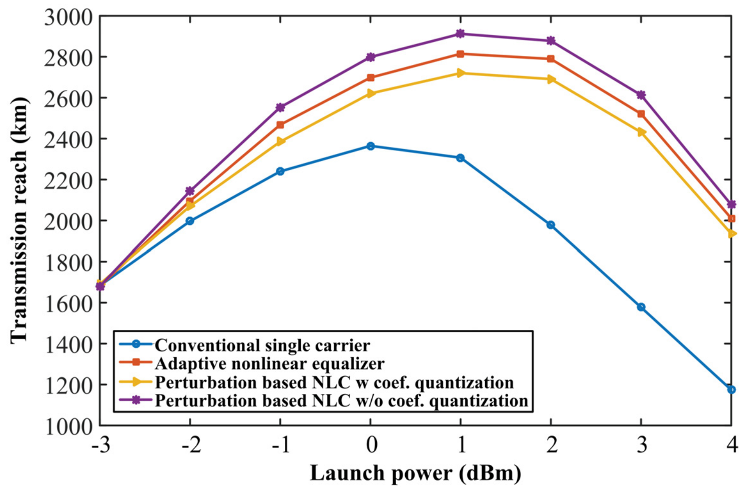

Fig. 5.10 Experimental maximum transmission distance versus launch power for 32 Gbaud SC-DP-16QAM at soft FEC BER threshold of 2×10^{-2}.

Next, we compare the achievable transmission distance for different launch powers with a forward error correction (FEC) pre-set BER threshold of 2×10^{-2}. The results are summarized in Fig. 5.10. In accordance with the results in Fig. 5.9, the achievable transmission distances of conventional single carrier transmission is significantly smaller without nonlinearity compensation. If we investigate the maximum transmission distance of all the systems at their respective optimum launch powers, transmission reach increases from 2365 km for only linear compensation to 2818, 2726 and 2904 km for adaptive nonlinear equalizer and perturbation based NLCs with and without coefficients quantization, respectively. In addition, the optimum launch power increases by 1 dB with fiber nonlinearity compensation.

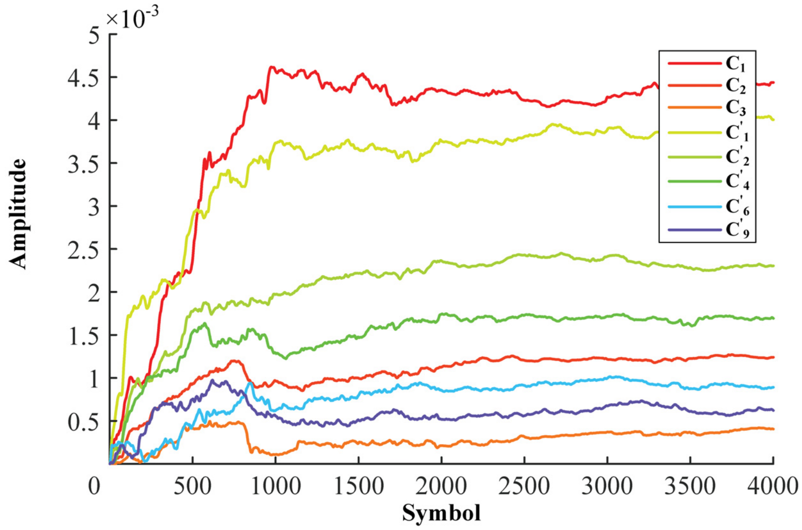

Fig. 5.11 Convergence of adaptive perturbation coefficients over time.

Finally, Fig. 5.11 shows convergence of the adaptive nonlinear equalizer over time. Equations (5.8) and (5.9) can be used to initialize the equalizer. Here, we used zero for the initial adaptive nonlinear coefficient values. We used a large step size at the beginning of the training sequence to achieve fast convergence. After 1000 and 2000 symbol equalization, the step size was divided by two and the algorithm switched to decision-directed mode. In contrast to previously proposed nonlinear equalizers [58], grouping multiple nonlinear triplets removed the requirement to use DD-LMS with multiple iterations per symbol and suboptimal convergence condition in order to increase the convergence rate and equalizer stability.

5.5 Conclusion

We proposed and experimentally demonstrated optimized perturbation based nonlinearity compensation and a novel adaptive low-complexity nonlinear equalizer. The proposed equalizers operate at one sample per symbol, and require only one computation step. In addition, it allows for compensation of nonlinear and linear impairments independently.

In order to further reduce the complexity and simplify implementation, we proposed a decision-directed least mean square (DD-LMS) algorithm for optimization of quantized perturbation coefficients for the fiber nonlinearity compensation. Our method shows robust tolerance to aggressive quantization. Furthermore, we have experimentally demonstrated that the number of quantization levels can be reduced from 15 to 8 after 2560 km single-mode fiber transmission when compared to the conventional linear quantization scheme.

In comparison to perturbation based nonlinearity compensation, our nonlinear equalizer does not require prior calculation of perturbation coefficients, symmetric dispersion maps or a large memory to store all possible perturbation coefficients for reconfigurable network scenarios. We achieved a transmission distance of 2818 km for a 32-Gbaud DP-16QAM system. The proposed equalizer performance is comparable to the perturbation based nonlinearity compensation and previously studied nonlinear equalization methods. In contrast to previously proposed adaptive nonlinear equalizers, our algorithm takes advantage of common symmetries of the perturbation coefficients and avoids replication of operations. In addition, it uses only a few adaptive coefficients by grouping multiple nonlinear terms and dedicating only one coefficient to each group. Finally, its computational complexity is smaller than previously proposed adaptive nonlinear equalization techniques by more than one order of magnitude.

Chapter 6

Conclusion

Coherent detection and digital signal processing greatly expanded the capacity of optical transmission systems. Next generation optical transmission systems are being designed to further push this capacity and hence they should bear the following four features: high speed, long transmission reach, agile, and cost effective. To satisfy this ever-increasing demand of capacity, the cost per bit need to be further reduced for the next generation optical transports. To fulfill this target, several aspects of coherent transmission systems should be thoroughly explored.

6.1 Summary

This thesis explored and reviewed the concepts behind multi-sub-band (MSB) communication, complexity reduction of chromatic dispersion (CD) compensation, CD mitigation and fiber nonlinearity compensation. The major contributions of this thesis are: (1) the first complete experimental demonstrations of multi-sub-band reduced-guard-interval orthogonal frequency-division multiplexing (MSB-RGO-OFDM) commutation technique, which reduces the required overhead and computational complexity in coherent optical OFDM systems, and (2) the extension and detailed analysis of multi-sub-banding to single carrier systems and their associated digital signal processing (DSP) algorithms for next generation agile and spectrally efficient transmission networks. In addition, the application of multi-band signal processing for crosstalk compensation between neighboring sub-band and methods for a more efficient implementation were also studied. Finally, the perturbation based fiber nonlinearity compensation technique was optimized, and a novel adaptive and low complexity equalizer for inter-channel nonlinear effects was developed. The key conclusions are organized as follows.

In Chapter 1, the new era in optical communication networks arising from rapid growth in traffic was discussed. The challenges facing fiber optical transmission systems as well as key features required for the next generation fiber optical transmission systems was reviewed. Then, a brief history and state of the art of fiber optical transmission systems was provided. Finally, the motivations and contributions of this thesis for mitigation of linear and nonlinear impairments in coherent optical transmission systems was summarized.

In Chapter 2, the effects of relevant linear and nonlinear impairments in the optical fiber channel, including fiber attenuation, amplified spontaneous emission noise, chromatic dispersion (CD), polarization mode dispersion and fiber nonlinearity were briefly described in the context of coherent long-haul transmissions. Then, a generic architecture of coherent optical transmission systems and associated DSP algorithms for mitigating or compensating the impairments was presented. Finally, the DSP algorithms utilized in our coherent transmission systems was described.

In Chapter 3, the concept of filter-bank based multi-sub-band communication were investigated in detail. First, the effect of CD on the OFDM signal was briefly explained.

Afterwards, the principles of MSB communication technique for CD mitigation, including its implementation and mathematical foundation, were reviewed. Finally, the experimental results and comparisons between the MSB-RGI-OFDM performance against the conventional single-carrier modulation formats were presented. At the same total data rate, both systems have comparable performance and transmission reach, whereas the method proposed here allowed for a significant reduction in computational complexity due to the removal of the pre/post CD compensation equalizer.

In Chapter 4, the application of the MSB communication technique in single-carrier modulation format for dispersion mitigation was investigated. MSB techniques offer efficient frequency-domain parallelization and lower computational complexity due to the elimination of the CD compensation from the receiver DSP. Early simulation studies were presented. Finally, experimental results of the filter-bank based multi-sub-band signaling were shown. It was shown that the proposed system offers longer transmission reach, better nonlinearity tolerance, and simplified realization of flexible optical transceivers. This demonstrates the potential of multi-sub-banding for the next generation flexible data-rate adaptive and spectrally efficient high-speed communication systems.

In Chapter 5, perturbation based fiber nonlinearity compensation (PB-NLC) equalization was reviewed. Next, the conventional PB-NLC technique was optimized and a novel adaptive low-complexity nonlinear equalizer was proposed. In the optimized PB-NLC, the complexity was reduced by using a decision-directed least mean square (DD-LMS) algorithm for the optimization of the quantized perturbation coefficients at the receiver. Next, an all adaptive nonlinear equalizer was proposed. This novel technique does not require any prior calculation or detailed knowledge of the transmission system. For efficient implementation, the fiber nonlinearities were compensated independently after the equalization of the linear impairments. Therefore, this algorithm can be easily implemented in currently deployed transmission systems after the conventional linear DSP stack. The complexity of the proposed algorithm is lower than previously studied adaptive nonlinear equalizers by more than an order of magnitude. In addition, this novel algorithm takes advantage of common symmetries of the perturbation coefficients and avoids replication of operations.

6.2 Future Work

Although the research objectives of this thesis have been realized, a number of interesting avenues are still to be explored. In this section, two research directions that will be important for the future of coherent long-haul optical communication are highlighted.

Because of advances in DSP and forward error correction techniques, the capacity of coherent single-mode fiber based optical communication systems are approaching the Shannon limit and is becoming ultimately limited by the fiber nonlinear effects. To further improve the performance of single-carrier systems, the multi-sub-band technique proposed in Chapters 3 and 4 could be combined with other nonlinearity compensation techniques such as digital back propagation and perturbation based nonlinearity equalization schemes. In this thesis, it was shown that in sub-band multiplexing technique dispersion induced delay spread and temporal pulse broadening can be significantly reduced. This results in a much shorter nonlinear channel memory and could be used to further improve the system margins and performance or reduce the computational complexity of nonlinearity compensation. For example, when digital backpropagation is used to compensate the nonlinearity of the MSB signals, the step size could be increased or, for the perturbation based nonlinearity compensation, the number of terms involved in finding the inverse nonlinear channel response can be decreased.

Hence, hardware implementation can be simpler. Therefore, it is of great importance to quantify the savings in the computational complexity of the digital nonlinearity compensation/mitigation algorithms when multi-sub-banding is being used.

The next step of research to satisfy the ever increasing demand in capacity from the Internet is to consider the sharing of common components in transmission systems to reduce the cost per bit. Moreover, the new link infrastructure should be able to be gradually deployed when the capacity of current links becomes exhausted. In the next 3 to 5 years, the optical transceiver capacity is expected to reach a data rate of 1 Tb/s per channel, which requires a parallelized structure with a high integration of transmitters and receivers to accommodate the bandwidth limit of components. This parallel structure, together with the flexible network, results in many new research opportunities. In this thesis, multi-sub-band signaling technique to achieve higher DSP efficiency as well as a simplified parallelization was discussed in Chapter 4. In Chapter 5, it was discussed that the flexible smart optical transceivers (with reconfigurable rate and modulation format) can be efficiently realized using digital sub-banding approach to realize a continuous adjustment in spectral efficiency. In addition, multi-band signal processing and equalization technique can be developed for a more efficient implementation. Overall, the advances in optical communication and signal processing has reshaped the world in the past decade, and it is going to be even more influential in the future.

References

[1] Cisco, "Cisco Global Cloud Index: Forecast and Methodology, 2014-2019," 2015.

[2] R. E. Wagner and R. A. Linke, "Heterodyne lightwave systems: moving towards commercial use," *LCS, IEEE*, vol. 1, no. 4, pp. 28–35, 1990.

[3] G. P. Agrawal, *Lightwave technology: telecommunication systems*. John Wiley & Sons, 2005.

[4] F. Kapron, D. Keck, and R. Maurer, "Radiation losses in glass optical waveguides," *Applied Physics Letters*, vol. 17, no. 10, pp. 423–425, 1970.

[5] I. Hayashi, M. Panish, P. Foy, and S. Sumski, "Junction lasers which operate continuously at room temperature," *Applied Physics Letters*, vol. 17, no. 3, pp. 109–111, 1970.

[6] K. Kao and G. A. Hockham, "Dielectric-fibre surface waveguides for optical frequencies," *Electrical Engineers, Proceedings of the Institution of*, vol. 113, no. 7, pp. 1151–1158, 1966.

[7] R. J. Sanferrare, "Terrestrial lightwave systems," *AT&T technical journal*, vol. 66, no. 1, pp. 95–107, 1987.

[8] S. J. Savory, "Digital coherent optical receivers: algorithms and subsystems," *Selected Topics in Quantum Electronics, IEEE Journal of*, vol. 16, no. 5, pp. 1164–1179, 2010.

[9] W. Shieh and I. Djordjevic, *OFDM for optical communications*. Academic Press, 2009.

[10] P. J. Winzer and R.-J. Essiambre, "Advanced modulation formats for high-capacity optical transport networks," *Journal of Lightwave Technology*, vol. 24, no. 12, pp. 4711–4728, 2006.

[11] C. Laperle, B. Villeneuve, Z. Zhang, D. McGhan, H. Sun, and M. O Sullivan, M.Sullivan, "Wavelength division multiplexing (WDM) and polarization mode dispersion (PMD) performance of a coherent 40Gbit/s dual-polarization quadrature phase shift keying (DP-QPSK) transceiver," in *National Fiber Optic Engineers Conference*, p. PDP16, Optical Society of America, 2007.

[12] G. Charlet, J. Renaudier, H. Mardoyan, P. Tran, O. B. Pardo, F. Verluise, M. Achouche, A. Boutin, F. Blache, J.-Y. Dupuy, *et al.*, "Transmission of 16.4-bit/s capacity over 2550 km using PDM QPSK modulation format and coherent receiver," in *National Fiber Optic Engineers Conference*, p. PDP3, Optical Society of America, 2008.

[13] X. Zhou, J. Yu, M.-F. Huang, Y. Shao, T. Wang, P. Magill, M. Cvijetic, L. Nelson, M. Birk, G. Zhang, *et al.*, "32Tb/s (320x114Gb/s) PDM-RZ-8QAM transmission over 580km of SMF-28 ultra-low-loss fiber," in *National Fiber Optic Engineers Conference*, p. PDPB4, Optical Society of America, 2009.

[14] X. Zhou, J. Yu, M.-F. Huang, Y. Shao, T. Wang, L. Nelson, P. Magill, M. Birk, P. I. Borel, D. W. Peckham, *et al.*, "64-Tb/s (640x107-Gb/s) PDM-36QAM transmission

over 320km using both pre-and post-transmission digital equalization," in *National Fiber Optic Engineers Conference*, p. PDPB9, Optical Society of America, 2010.

[15] D. Qian, M. F. Huang, E. Ip, Y. K. Huang, Y. Shao, J. Hu, and T. Wang, "101.7-Tb/s (370x294-Gb/s) PDM-128QAM-OFDM transmission over 3x55-km SSMF using pilot-based phase noise mitigation," in *National Fiber Optic Engineers Conference*, p. PDP16, 2011.

[16] X. Liu, S. Chandrasekhar, T. Lotz, P. Winzer, H. Haunstein, S. Randel, S. Corteselli, B. Zhu, and D. Peckham, "Generation and FEC-decoding of a 231.5-Gb/s PDM-OFDM signal with 256-iterative-polar-modulation achieving 11.15-b/s/Hz intrachannel spectral efficiency and 800-km reach," in *Optical Fiber Communication Conference*, pp. PDP5B–3, Optical Society of America, 2012.

[17] G. Raybon, A. Adamiecki, P. Winzer, C. Xie, A. Konczykowska, F. Jorge, J.-Y. Dupuy, L. L. Buhl, C. Sethumadhavan, S. Draving, *et al.*, "Single-carrier 400G interface and 10-channel WDM transmission over 4800 km using all-ETDM 107-Gbaud PDM-QPSK," in *Optical Fiber Communication Conference*, pp. PDP5A–5, Optical Society of America, 2013.

[18] J.-X. Cai, H. Zhang, H. G. Batshon, M. Mazurczyk, O. Sinkin, Y. Sun, A. Pilipetskii, and D. Foursa, "Transmission over 9,100 km with a capacity of 49.3 Tb/s using variable spectral efficiency 16 QAM based coded modulation," in *Optical Fiber Communication Conference*, pp. Th5B–4, Optical Society of America, 2014.

[19] J.-X. Cai, H. G. Batshon, M. Mazurczyk, H. Zhang, Y. Sun, O. V. Sinkin, D. Foursa, and A. N. Pilipetskii, "64QAM based coded modulation transmission

over transoceanic distance with¿ 60 Tb/s capacity," in *Optical Fiber Communication Conference*, pp. Th5C–8, Optical Society of America, 2015.

[20] M. G. Taylor, "Coherent detection method using DSP for demodulation of signal and subsequent equalization of propagation impairments," *Photonics Technology Letters, IEEE*, vol. 16, no. 2, pp. 674–676, 2004.

[21] "Verizon, Nortel light first commercial 100G wave," tech. rep., available at http://www.telecomasia.net/content/verizon-nortel-light-first-commercial-100g-wave, 2009.

[22] P. Winzer, "Beyond 100G ethernet," *Communications Magazine, IEEE*, vol. 48, no. 7, pp. 26–30, 2010.

[23] T. A. Strasser and J. Taylor, "ROADMS unlock the edge of the network," *Communications Magazine, IEEE*, vol. 46, no. 7, pp. 146–149, 2008.

[24] D. L. McGhan, W. Leckie, and C. Chen, "Reconfigurable coherent transceivers for optical transmission capacity and reach optimization," in *Optical Fiber Communication Conference*, pp. OW4C–7, Optical Society of America, 2012.

[25] H. Y. Choi, T. Tsuritani, and I. Morita, "BER-adaptive flexible-format transmitter for elastic optical networks," *Optics express*, vol. 20, no. 17, pp. 18652–18658, 2012.

[26] G.-H. Gho and J. M. Kahn, "Rate-adaptive modulation and coding for optical fiber transmission systems," *Journal of Lightwave Technology*, vol. 30, no. 12, pp. 1818–1828, 2012.

[27] X. Zhou, L. E. Nelson, and P. Magill, "Rate-adaptable optics for next generation long-haul transport networks," *Communications Magazine, IEEE*, vol. 51, no. 3, pp. 41–49, 2013.

[28] O. Gerstel, M. Jinno, A. Lord, and S. B. Yoo, "Elastic optical networking: A new dawn for the optical layer?," *Communications Magazine, IEEE*, vol. 50, no. 2, pp. s12–s20, 2012.

[29] M. Jinno, T. Ohara, Y. Sone, A. Hirano, O. Ishida, and M. Tomizawa, "Elastic and adaptive optical networks: possible adoption scenarios and future standardization aspects," *Communications Magazine, IEEE*, vol. 49, no. 10, pp. 164–172, 2011.

[30] A. Davis, S. Wright, M. Pettitt, J. King, and K. Richards, "Coherent optical receiver for 680 Mbit/s using phase diversity," *Electronics Letters*, vol. 22, no. 1, p. 9, 1986.

[31] T. Okoshi, "Recent advances in coherent optical fiber communication systems," *Journal of Lightwave Technology*, vol. 5, no. 1, pp. 44–52, 1987.

[32] A. Davis, M. Pettitt, J. King, and S. Wright, "Phase diversity techniques for coherent optical receivers," *Journal of Lightwave Technology*, vol. 5, no. 4, pp. 561–572, 1987.

[33] L. G. Kazovsky, "Phase-and polarization-diversity coherent optical techniques," *Journal of Lightwave Technology*, vol. 7, no. 2, pp. 279–292, 1989.

[34] P. Schvan, D. Pollex, and T. Bellingrath, "A 22GS/s 6b DAC with integrated digital ramp generator," in *Solid-State Circuits Conference, 2005. Digest of Technical Papers. ISSCC. 2005 IEEE International*, pp. 122–588, IEEE, 2005.

[35] Y. M. Greshishchev, D. Pollex, S.-C. Wang, M. Besson, P. Flemeke, S. Szilagyi, J. Aguirre, C. Falt, N. Ben-Hamida, R. Gibbins, *et al.*, "A 56GS/s 6b DAC in

65nm CMOS with 256× 6b memory," in *2011 IEEE International Solid-State Circuits Conference*, 2011.

[36] P. Schvan, J. Bach, C. Falt, P. Flemke, R. Gibbins, Y. M. Greshishchev, N. Ben-Hamida, D. Pollex, J. Sitch, S.-C. Wang, *et al.*, "A 24GS/s 6b ADC in 90nm CMOS," in *ISSCC*, pp. 544–545, 2008.

[37] M. Chu, P. Jacob, J.-W. Kim, M. R. LeRoy, R. P. Kraft, and J. F. McDonald, "A 40 Gs/s time interleaved ADC using SiGe BiCMOS technology," *Solid-State Circuits, IEEE Journal of*, vol. 45, no. 2, pp. 380–390, 2010.

[38] C. Laperle and M. O'Sullivan, "Advances in high-speed DACs, ADCs, and DSP for optical coherent transceivers," *J. Lightw. Technol*, vol. 32, no. 4, pp. 629–643, 2014.

[39] G. P. Agrawal, *Nonlinear fiber optics*. Academic press, 2007.

[40] T. Li, *Optical fiber communications: fiber fabrication*. Elsevier, 2012.

[41] M. Cvijetic and I. Djordjevic, *Advanced optical communication systems and networks*. Artech House, 2013.

[42] P. Mamyshev and N. Mamysheva, "Pulse-overlapped dispersion-managed data transmission and intrachannel four-wave mixing," *Optics Letters*, vol. 24, no. 21, pp. 1454–1456, 1999.

[43] M. Kuschnerov, T. Bex, and P. Kainzmaier, "Energy efficient digital signal processing," in *Optical Fiber Communication Conference*, pp. Th3E–7, Optical Society of America, 2014.

[44] B. S. G. Pillai, B. Sedighi, K. Guan, N. P. Anthapadmanabhan, W. Shieh, K. J. Hinton, and R. S. Tucker, "End-to-end energy modeling and analysis of long-haul

coherent transmission systems," *Journal of Lightwave Technology*, vol. 32, no. 18, pp. 3093–3111, 2014.

[45] J. N. Damask, *Polarization optics in telecommunications*, vol. 101. Springer Science & Business Media, 2004.

[46] E. Ip and J. M. Kahn, "Digital equalization of chromatic dispersion and polarization mode dispersion," *Journal of Lightwave Technology*, vol. 25, no. 8, pp. 2033–2043, 2007.

[47] S. Ten and M. Edwards, "An Introduction to the Fundamentals of PMD in Fibers," *white paper, avaiable from:¡ www.corning.com/WorkArea/downloadasset.*, 2006.

[48] R.-J. Essiambre, G. Kramer, P. J. Winzer, G. J. Foschini, and B. Goebel, "Capacity limits of optical fiber networks," *Journal of Lightwave Technology*, vol. 28, no. 4, pp. 662–701, 2010.

[49] P. J. Winzer and R.-J. Essiambre, "Advanced optical modulation formats," *Proceedings of the IEEE*, vol. 94, no. 5, pp. 952–985, 2006.

[50] P. P. Mitra and J. B. Stark, "Nonlinear limits to the information capacity of optical fibre communications," *Nature*, vol. 411, no. 6841, pp. 1027–1030, 2001.

[51] E. Ip and J. M. Kahn, "Compensation of dispersion and nonlinear impairments using digital backpropagation," *Journal of Lightwave Technology*, vol. 26, no. 20, pp. 3416–3425, 2008.

[52] X. Li, X. Chen, G. Goldfarb, E. Mateo, I. Kim, F. Yaman, and G. Li, "Electronic post-compensation of WDM transmission impairments using coherent detection and digital signal processing," *Optics Express*, vol. 16, no. 2, pp. 880–888, 2008.

[53] L. B. Du and A. J. Lowery, "Improved single channel backpropagation for intra-channel fiber nonlinearity compensation in long-haul optical communication systems," *Optics Express*, vol. 18, no. 16, pp. 17075–17088, 2010.

[54] E. F. Mateo, X. Zhou, and G. Li, "Improved digital backward propagation for the compensation of inter-channel nonlinear effects in polarization-multiplexed WDM systems," *Optics Express*, vol. 19, no. 2, pp. 570–583, 2011.

[55] Y. Gao, J. H. Ke, K. P. Zhong, J. C. Cartledge, and S. S.-H. Yam, "Assessment of intrachannel nonlinear compensation for 112 Gb/s dual-polarization 16QAM systems," *Journal of Lightwave Technology*, vol. 30, no. 24, pp. 3902–3910, 2012.

[56] T. Hoshida, L. Dou, W. Yan, L. Li, Z. Tao, S. Oda, H. Nakashima, C. Ohshima, T. Oyama, and J. C. Rasmussen, "Advanced and feasible signal processing algorithm for nonlinear mitigation," in *Optical Fiber Communication Conference*, pp. OTh3C–3, Optical Society of America, 2013.

[57] Y. Gao, J. C. Cartledge, J. D. Downie, J. E. Hurley, D. Pikula, and S. S.-H. Yam, "Nonlinearity compensation of 224 Gb/s dual-polarization 16-QAM transmission over 2700 km," *Photonics Technology Letters, IEEE*, vol. 25, no. 1, pp. 14–17, 2013.

[58] Z. Tao, L. Dou, W. Yan, L. Li, T. Hoshida, and J. C. Rasmussen, "Multiplier-free intrachannel nonlinearity compensating algorithm operating at symbol rate," *Journal of Lightwave Technology*, vol. 29, no. 17, pp. 2570–2576, 2011.

[59] Y. Gao, J. C. Cartledge, A. S. Karar, S. S.-H. Yam, M. O Sullivan, M.Sullivan, C. Laperle, A. Borowiec, and K. Roberts, "Reducing the complexity of perturbation based nonlinearity pre-compensation using symmetric EDC and pulse shaping," *Optics express*, vol. 22, no. 2, pp. 1209–1219, 2014.

[60] Q. Zhuge, M. Reimer, A. Borowiec, M. O Sullivan, M.Sullivan, and D. V. Plant, "Aggressive quantization on perturbation coefficients for nonlinear pre-distortion," *Proc. OFC/NFOEC2014, paper Tu4D7*, 2014.

[61] G. P. Agrawal, *Fiber-optic communication systems*. Wiley Online Library, 1997.

[62] K. Onohara, Y. Miyata, T. Sugihara, K. Kubo, H. Yoshida, and T. Mizuochi, "Soft decision FEC for 100G transport systems," in *Optical Fiber Communication Conference*, p. OThL1, Optical Society of America, 2010.

[63] R. Schmogrow, S. Ben-Ezra, P. C. Schindler, B. Nebendahl, C. Koos, W. Freude, and J. Leuthold, "Pulse-shaping with digital, electrical, and optical filters: a comparison," *Journal of Lightwave Technology*, vol. 31, no. 15, pp. 2570–2577, 2013.

[64] R. I. Killey, P. M. Watts, V. Mikhailov, M. Glick, and P. Bayvel, "Electronic dispersion compensation by signal predistortion using digital processing and a dual-drive Mach-Zehnder modulator," *IEEE Photonics Technology Letters*, vol. 17, no. 3, pp. 714–716, 2005.

[65] R. Waegemans, S. Herbst, L. Holbein, P. Watts, P. Bayvel, C. Fürst, and R. I. Killey, "10.7 Gb/s electronic predistortion transmitter using commercial FPGAs and D/A converters implementing real-time DSP for chromatic dispersion and SPM compensation," *Optics express*, vol. 17, no. 10, pp. 8630–8640, 2009.

[66] X. Xu, B. Châtelain, Q. Zhuge, M. Morsy-Osman, M. Chagnon, M. Qiu, and D. Plant, "Frequency domain M-shaped pulse for SPM nonlinearity mitigation in coherent optical communications," in *National Fiber Optic Engineers Conference*, pp. JTh2A–38, Optical Society of America, 2013.

[67] X. Xu, Q. Zhuge, B. Châtelain, M. Qiu, M. Chagnon, M. Morsy-Osman, W. Wang, and D. V. Plant, "Nonlinearity-tolerant frequency domain root m-shaped pulse for spectrally efficient coherent transmissions," in *Optical Fiber Communication Conference*, pp. W1G–3, Optical Society of America, 2014.

[68] X. Xu, Q. Zhuge, B. Châtelain, M. Chagnon, M. Morsy-Osman, M. Malekiha, M. Qiu, Y. Gao, W. Wang, and D. V. Plant, "Experimental investigation on the nonlinear tolerance of root m-shaped pulse in spectrally efficient coherent transmissions," *Optics express*, vol. 23, no. 2, pp. 882–894, 2015.

[69] H. Sun, K.-T. Wu, and K. Roberts, "Real-time measurements of a 40 Gb/s coherent system," *Optics Express*, vol. 16, no. 2, pp. 873–879, 2008.

[70] Q. Zhuge, X. Xu, M. Morsy-Osman, M. Chagnon, M. Qiu, and D. Plant, "Time domain hybrid QAM based rate-adaptive optical transmissions using high speed DACs," in *Optical Fiber Communication Conference*, pp. OTh4E–6, Optical Society of America, 2013.

[71] I. Kaminow, T. Li, and A. E. Willner, *Optical fiber telecommunications VB: systems and networks*. Academic press, 2010.

[72] I. Fatadin, S. J. Savory, and D. Ives, "Compensation of quadrature imbalance in an optical QPSK coherent receiver," *Photonics Technology Letters, IEEE*, vol. 20, no. 20, pp. 1733–1735, 2008.

[73] T. Tanimura, S. Oda, T. Tanaka, T. Hoshida, Z. Tao, and J. C. Rasmussen, "A simple digital skew compensator for coherent receiver," *ECOC 2009*, 2009.

[74] S. J. Savory, "Digital filters for coherent optical receivers," *Optics Express*, vol. 16, no. 2, pp. 804–817, 2008.

[75] E. M. Ip and J. M. Kahn, "Fiber impairment compensation using coherent detection and digital signal processing," *Journal of Lightwave Technology*, vol. 28, no. 4, pp. 502–519, 2010.

[76] R. Kudo, T. Kobayashi, K. Ishihara, Y. Takatori, A. Sano, and Y. Miyamoto, "Coherent optical single carrier transmission using overlap frequency domain equalization for long-haul optical systems," *Journal of Lightwave Technology*, vol. 27, no. 16, pp. 3721–3728, 2009.

[77] R. A. Soriano, F. N. Hauske, N. G. Gonzalez, Z. Zhang, Y. Ye, and I. T. Monroy, "Chromatic dispersion estimation in digital coherent receivers," *Journal of Lightwave Technology*, vol. 29, no. 11, pp. 1627–1637, 2011.

[78] Q. Sui, A. P. T. Lau, and C. Lu, "Fast and robust blind chromatic dispersion estimation using auto-correlation of signal power waveform for digital coherent systems," *Journal of Lightwave Technology*, vol. 31, no. 2, pp. 306–312, 2013.

[79] F. M. Gardner, "A BPSK/QPSK timing-error detector for sampled receivers," *IEEE Transactions on communications*, vol. 34, pp. 423–429, 1986.

[80] M. Oerder and H. Meyr, "Digital filter and square timing recovery," *IEEE Transactions on communications*, vol. 36, pp. 605–612, 1988.

[81] T. Nakagawa, M. Matsui, T. Kobayashi, K. Ishihara, R. Kudo, M. Mizoguchi, and Y. Miyamoto, "Non-data-aided wide-range frequency offset estimator for QAM

optical coherent receivers," in *Optical Fiber Communication Conference*, p. OMJ1, Optical Society of America, 2011.

[82] A. Leven, N. Kaneda, U.-V. Koc, and Y.-K. Chen, "Frequency estimation in intradyne reception," *IEEE Photonics Technology Letters*, vol. 6, no. 19, pp. 366–368, 2007.

[83] P. Winzer, A. Gnauck, C. Doerr, M. Magarini, and L. Buhl, "Spectrally efficient long-haul optical networking using 112-Gb/s polarization-multiplexed 16-QAM," *Journal of lightwave technology*, vol. 28, no. 4, pp. 547–556, 2010.

[84] A. Viterbi, "Nonlinear estimation of PSK-modulated carrier phase with application to burst digital transmission," *Information Theory, IEEE Transactions on*, vol. 29, no. 4, pp. 543–551, 1983.

[85] U. Mengali, *Synchronization techniques for digital receivers.* Springer Science & Business Media, 2013.

[86] Z. Wang and G. B. Giannakis, "Wireless multicarrier communications," *Signal Processing Magazine, IEEE*, vol. 17, no. 3, pp. 29–48, 2000.

[87] C. Chen, Q. Zhuge, and D. V. Plant, "Zero-guard-interval coherent optical OFDM with overlapped frequency-domain CD and PMD equalization," *Optics express*, vol. 19, no. 8, pp. 7451–7467, 2011.

[88] X. Liu, S. Chandrasekhar, B. Zhu, P. Winzer, A. H. Gnauck, and D. W. Peckham, "448-Gb/s reduced-guard-interval CO-OFDM transmission over 2000 km of ultra-large-area fiber and five 80-GHz-grid ROADMs," *Journal of Lightwave Technology*, vol. 29, no. 4, pp. 483–490, 2011.

[89] W. Shieh, H. Bao, and Y. Tang, "Coherent optical OFDM: theory and design," *Optics express*, vol. 16, no. 2, pp. 841–859, 2008.

[90] H. Minn, V. K. Bhargava, and K. Letaief, "A robust timing and frequency synchronization for OFDM systems," *Wireless Communications, IEEE Transactions on*, vol. 2, no. 4, pp. 822–839, 2003.

[91] H. Abdzadeh-Ziabari and M. G. Shayesteh, "Robust timing and frequency synchronization for OFDM systems," *Vehicular Technology, IEEE Transactions on*, vol. 60, no. 8, pp. 3646–3656, 2011.

[92] W. Shieh, "Maximum-likelihood phase and channel estimation for coherent optical OFDM," *Photonics Technology Letters, IEEE*, vol. 20, no. 8, pp. 605–607, 2008.

[93] X. Liu and F. Buchali, "Intra-symbol frequency-domain averaging based channel estimation for coherent optical OFDM," *Optics Express*, vol. 16, no. 26, pp. 21944–21957, 2008.

[94] X. Yi, W. Shieh, and Y. Ma, "Phase noise effects on high spectral efficiency coherent optical OFDM transmission," *Journal of Lightwave Technology*, vol. 26, no. 10, pp. 1309–1316, 2008.

[95] R. v. Nee and R. Prasad, *OFDM for wireless multimedia communications*. Artech House, Inc., 2000.

[96] J. A. Bingham, "Multicarrier modulation for data transmission: An idea whose time has come," *Communications Magazine, IEEE*, vol. 28, no. 5, pp. 5–14, 1990.

[97] W. Y. Zou and Y. Wu, "COFDM: An overview," *Broadcasting, IEEE Transactions on*, vol. 41, no. 1, pp. 1–8, 1995.

[98] W. Shieh and C. Athaudage, “Coherent optical orthogonal frequency division multiplexing,” *Electronics letters*, vol. 42, no. 10, p. 1, 2006.

[99] X. Liu, S. Chandrasekhar, and P. J. Winzer, “Digital signal processing techniques enabling multi-Tb/s superchannel transmission: an overview of recent advances in DSP-enabled superchannels,” *Signal Processing Magazine, IEEE*, vol. 31, no. 2, pp. 16–24, 2014.

[100] A. Tolmachev and M. Nazarathy, “Filter-bank based efficient transmission of reduced-guard-interval OFDM,” *Optics express*, vol. 19, no. 26, pp. B370–B384, 2011.

[101] C. Liu, J. Pan, T. Detwiler, A. Stark, Y.-T. Hsueh, G.-K. Chang, and S. E. Ralph, “Super receiver design for superchannel coherent optical systems,” in *SPIE OPTO*, pp. 828405–828405, International Society for Optics and Photonics, 2012.

[102] M. Nazarathy, A. Tolmachev, and S. Ben-Ezra, “Sub-banding DSP for flexible optical transceivers,” in *Transparent Optical Networks (ICTON), 2012 14th International Conference on*, pp. 1–4, IEEE, 2012.

[103] N. Sambo, P. Castoldi, A. D’Errico, E. Riccardi, A. Pagano, M. S. Moreolo, J. M. Fabrega, D. Rafique, A. Napoli, S. Frigerio, *et al.*, “Next generation sliceable bandwidth variable transponders,” *Communications Magazine, IEEE*, vol. 53, no. 2, pp. 163–171, 2015.

[104] M. Nazarathy and A. Tolmachev, “Digitally sub-banded coherent optical OFDM transmission,” in *Optical Fiber Communication Conference*, pp. Tu3G–1, Optical Society of America, 2014.

[105] M. Nazarathy and A. Tolmachev, "Subbanded DSP architectures based on underdecimated filter banks for coherent OFDM receivers: Overview and recent advances," *Signal Processing Magazine, IEEE*, vol. 31, no. 2, pp. 70–81, 2014.

[106] A. Tolmachev and M. Nazarathy, "Low-complexity multi-band polyphase filter bank for reduced-guard-interval coherent optical OFDM," in *Signal Processing in Photonic Communications*, p. SPMB3, Optical Society of America, 2011.

[107] F. J. Harris, C. Dick, and M. Rice, "Digital receivers and transmitters using polyphase filter banks for wireless communications," *Microwave Theory and Techniques, IEEE Transactions on*, vol. 51, no. 4, pp. 1395–1412, 2003.

[108] J. G. Proakis, "Digital communications. 1995," *McGraw-Hill, New York*.

[109] A. Bar, A. Tolmachev, and M. Nazarathy, "In-Service monitoring of chromatic dispersion with filter-bank digitally sub-banded OFDM," *IEEE Photonics Technol. Lett.*, vol. 25, no. 22, pp. 2189–2192, 2013.

[110] Q. Yang, Z. He, Z. Yang, S. Yu, X. Yi, and W. Shieh, "Coherent optical DFT-spread OFDM transmission using orthogonal band multiplexing," *Optics express*, vol. 20, no. 3, pp. 2379–2385, 2012.

[111] N. Kaneda, Q. Yang, X. Liu, S. Chandrasekhar, W. Shieh, and Y.-K. Chen, "Real-time 2.5 GS/s coherent optical receiver for 53.3-Gb/s sub-banded OFDM," *Journal of lightwave technology*, vol. 28, no. 4, pp. 494–501, 2010.

[112] Q. Yang, "Digital signal processing for multi-gigabit real-time OFDM," in *Signal Processing in Photonic Communications*, p. SPMB2, Optical Society of America, 2011.

[113] Q. Zhuge, M. Morsy-Osman, M. Chagnon, X. Xu, M. Qiu, and D. V. Plant, "Terabit bandwidth-adaptive transmission using low-complexity format-transparent digital signal processing," *Optics express*, vol. 22, no. 3, pp. 2278–2288, 2014.

[114] M. Malekiha, I. Tselniker, M. Nazarathy, A. Tolmachev, and D. V. Plant, "Experimental demonstration of low-complexity fiber chromatic dispersion mitigation for reduced guard-interval OFDM coherent optical communication systems based on digital spectrum sub-band multiplexing," *Optics express*, vol. 23, no. 20, pp. 25608–25619, 2015.

[115] X. Liu, P. Winzer, C. Sethumadhavan, S. Randel, and S. Corteselli, "Multiband DFT-spread-OFDM equalizer with overlap-and-add dispersion compensation for low-overhead and low-complexity channel equalization," in *Optical Fiber Communication Conference*, pp. OW3B–2, Optical Society of America, 2013.

[116] J. Munir, A. Mezghani, H. Khawar, I. Slim, and J. A. Nossek, "Chromatic dispersion compensation using filter bank based complex-valued all-pass filter," in *SCC 2015; 10th International ITG Conference on Systems, Communications and Coding; Proceedings of*, pp. 1–6, VDE, 2015.

[117] M. Qiu, Q. Zhuge, M. Chagnon, Y. Gao, X. Xu, M. Morsy-Osman, and D. V. Plant, "Digital subcarrier multiplexing for fiber nonlinearity mitigation in coherent optical communication systems," *Optics express*, vol. 22, no. 15, pp. 18770–18777, 2014.

[118] P. J. Winzer, "High-spectral-efficiency optical modulation formats," *Journal of Lightwave Technology*, vol. 30, no. 24, pp. 3824–3835, 2012.

[119] T. Zeng, "Superchannel transmission system based on multi-channel equalization," *Optics express*, vol. 21, no. 12, pp. 14799–14807, 2013.

[120] R. Dar, M. Shtaif, and M. Feder, “New bounds on the capacity of the nonlinear fiber-optic channel,” *Optics letters*, vol. 39, no. 2, pp. 398–401, 2014.

[121] A. Mecozzi and R.-J. Essiambre, “Nonlinear shannon limit in pseudolinear coherent systems,” *Journal of Lightwave Technology*, vol. 30, no. 12, pp. 2011–2024, 2012.

[122] D. Rafique, J. Zhao, and A. D. Ellis, “Digital back-propagation for spectrally efficient WDM 112 Gbit/s PM m-ary QAM transmission,” *Optics express*, vol. 19, no. 6, pp. 5219–5224, 2011.

[123] E. Ip, “Nonlinear compensation using backpropagation for polarization-multiplexed transmission,” *Journal of Lightwave Technology*, vol. 28, no. 6, pp. 939–951, 2010.

[124] F. Zhang, Q. Zhuge, M. Qiu, W. Wang, M. Chagnon, and D. V. Plant, “XPM Model-Based Digital Backpropagation for Subcarrier-Multiplexing Systems,” *Journal of Lightwave Technology*, vol. 33, no. 24, pp. 5140–5150, 2015.

[125] F. P. Guiomar, J. D. Reis, A. L. Teixeira, and A. N. Pinto, “Mitigation of intra-channel nonlinearities using a frequency-domain volterra series equalizer,” *Optics express*, vol. 20, no. 2, pp. 1360–1369, 2012.

[126] Y. Gao, F. Zhang, L. Dou, Z. Chen, and A. Xu, “Intra-channel nonlinearities mitigation in pseudo-linear coherent QPSK transmission systems via nonlinear electrical equalizer,” *Optics Communications*, vol. 282, no. 12, pp. 2421–2425, 2009.

[127] J. Pan and C.-H. Cheng, “Wiener–Hammerstein model based electrical equalizer for optical communication systems,” *Journal of Lightwave Technology*, vol. 29, no. 16, pp. 2454–2459, 2011.

[128] D. Maiti and M. Brandt-Pearce, “Modified nonlinear decision feedback equalizer for long-haul fiber-optic communications,” *Journal of Lightwave Technology*, vol. 33, no. 18, pp. 3763–3772, 2015.

[129] S. Gringeri, B. Basch, V. Shukla, R. Egorov, and T. J. Xia, “Flexible architectures for optical transport nodes and networks,” *IEEE Communications Magazine*, vol. 48, no. 7, pp. 40–50, 2010.

[130] M. Abramowitz, I. A. Stegun, *et al.*, “Handbook of mathematical functions,” *Applied mathematics series*, vol. 55, p. 62, 1966.

[131] Z. Li, W.-R. Peng, F. Zhu, and Y. Bai, “MMSE-Based Optimization of Perturbation Coefficients Quantization for Fiber Nonlinearity Mitigation,” *Journal of Lightwave Technology*, vol. 33, no. 20, pp. 4311–4317, 2015.

[132] T. Wuth, M. W. Chbat, and V. F. Kamalov, “Multi-rate (100G/40G/10G) transport over deployed optical networks,” in *OFC/NFOEC 2008-2008 Conference on Optical Fiber Communication/National Fiber Optic Engineers Conference*, 2008.

[133] A. Ghazisaeidi, J. Renaudier, M. Salsi, P. Tran, G. Charlet, and S. Bigo, “System benefits of digital dispersion pre-compensation for non-dispersion-managed PDM-WDM transmission,” in *39th European Conference and Exhibition on Optical Communication (ECOC 2013)*, 2013.

[134] S. J. Lee, “A new non-data-aided feedforward symbol timing estimator using two samples per symbol,” *Communications Letters, IEEE*, vol. 6, no. 5, pp. 205–207, 2002.

[135] T. M. Schmidl and D. C. Cox, "Robust frequency and timing synchronization for OFDM," *Communications, IEEE Transactions on*, vol. 45, no. 12, pp. 1613–1621, 1997.

[136] X. Xu, B. Châtelain, and D. V. Plant, "Decision directed least radius distance algorithm for blind equalization in a dual-polarization 16-QAM system," in *Proceedings of OFC*, 2012.

[137] Q. Zhuge, M. Morsy-Osman, X. Xu, M. E. Mousa-Pasandi, M. Chagnon, Z. A. El-Sahn, and D. V. Plant, "Pilot-aided carrier phase recovery for M-QAM using superscalar parallelization based PLL," *Optics express*, vol. 20, no. 17, pp. 19599–19609, 2012.

[138] Z. Dong, Q. Sui, A. P. T. Lau, K. Zhong, L. Li, Z. Li, and C. Lu, "Optical performance monitoring in DSP-based coherent optical systems," in *Optical Fiber Communication Conference*, pp. W4D–1, Optical Society of America, 2015.